OPTIMAL TRANSMISSION SWITCHING IN POWER SYSTEMS WITH LARGE-SCALE RENEWABLE RESOURCES

A Dissertation

by

TIAN LAN

Submitted to the Office of Graduate and Professional Studies of
Texas A&M University
in partial fulfillment of the requirements for the degree of

DOCTOR OF PHILOSOPHY

Chair of Committee,	Garng M. Huang
Committee Members,	Chanan Singh
	Shankar P. Bhattacharyya
	Erick Moreno-Centeno
Head of Department,	Miroslav M. Begovic

December 2018

Major Subject: Electrical Engineering

ABSTRACT

In the past decade, there has been a rapid growth for renewable generations in power systems worldwide. However, the natural intermittency of wind and solar causes a variable output for renewable generations in power systems. Under this new situation, the optimal network topology of a power system can vary with time. This research focuses on an emerging topology control technology, optimal transmission switching, to improve the flexibility and efficiency of power systems with large-scale renewable generations. Novel optimization and stability enhancement approaches for optimal transmission switching are developed considering the grid uncertainties caused by the highly variable renewable generations and load fluctuation.

Three major problems of optimal transmission switching are resolved in this research. First, novel optimization approaches are developed to calculate accurate switching plans for optimal transmission switching actions. Different from the existing approaches, the proposed approaches are focused on the alternating current optimal power flow for a better accuracy. New elements like renewable generations and energy storage devices are included in the optimization problems. In addition, grid uncertainties are taken into consideration and stochastic programming is used in the decision-making process. A scalable decomposition approach is proposed to solve the stochastic programming problem of the alternating current optimal power flow based optimal transmission switching.

Second, transient stability issues in the transmission switching actions are investigated and transient stability enhancement methods are proposed. And a new transient stability index, critical switching flow, is proposed for transmission switching actions. Based on the new quantitative index, a preventive stabilizing redispatch scheme is developed. The proposed scheme considers

the grid uncertainties in the day-ahead planning and can be applied to avoid unstable switching actions in the online operation.

Third, the cyber-security issues associated with transmission switching actions are analyzed. The potential threat of false data injection attack is discussed. The cyber-attack may compromise the state estimator and make a risky switching action stable in the online stability check. As a result, a catastrophic instability will be led by the cyber-attack. The countermeasure is given to defend the cyber-attack.

Numerical results on the different test systems justify the proposed approaches in this research. The developed approaches will facilitate the implementation of optimal transmission switching in the real world.

DEDICATION

To my parents and beloved wife.

ACKNOWLEDGEMENTS

First and foremost, I would like to express my deepest appreciation to my advisor Dr. Garng M. Huang. When I started my Ph.D. career in 2013, I was a student who just came to a new country without funding and even without an advisor. It was Dr. Huang who spotted my talent and provided me with enough funding for my entire Ph.D. career. I am very grateful for what Dr. Huang has done for me. Working with Dr. Huang is my greatest honor and fortune. His rigorous scientific attitude has deeply inspired me and I have been trained to hold the same attitude not only in my Ph.D. career but also in my future career for the rest of my life.

I would also thank Dr. Chanan Singh, Dr. Shankar P. Bhattacharyya and Dr. Erick Moreno-Centeno for serving my committee members. I have learned a lot from their courses and they provide me with previous guidance and support throughout my research.

It has been a great experience to work with my colleagues: Yenpo Ho, Wenzong Wang, Chenyan Guo, Zhangxin Zhou, Shijia Zhao, Hangtian Lei, Bo Chen, Xinbo Geng, Hao Ming and Cheng Qian. We had many interesting discussions about our research as well as our life. In addition, I would also thank my friends: Tiangang Song, Yifei Zhang, Chan Huang, Yifeng Cheng, Bizhu He, Xijun Shi, Xuan Zhou, Zhongming Chen, Ting Chen, Xiaolu Zhou, Xie Xie, Yang Song, Han Wang, Hongyang Di and Wei Xie for making my life colorful and enjoyable during my Ph.D. career.

Finally, my special thanks go to my family for their support, encouragement and even sacrifice in my pursuit of the Ph.D. degree. I will never forget that my parents, Yueming Lan and Tingmei Zhou, flew all over the world to have several short reunions with me. Meeting and getting married to my wife, Tian Su, at Texas A&M University is the most precious and romantic thing

during my Ph.D. time. She always gives unconditional love and understanding to me. I will always remember her sacrifice for being alone when I have to stay in Qatar for my research. She is the source of my impetus for working hard in my Ph.D. career.

CONTRIBUTORS AND FUNDING SOURCES

This work was supervised by a dissertation committee consisting of Professor Garng M. Huang (advisor) and Professors Chanan Singh, Shankar P. Bhattacharyya of the Department of Electrical and Computer Engineering and Professor Erick Moreno-Centeno of the Department of Industrial and Systems Engineering. All work for the dissertation was completed independently by the student.

Graduate study was supported by a one-time graduate merit scholarship from the Department of Electrical and Computer Engineering at Texas A&M University.

The work was in part supported by U.S. Department of Energy, ARPA-E program, Robust Adaptive Topology Control (RATC), project award number: DE-AR0000220.

This publication was made possible by NPRP grant # 7-106-2-053 from the Qatar National Research Fund (a member of Qatar Foundation). The statements made herein are solely the responsibility of the authors.

NOMENCLATURE

DCOPF	Direct current optimal power flow
ACOPF	Alternating current optimal power flow
OTS	Optimal transmission switching
DC-OTS	DCOPF based OTS
AC-OTS	ACOPF based OTS
LP	Linear programming
NLP	Nonlinear programming
MILP	Mixed-integer linear programming
MINLP	Mixed-integer nonlinear programming
MISOCP	Mixed-integer second-order cone programming
SP	Stochastic programming
CCT	Critical clearing time
TSI	Transient stability index
TEF	Transient energy function
EMS	Energy management system
FDIA	False data injection attack
BESS	Battery energy storage device
WSCC	Western systems coordinating council
SOC	State of charge
B&B	Branch and bound
GAMS	General Algebraic Modeling System

GBD	Generalized Benders decomposition
TCSC	Thyristor-controlled series compensation
CSF	Critical switching flow
PDF	Probability density function
COI	Center of inertia
UEP	Unstable equilibrium point
PCSF	Practical CSF
SCOPF	Security constrained OPF
COV	Coefficient of variation
RTS	Reliability test system
SCADA	Supervisory control and data acquisition
PMU	Phasor measurement unit
LMP	Locational marginal price

TABLE OF CONTENTS

Page

LIST OF FIGURES

Page

LIST OF TABLES

Page

1. INTRODUCTION

1.1 Motivation

Electric power system is one of the most important infrastructures in modern societies. In the past decade, great efforts have been taken to build a more reliable and more cost-efficient smart grid. In the vision of a smart grid, large-scale renewable generations are integrated to reduce the consumption of fossil fuel and thus reduce the system operational cost for a sustainable development. However, the integration of large-scale renewable generations brings new challenges to power systems. Due to the intermittent nature of wind and solar, the renewable outputs can change fast with time and it is extremely hard to get an accurate forecast. Since the renewable generations are usually installed in different geographic areas, the variable renewable outputs together with the load fluctuation may cause transmission congestions in different areas in the daily operation. Under this new situation, the optimal network topology of a power system is no longer fixed during a day.

Optimal transmission switching (OTS) is proposed by the academia in the past few years to actively adjust the system topology and generation dispatch collaboratively to optimize the system operational cost. Therefore, this new technology has the potential to improve the efficiency of power systems with large-scale renewable generations. However, at the infantile stage, two categorizes of studies are needed to implement the new technology in the real world. First, optimization and planning schemes should be developed for OTS in systems with large-scale renewable generations. Second, the security concerns of the new technology, especially the impact of large-scale renewable generations, should be fully investigated before actual implementation. The system must be kept stable all the time to avoid disastrous consequences.

Driven by the promising future of OTS, this dissertation is aimed at resolving the key issues to enable the new technology to achieve its full potential.

1.2 Literature review

The concept of OTS for economic benefits was first introduced in [1] in 2005. Transmission lines are considered as dispatchable devices in OTS. The implementation of OTS in the real world requires advanced optimization approaches and security analysis.

1.2.1 Existing works on optimization methods for OTS

A series of studies of OTS are presented in the deterministic optimization area led by the concept in [1]. The mathematical formulation of OTS was first proposed and investigated in [2] in 2008. The OTS problem is formulated as a mixed-integer linear programming (MILP) problem with the direct current optimal power flow (DCOPF). The DCOPF is used in most research papers for OTS problems in [3]-[10]. The sensitivity analysis and the contingency analysis for the OTS are shown in [3]-[4] respectively. A co-optimization of generation unit commitment and OTS with N-1 reliability is proposed in [5]. Reference [6] summarizes the transmission switching actions and network topology optimization. A fast heuristic for OTS is developed in [7] by providing candidate lines. The line switching actions are considered in the line capacity expansion problem in [8]. In [9], OTS is incorporated in the day-ahead unit commitment and scheduling stage. And an OTS formulation with short-circuit current limitation constraints is proposed in [10]. Besides the DCOPF based OTS (DC-OTS), the alternating current optimal power flow (ACOPF) based OTS (AC-OTS) is adopted in [11]-[16]. The discrepancy between the DC-OTS and the AC-OTS is analyzed in detail in [11]. The AC-OTS is proven to be more accurate in OTS problems. Reference [12] proposes an AC-OTS formulation considering voltage security and N-1 contingency analysis. A new heuristic for solving the AC-OTS is proposed in [13]. A mixed-

integer second-order cone programming (MISOCP) relaxation is proposed in [14] for the AC-OTS. In [15], another MISOCP relaxation model is proposed for AC-OTS and combined with an AC feasibility check. Reference [16] investigates the primal and dual bound of the AC-OTS using a series of relaxations and a generic mixed-integer nonlinear programming (MINLP) solver.

Apart from the aforementioned deterministic optimization studies, a few probabilistic and stochastic studies are also performed for OTS to deal with grid uncertainties. In [17], a two-point estimation method is proposed for the probabilistic analysis using the DC-OTS. Reference [18] proposes a stochastic programming (SP) formulation for OTS problems under uncertainties using the piece-wise linearized power flow equations, which are solved in the Benders decomposition.

From the previous optimization studies, it can be seen that two important studies are needed. First, a lot of new equipment, such as energy storage devices, are installed in the grid now. The co-optimization of OTS and the new equipment should be investigated. Second, the integration of renewable generations increases the grid uncertainties greatly. As a result, we should consider the uncertainties in the decision-making of OTS operations. And in both studies, the ACOPF should be used to consider voltage and reactive power issues for a better accuracy. The linearized or piece-wise linearized power flow equations cannot represent the physical system and thus may result in an inaccurate result in the optimization problems.

1.2.2 Existing works on security analysis for OTS

Another important part of implementing OTS is the potential security concern. A line switching action may introduce a large disturbance in the system and thus transient instability becomes a potential security concern. In previous literature [19], transient instability is observed in line switching actions. As a result, some beneficial switching plans are abandoned for the sake of security. Therefore, the key problem is how to enhance system stability to enable beneficial

switching actions. To achieve that, a proper index that can be calculated offline and then used online to provide preventive stabilizing control guidelines is desired for transmission switching actions. Critical clearing time (CCT) [20]-[21], transient stability index (TSI) [22] and transient energy function (TEF) [23]-[27] are widely used indices to assess transient stability. CCT is the maximum time during which a disturbance can be applied without the system losing its stability. It is a traditional transient stability metric for short circuit faults on a power system [21]. However, a line switching action is not a fault and will not be cleared after it is implemented. There is no CCT defined for transmission switching actions. TSI is calculated based on the maximum angle separation of any two generators in the system at the same time in the post-fault response. The trajectory of a system following a disturbance can be assessed by evaluating the TSI [22]. It is good to use TSI for transient stability evaluation after a contingency happens, but TSI cannot provide any information about how to avoid instability. The energy-based TEF is a specific form of the more general Lyapunov functions for stability study [24]. The fundamental goal of TEF is to calculate the transient energy that the post-fault system is capable of absorbing and compare it with the system initial energy after fault clearing to determine stability. TEF allows fast screening of the contingencies while providing a mathematically rigorous certificate of stability. However, limited scalability and natural conservativeness of classical TEF restrict its applicability [27]. Moreover, TEF is unable to provide explicit control instructions for stability enhancement since the complex calculation of TEF consists of generator rotor angles, generator outputs and loads. Therefore, the aforementioned indices are unsuitable for preventive stabilizing control in transmission switching actions. In addition, these indices are usually used for deterministic studies where the uncertainties in the grid are not considered. Apparently, a new transient stability index

and the corresponding preventive scheme is needed for the implementation of transmission switching actions.

In addition to the transient stability concern, the cyber-security is also a potential concern for transmission switching actions such as OTS. In fact, a modern power system is a complicated cyber-physical system, in which many applications heavily rely on the result of the state estimation in the energy management system (EMS). Therefore, the cyber-security has become a key factor. As shown in the previous literature [28], both the DC state estimation and the AC state estimation could be vulnerable to false data injection attack (FDIA). And the impacts of FDIA include the economic attack, the load redistribution attack and the energy deceiving attack [29]. Considering the cyber-security concerns in modern power systems, it is necessary to assess and enhance the cyber-security for new applications like OTS.

1.3 Challenges

According to Section 1.2, the main challenges of implementing OTS in modern power systems are summarized in this section. The associated technical and mathematical issues are also introduced briefly.

1) **Incorporate new devices such as energy storage devices into OTS**: The AC-OTS problem is a nonconvex MINLP problem, which is also NP-hard. Solving this problem for a single hour case is fairly difficult and time-consuming. When energy storages devices are incorporated, we must consider the 24 hours together to co-optimize OTS actions and energy storage. In mathematical perspective, this is a multi-stage nonconvex MINLP problem and is even more difficult to solve due to the linkage between stages and the increased size of the optimization problem.

2) **Consider the uncertainties of the grid in the decision-making of OTS**: In most previous research on OTS problems, all parameters are known and deterministic optimization is used. When considering the grid uncertainties, SP should be used. The probability distributions of uncertain parameters are used to represent the uncertainties. And the impact of the uncertainties is evaluated by a mean value function in the objective function to obtain the optimal decision. In general, a lot of random scenarios are needed to represent the uncertainties and the size of the optimization problem is much bigger than the deterministic optimization problem.
3) **Enhance system transient stability for OTS actions in the online operation**: The switching actions could introduce a large disturbance in the system and result in transient instability. An important technical issue is how to identify the instability and what to do to avoid the instability in the online operation. The existing time-domain simulation method is good enough to find instability in the online dynamic study. However, it cannot give explicit control instructions to enhance transient stability for the switching action.
4) **Enhance cyber-security for OTS actions**: A modern power system is a cyber-physical system. The operation of the system heavily relies on data acquisition and analysis in the EMS. It is essential to investigate whether somebody may launch a cyber-attack and take advantage of the OTS actions to affect the system operation. If such cyber-attack is possible, the corresponding defending scheme should be developed.

1.4 Main contributions

This dissertation focuses on the aforementioned challenges of OTS in the perspective of optimization and security analysis, in which the grid uncertainties caused by large-scale renewable generations and load fluctuations are considered. The main contributions are as follows:

- A new co-optimization of the AC-OTS and battery energy storage device (BESS) is proposed. The AC-OTS and BESS can work collaboratively to further improve the power system efficiency.
- The grid uncertainties caused by large-scale renewable generations and load fluctuation are considered in the decision-making process of OTS by using SP. The SP formulations for the AC-OTS and the DC-OTS are proposed and compared through a comprehensive numerical study.
- A reliable decomposition approach is developed to solve the SP formulation of the AC-OTS efficiently. The proposed decomposition approach has a good scalability and thus can deal with a large number of random scenarios in the decision-making process.
- The transient stability analysis for transmission switching actions is investigated. The general transient stability enhancement methods are provided.
- A new transient stability index for transmission switching actions is developed. Based on the new index, a preventive stabilizing redispatch scheme is proposed for switching actions. In the proposed scheme, the knowledge obtained in the offline probabilistic stability study could be utilized to avoid instability in online operations.
- The cyber-security of switching actions is investigated. A cyber-attack in the power system may finally lead to catastrophic instability in the physical system. The corresponding countermeasure is provided for transmission switching actions.

1.5 Dissertation organization

The rest of the dissertation is organized as follows.

Section 2 presents the deterministic optimization approaches for OTS. The basic DC-OTS and AC-OTS formulations are first introduced. Then the AC-OTS with BESS is shown to further improve the power system efficiency. Solution strategies are followed, where the branch and bound (B&B) algorithm and the proposed approximation method are illustrated. Numerical examples are shown on the IEEE-118 bus system.

Section 3 deals with the grid uncertainties caused by large-scale renewable resources and load fluctuations in OTS decision-making. The fundamentals of SP are introduced in the beginning. Then the mathematical formulations of the stochastic AC-OTS and DC-OTS are given. Multiple solution strategies are demonstrated next. Finally, numerical analysis on the IEEE-118 bus system is shown to compare the traditional deterministic DC-OTS and the two proposed stochastic OTS methods.

Section 4 proposes a novel decomposition approach to solve the SP formulation of AC-OTS efficiently and accurately. A brief introduction is presented in the beginning to illustrate why a new decomposition approach is necessary for solving the SP problems of AC-OTS. Then the new mathematical formulations of the stochastic AC-OTS are presented and followed by the explanation of the proposed solution strategy. The numerical results on different systems confirm the validity of the proposed decomposition approach in OTS problems.

Section 5 consists of a comprehensive transient stability analysis for transmission switching actions. The numerical integration and the transient energy function (TEF) method are introduced first for power system transient stability study. A discussion on the advantages and disadvantages of the two methods is given. Then, transient stability enhancement methods are

proposed for transmission switching actions and numerical examples are shown on the simplified western systems coordinating council (WSCC) 9 bus system.

Section 6 proposes a preventive stabilizing redispatch scheme for transmission switching actions. In the beginning, the derivation of a new transient stability index is presented using the TEF theory. Then a Monte Carlo simulation based algorithm is given to calculate the proposed transient stability index in the offline study. The preventive stabilizing redispatch scheme is illustrated in detail next and a couple of numerical examples are presented on the IEEE-118 bus system to show how the scheme works.

Section 7 explores the cyber-security issues associated with transmissions switching actions. FDIA against the AC state estimation is introduced first. And the undetected FDIA in transmission switching actions is analyzed. Finally, the countermeasure is given to defend the cyber-attack. Numerical examples on the IEEE reliability test system (RTS) demonstrate the potential risk and the effectiveness of the proposed countermeasure.

Section 8 summarizes the research works in this dissertation and discusses the potential research topics in the future.

2. DETERMINISTIC OPTIMIZATION FOR OPTIMAL TRANSMISSION SWITCHING*

In Section 2, the deterministic optimization methods for OTS are presented. The basic DC-OTS and AC-OTS are shown first. Then we include a new device, BESS, in OTS to further optimize the system operation cost. The combination of OTS and BESS makes the optimization problem rather complicated as we need to solve a multi-stage nonconvex MINLP problem. An approximation method is therefore proposed to accelerate the computation. Numerical examples are given on the IEEE-118 bus system.

The symbols used in Section 2 are listed as follows.

1) Notations for the optimization problems:

Sets:

$g \in G$	Set of all conventional generators.
$r \in R$	Set of all renewable generators.
$e \in E$	Set of all BESS.
$b \in B$	Set of all buses.
$k \in L$	Set of all lines
$t \in T$	Set of all hours. $T = \{1,2 \dots\ t_{total}\}$
T_j	Set of hours for jth subproblem. The whole problem is divided into q subproblems. $T_j = \{(j-1) * t_{total}/q + 1, j * t_{total}/q\}$

* © [2017] IEEE. Reprinted, with permission, from [T. Lan and G. M. Huang, An intelligent parallel scheduling method for optimal transmission switching in power systems with batteries, 2017 19th International Conference on Intelligent System Application to Power Systems (ISAP), 09/2017]
© [2018] IEEE. Reprinted, with permission, from [T. Lan, Z. Zhou and G. M. Huang, An approximation for parallelism in ACOPF based stochastic optimal transmission switching with battery energy storage systems, 2018 IEEE 12th International Conference on Compatibility, Power Electronics and Power Engineering (CPE-POWERENG 2018), 04/2018]

$ec \in EC$ Set of equality constraints. $EC = \{1, 2 \dots ec_{total}\}$

$ic \in IC$ Set of inequality constraints. $IC = \{1, 2 \dots ic_{total}\}$

$\Omega_{g,b}$ Set of conventional generators connected to bus b

$\Omega_{r,b}$ Set of renewable generators connected to bus b

$\Omega_{e,b}$ Set of BESS connected to bus b

$\Omega_{m=b}$ Set of lines with from end connected to bus b.

Parameters:

C_g Linear generation cost of generator g.

C_{shed} Linear penalty cost of load shedding.

V_b^{max}, V_b^{min} Max. and min. voltage of bus b.

P_g^{max}, V_g^{min} Max. and min. generation of generator g.

Q_g^{max}, Q_g^{min} Max. and min. reactive power of generator g.

$P_{r,t}^{max}$, $P_{r,t}^{min}$ Max. and min. generation of renewable generator r at hour t.

$Q_{r,t}^{max}$, $Q_{r,t}^{min}$ Max. and min. reactive power of renewable generator r at hour t.

t_{kmn} Transformer tap ratio of line k (from m to n). $t_{kmn} = 1$ for non-transformer branch

$g_{kmn} + jb_{kmn}$ Admittance of line k (from m to n).

B_{kmn}^{shunt} Shunt capacitance of line k (from m to n).

c_{kmn} Binary index. $c_{kmn} = 1$ if m is the tap side of transformer; $c_{kmn} = 0$ if n is the tap side or line k is non-transformer branch.

S_{kmn}^{max} Thermal limit of line k (from m to n).

$G_b + jB_b$ Fixed shunt admittance of bus b.

$P_{b,t}^{load}, Q_{b,t}^{load}$ Real and reactive load of bus *b* at hour *t*.

N Number of allowed switching actions for each hour.

M Large number. $M = \max(S_{kmn}^{max})$.

η_e^{in} Charging efficiency of BESS *e*.

η_e^{out} Discharging efficiency of BESS *e*.

E_e^{max}, E_e^{min} Max. and min. state of charge of BESS *e*.

$P_e^{in,max}$ Max. charging power of BESS *e*.

$P_e^{in,min}$ Min. charging power of BESS *e*.

$P_e^{out,max}$ Max. discharging power of BESS *e*.

$P_e^{out,min}$ Min. discharging power of BESS *e*.

Q_e^{max}, Q_e^{min} Max. and min. reactive power of BESS *e*.

Variables:

$P_{g,t}, Q_{g,t}$ Real power and reactive power generation of generator *g* at hour *t*.

$P_{r,t}, Q_{r,t}$ Real power and reactive power of renewable generator *r* at hour *t*.

$LSp_{b,t}$ Real power load shedding at bus *b* at hour *t.*

$V_{b,t}, \delta_{b,t}$ Voltage magnitude and angle of bus b at hour *t*.

$P_{kmn,t}, Q_{kmn,t}$ Real and reactive power flow of line *k* through *m* to *n* at hour *t*.

$z_{k,t}$ Binary variable of line status at hour *t*. 0 for in service, 1 for out of service.

$P_{e,t}^{in}, P_{e,t}^{out}$ Charging and discharging power of BESS *e* at hour *t*.

$E_{e,t}$ State of charge (SOC) of BESS *e* at hour *t*.

$Q_{e,t}$ reactive power of BESS *e* at hour *t*.

2) Notations for the B&B algorithm:

$x(j), y(j)$	The optimal solution for the LP/NLP relaxation of problem (*j*), where $x(j)$ is the binary variable and $y(j)$ is the continuous variable.
$z(j)$	The optimal objective value of the LP/NLP relaxation of problem (*j*).
x^*, y^*	The incumbent solution for the LP/NLP of problem, where x^* is the solution for binary variable and y^* is the solution for continuous variable.
S_{Active}	Set of active nodes in the B&B algorithm

2.1 Basic mathematical formulations for OTS

In the mathematical formulations for OTS, a binary variable is used to represent the on/off status of a transmission line. The two basic formulations for OTS are shown in this section.

2.1.1 The basic DC-OTS formulation

The basic DC-OTS formulation [2] is shown in (2-1)-(2-8). The objective is to minimize the system operational cost as shown in (2-1). Equation (2-2) is the generation limit constraint. Line status (on/off) is modeled as a binary variable in (2-3). And the number of allowed switching actions is shown in (2-4). The line flow constraint is shown in (2-5). A big *M* is used in the flow calculation in (2-6)-(2-7). When a line is switched off ($z_k = 1$), the voltage angles will not be constrained by (2-6)-(2-7). Power balance constraint is enforced by (2-8).

$$\text{min} \quad \sum_{g \in G} C_g P_g \tag{2-1}$$

$$\text{s.t.} \quad P_g^{min} \le P_g \le P_g^{max}, \quad \forall g \tag{2-2}$$

$$z_k \in \{0,1\}, \quad \forall k \tag{2-3}$$

$$\sum_{k \in L} z_k \le N \tag{2-4}$$

$$-(1 - z_k) S_{kmn}^{max} \le P_{kmn} \le (1 - z_k) S_{kmn}^{max}, \quad \forall k \tag{2-5}$$

$$b_{kmn}(\delta_m - \delta_n) - P_{kmn} + (z_k) M \ge 0, \quad \forall k \tag{2-6}$$

$$b_{kmn}(\delta_m - \delta_n) - P_{kmn} - (z_k)M \leq 0, \quad \forall k \tag{2-7}$$

$$\sum_{g\in\Omega_{g,b}} P_g^{gen} - P_b^{load} = \sum_{k\in\Omega_{m=b}} P_{kbn} + G_b, \quad \forall b \tag{2-8}$$

The DC-OTS uses the linearized power flow equations for simplicity and it is a convex MILP problem. The voltage issues and the reactive power issues are ignored. Usually, an AC feasibility check is needed for the obtained switching solution from the DC-OTS.

2.1.2 The basic AC-OTS formulation

The basic AC-OTS formulation is shown in (2-9)-(2-19). The objective is to minimize the system operational cost as shown in (2-9). Constraint (2-10) is the bus voltage limit. Real and reactive power generation limits are shown in (2-11)-(2-12) for conventional generators. Line flows are calculated using AC power flow equations in (2-13)-(2-14), where δ_{mn} stands for $(\delta_m - \delta_n)$. Transformer branch is taken into consideration and a binary index c_{kmn} is used to indicate the tap side of the transformer. Line status is modeled as a binary variable as shown in (2-15) and the number of switching actions allowed is presented in (2-16). Equation (2-17) is the line flow constraint. When a line is in service ($z_k = 0$), the corresponding line flow is constrained by the line capacity. And when a line is out of service ($z_k = 1$), the constraint (2-17) is no longer valid for the line. Constraints (2-18)-(2-19) represent the power balance equations, which contain conventional generators and renewable generators.

$$\text{min} \qquad \sum_{g\in G} C_g P_g \tag{2-9}$$

$$\text{s.t.} \qquad V_b^{min} \leq V_{b,} \leq V_b^{max}, \ \forall b \tag{2-10}$$

$$P_g^{min} \leq P_g \leq P_g^{max}, \quad \forall g \tag{2-11}$$

$$Q_g^{min} \leq Q_g \leq Q_g^{max}, \ \forall g \tag{2-12}$$

$$P_{kmn} = -\frac{V_m V_n}{t_{kmn}}(g_{kmn}\, cos(\delta_{mn}) + b_{kmn}\, sin(\delta_{mn}))$$

$$+V_m^2 g_{kmn}(1-c_{kmn}) + \left(\frac{V_m^2 g_{kmn}}{t_{kmn}^2}\right) c_{kmn}, \ \forall k \tag{2-13}$$

$$Q_{kmn} = -\frac{V_m V_n}{t_{kmn}}(g_{kmn}\, sin(\delta_{mn}) - b_{kmn}\, cos(\delta_{mn}))$$

$$-V_m^2\left(b_{kmn} + \frac{B_{kmn}^{shunt}}{2}\right)(1-c_{kmn}) - V_m^2\left(\frac{b_{kmn}}{t_{kmn}^2} + \frac{B_{kmn}^{shunt}}{2}\right) c_{kmn}, \ \forall k \tag{2-14}$$

$$z_k \in \{0,1\}, \quad \forall k \tag{2-15}$$

$$\sum_{k\in L} z_k \leq N \tag{2-16}$$

$$\left((1-z_k) * P_{kmn,}\right)^2 + ((1-z_k) * Q_{kmn})^2 \leq ((1-z_k) * S_{kmn}^{max})^2, \ \forall k \tag{2-17}$$

$$\sum_{g\in\Omega_{g,b}} P_g = \sum_{k\in\Omega_{m=b}}(1-z_k) * P_{kbn} + P_b^{load} + V_{b,s}^2 G_b, \quad \forall b \tag{2-18}$$

$$\sum_{g\in\Omega_{g,b}} Q_g = \sum_{k\in\Omega_{m=b}}(1-z_k) * Q_{kbn} + Q_b^{load} - V_b^2 B_b, \quad \forall b \tag{2-19}$$

The AC-OTS considers the voltage and reactive issues of the physical system. Therefore, the obtained switching solution is directly applicable. However, the problem becomes a nonconvex MINLP problem due to the use of AC power flow equations. The NP-hard problem is usually very time-consuming to solve.

2.2 The co-optimization of the AC-OTS and BESS

OTS is proposed to reduce transmission congestion and thus the system operational cost in previous literature [2]-[6] as shown in Section 1.2. Energy storage devices, for example BESS, are also proposed as a tool for congestion management [30], load shedding management [31] and voltage profile improvement [32]. By optimally charging and discharging batteries, excessive cheap generation, i.e. renewable generations, can be stored in light loading hours and used in heavy loading hours. This will greatly relieve the congestion of transmission lines since part of power can be supplied locally by batteries.

In this section, the co-optimization of the AC-OTS and BESS is presented in power systems with large-scale renewable generations. The co-optimization of the two methods will further improve the power system efficiency.

The mathematical formulation is shown in (2-20)-(2-38). The main differences from Section 2.1.2 are:

1) Multiple hours instead of a single hour is considered in (2-20)-(2-38). The optimal switching plan and the optimal charging and discharging strategy are decided considering the daily fluctuation of loads and renewable generations.
2) Real power load shedding is allowed. The allowed load shedding should not exceed the current load, which is shown in (2-33). And the penalty cost of load shedding is included in the objective function (2-20).
3) Renewable generations are included in (2-24)-(2-25). The available renewable generations may be different in each hour because of the natural intermittency. That is the reason why a subscript *t* is used in (2-24)-(2-25) for renewable generators.
4) The model for BESS is shown in (2-34)-(2-38) [30], [33]. Constraint (2-34) is the power balance constraint for the energy storage device. The energy storage capacity is presented in (2-35). The limits of charging and discharging power are shown in (2-36)-(2-37). The reactive power supplied by a battery is represented in constraint (2-38).
5) The power balance equations (2-31)-(2-32) are modified to include the impact of renewable generations, load shedding and BESS.

$$\min \quad \mathrm{TC} = \sum_{t\in T}\sum_{g\in G} C_g P_{g,t} + \sum_{t\in T}\sum_{b\in B} C_{shed} LSp_{b,t} \tag{2-20}$$

$$\text{s.t.} \qquad V_b^{min} \le V_{b,\,t} \le V_b^{max},\ \forall b,t \tag{2-21}$$

$$P_g^{min} \le P_{g,\,t} \le P_g^{max},\ \forall g,t \tag{2-22}$$

$$Q_g^{min} \le Q_{g,t} \le Q_g^{max},\ \forall g,t \tag{2-23}$$

$$P_{r,t}^{min} \le P_{r,\,t} \le P_{r,t}^{max},\ \forall r,t \tag{2-24}$$

$$Q_{r,t}^{min} \le Q_{r,\,t} \le Q_{r,t}^{max},\ \forall r,t \tag{2-25}$$

$$P_{kmn,t} = -\frac{V_{m,t}V_{n,t}}{t_{kmn}}\left(g_{kmn}\,cos\left(\delta_{mn,t}\right) + b_{kmn}\,sin\left(\delta_{mn,t}\right)\right)$$

$$+V_{m,t}^2 g_{kmn}(1-c_{kmn}) + \left(\frac{V_{m,t}^2 g_{kmn}}{t_{kmn}^2}\right)c_{kmn},\quad \forall k,t \tag{2-26}$$

$$Q_{kmn,t} = -\frac{V_{m,t}V_{n,t}}{t_{kmn}}\left(g_{kmn}\,sin(\delta_{mn.t}) - b_{kmn}\,cos\left(\delta_{mn,t}\right)\right)$$

$$-V_{m,t}^2\left(b_{kmn} + \frac{B_{kmn}^{shunt}}{2}\right)(1-c_{kmn}) - V_{m,t}^2\left(\frac{b_{kmn}}{t_{kmn}^2} + \frac{B_{kmn}^{shunt}}{2}\right)c_{kmn},\ \forall k,t \tag{2-27}$$

$$z_{k,t} \in \{0,1\},\quad \forall k,t \tag{2-28}$$

$$\textstyle\sum_k z_{k,t} \le N,\quad \forall t \tag{2-29}$$

$$\left(\left(1-z_{k,t}\right) * P_{kmn,\,t}\right)^2 + \left(\left(1-z_{k,t}\right) * Q_{kmn,t}\right)^2 \le \left(\left(1-z_{k,t}\right) * S_{kmn}^{max}\right)^2,\ \forall k,t \tag{2-30}$$

$$\textstyle\sum_{g\in\Omega_{g,b}} P_{g,t} + \sum_{r\in\Omega_{r,b}} P_{r,t} + \sum_{e\in\Omega_{e,b}}\left(P_{e,t}^{out} - P_{e,t}^{in}\right)$$

$$= \textstyle\sum_{k\in\Omega_{m=b}}\left(1-z_{k,t}\right) * P_{kbn,t} + \left(P_{b,t}^{load} - LSp_{b,t}\right) + V_{b,t}^2 G_b,\quad \forall b,t \tag{2-31}$$

$$\textstyle\sum_{g\in\Omega_{g,b}} Q_{g,t} - Q_{b,t}^{load} + Q_{s,t} = \sum_{k\in\Omega_{m=\,b}}\left(1-z_{k,t}\right) * Q_{kbn,t} - V_{b,t}^2 B_b,\quad \forall b,t \tag{2-32}$$

$$0 \le LSp_{b,t} \le P_{b,t}^{load},\quad \forall b,t \tag{2-33}$$

$$E_{e,t} = E_{e,t-1} + P_{e,t}^{in}\eta_e^{in} - P_{e,t}^{out}/\eta_e^{out},\quad \forall e,t \tag{2-34}$$

$$E_e^{min} \le E_{e,t} \le E_e^{max},\quad \forall e,t \tag{2-35}$$

$$P_e^{in,\,min} \le P_{e,t}^{in} \le P_e^{in,\,max},\quad \forall e,t \tag{2-36}$$

$$P_e^{out,\,min} \le P_{e,t}^{out} \le P_e^{out,\,max},\quad \forall e,t \tag{2-37}$$

$$Q_e^{min} \le Q_{e,t} \le Q_e^{max},\quad \forall e,t \tag{2-38}$$

2.3 Solution strategies

In this section, the widely used B&B algorithm is introduced for solving OTS problems. And the proposed approximation method is then presented to accelerate the computation for the problem of AC-OTS with BESS.

2.3.1 The branch and bound algorithm

The B&B [34] is an algorithm for combinatorial optimization problems. It recursively branches on the fractional variables to split the search space into smaller spaces and solves the relaxation of LP/NLP problem on these smaller spaces. The B&B algorithm keeps track of the upper bound and lower bound of the original combinatorial optimization problem, and uses these bounds to prune the search space, eliminating candidate solutions that can be proved not better than the incumbent solution. For convex problems, the B&B algorithm can guarantee that a global optimum will be found. And for nonconvex problems, the B&B algorithm is a heuristic that may only find a local optimum.

A brief introduction of the B&B algorithm for solving a MILP minimization problem or a MINLP minimization problem is shown as follows:

1) Procedures of the B&B algorithm:

Step 1) Initialization: Set $UB = +\infty$, $LB = -\infty$, j=1.

Step 2) Solve the LP/NLP relaxation of problem (j) for the initial node j. Update the upper bound (*UB)* and the lower bound *(LB)* according to the bounds calculation rules and mark the node j as inactive. Set the initial node j as the current node c.

Step 3) Branch on a fractional variable in $x(c)$ and mark the two direct descendants of problem (c) as active nodes. Solve the two direct descendants, problem (j+1) and problem (j+2).

Step 4) Update the *UB, LB* by applying the bounds calculation rules to each descendant problem.

Step 5) Convergence test. If $(UB - LB) \leq e|UB|$, stop the calculation and the incumbent solution x^*, y^* is the optimal solution. Otherwise, *j*=*j*+2 and continue the search with **Step 6)**.

Step 6) Choose the active node with the lowest objective value as the current node *c*. Mark the node *c* as inactive. Repeat **Step 3)-Step 6)** until the optimal solution is found.

Bounds calculation rules:

If the relaxation of problem (*j*) is feasible:

1) $z(j) \geq UB$: Prune the node *j*.

2) $z(j) < UB$:

Case 1: $x(j)$ is an integer solution

Mark the node as inactive. $UB = min\{UB, z(j)\}$. If the upper bound is updated, update the incumbent solution $x^* = x(j), y^* = y(j)$.

Case 2: $x(j)$ is not an integer solution, $LB = min\{z(j)\}, j \in S_{Active}$

If the relaxation of problem (*j*) is infeasible: Prune the node *j*.

2) A simple example:

$$Q = \begin{cases} \min & z = (x-1)^2 + (y_1 - 0.4)^2 + (y_2 - 0.8)^2 + (y_3 - 0.6)^2 \\ s.t. & x \leq 3 \\ & x \epsilon R, y_i \; is \; binary \; i = 1,2,3 \end{cases}$$

Clearly, the optimal solution is x=1, $y_1 = 0$, $y_2 = 1$, $y_3 = 1$ objective value is $z = 0.36$.

Initialization: Set $UB = +\infty$, $LB = -\infty$, $e = 0.01$. Start from the initial node and solve the relaxed NLP problem Q_1.

$$Q_1 = \begin{cases} \min & z = (x-1)^2 + (y_1 - 0.4)^2 + (y_2 - 0.8)^2 + (y_3 - 0.6)^2 \\ s.t. & x \leq 3 \\ & x \epsilon R \, , y_i \epsilon [0,1] \end{cases}$$

The solution is $x = 1$, $y_1 = 0.4$, $y_2 = 0.8$, $y_3 = 0.6$, $z = 0$. The solution is not an integer solution. Set $LB = 0$. Mark the node as inactive and set the node as current node.

Starting from the current node, branch on a non-integral variable y_2 and solve the relaxed NLP problems. Mark the two direct descendants of problem (c) as active nodes.

$$Q_2 = \begin{cases} \min & z = (x-1)^2 + (y_1 - 0.4)^2 + (y_2 - 0.8)^2 + (y_3 - 0.6)^2 \\ s.t. & x \leq 3 \\ & x \epsilon R, y_i \epsilon [0,1]\ i = 2,3, y_1 = 1 \end{cases}$$

$$Q_3 = \begin{cases} \min & z = (x-1)^2 + (y_1 - 0.4)^2 + (y_2 - 0.8)^2 + (y_3 - 0.6)^2 \\ s.t. & x \leq 3 \\ & x \epsilon R, y_i \epsilon [0,1]\ i = 2,3, y_1 = 0 \end{cases}$$

Solve the two subproblems.

For Q_2, $x = 1$, $y_1 = 1$, $_2 = 0.8$, $y_3 = 0.6$, $z = 0.36$.

For Q_3, $x = 1$, $y_1 = 0$, $y_2 = 0.8$, $y_3 = 0.6$, $z = 0.16$.

Update bounds: $LB = 0.16$, $UB = +\infty$.

Convergence test: $(UB - LB) \leq e|UB|$ not satisfied, continue.

Choose Q_3, as the current node *c* since it gives a lower objective value. Mark the node *c* as inactive and go to the next branching step. The comprehensive process can be found in Figure 2-1.

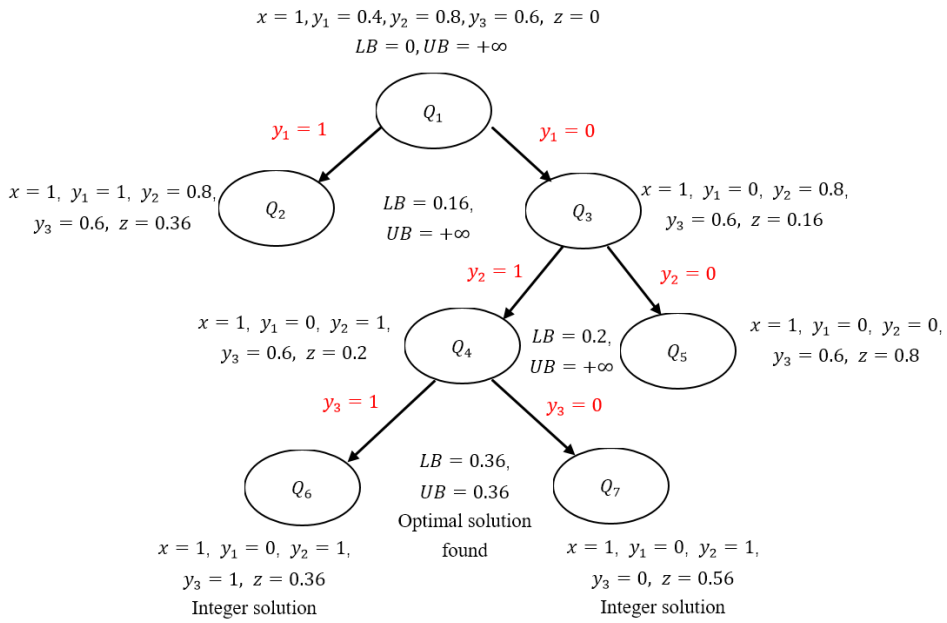

Figure 2-1: The calculation procedures using the B&B algorithm

3) Drawbacks of the B&B algorithm in OTS problems

Although the B&B algorithm can solve OTS problems by systematical enumerations, sometimes the computation time is extremely long. In the worst cases, all binary combinations must be enumerated to find the optimal solution.

For the problem of AC-OTS with BESS, the possible combinations of binary variables increase exponentially when more hours are considered. As a sequence, the computation time will increase exponentially in the B&B algorithm in the worst case. It is impractical to use the B&B algorithm directly to calculate the optimal switching plan. Thus, in the coming section, an approximation method is developed to accelerate the computation while achieving the same level of optimality.

2.3.2 The proposed approximation method

We can see from Section 2.2 that the only connection between hour t and hour t-1 is through the SOC of batteries in (2-34), where $E_{e,t}$ is determined by previous state $E_{e,t-1}$ and current charging/discharging power $P_{e,t}^{in}$, $P_{e,t}^{out}$. In the proposed scheme, we first estimate the optimal SOC and then break the whole problem into q independent subproblems, which are suitable for parallel computing. Suppose there are *x* binary variables in each hour and *y* hours are considered, the total combination is 2^{x*y} in the original problem. In contrast, the total combination is reduced to $2^{x*y/q}$ in each subproblem. The computation is therefore accelerated as fewer enumerations are needed in the B&B algorithm and subproblems can be solved simultaneously.

1) Procedures:

The framework of the proposed scheme is shown in Figure 2-2. The details are shown in the following steps:

Step 1) The power system scheduling problem is solved with BESS only for a given time period *T* (i.e. 24 hours). OTS is disabled and an NLP problem is solved. The aim of this step is to estimate the optimal SOC of BESS for each hour.

Step 2) Decide the number of periods (q) that the original problem will be decoupled into, which is also the number of subproblems in this approximation method. For example, if $q = 4$, each subproblem will contain 6 hours, namely hour 1-6, hour 7-12, hour 13-18 and hour 19-24.

Step 3) The estimated SOC of the starting hour and the ending hour are added in each subproblem as an additional constraint, which makes subproblems independent from each other. In

the aforementioned example, the estimated values of $E_{s,6}$, $E_{s,12}$, $E_{s,18}$, $E_{s,24}$ are added in the subproblems.

Step 4) Solve the subproblems in parallel computing. Several computers could be used to solve the subproblems simultaneously and reduce the computational time.

Step 5) Combine the obtained results from parallel computing. Determine if there is a need to increase or decrease the number of subproblems. It is worth mentioning that in general more subproblems will lead to a higher computational efficiency but a lower accuracy since we have more approximation and simplification there. Thus, a trade-off should be taken here considering the existing computing power.

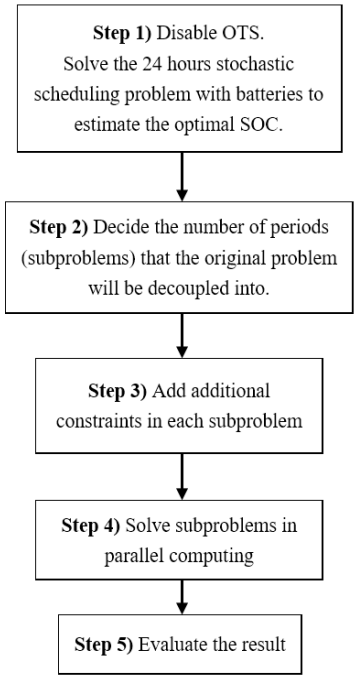

Figure 2-2: The proposed approximation method: Reprinted with permission from [© 2018, IEEE]

2) Optimality analysis:

The KKT conditions of the original problem (2-20)-(2-38) and the simplified problem in the approximation method are analyzed in this part. The original problem can be represented by (2-39)-(2-42). There are w variables ($X_{n,t}$), e_{total} equality constraints (f_e) and i_{total} inequality constraints (g_i) for each hour. The objective function $c(X_{1,t}, X_{2,t}, \dots X_{w,t})$ is a function of all variables. And the last variable $X_{w,t}$ represents the SOC of BESS.

$$\min \quad \sum_{t\in T} c(X_{1,t}, X_{2,t}, \dots X_{w,t}) \tag{2-39}$$

$$\text{s.t.} \quad f_{ec}\left(X_{1,t}, X_{2,t}, \dots X_{w,t}\right) = 0\ , \forall ec \in EC, \forall\ t \in T \tag{2-40}$$

$$g_{ic}\left(X_{1,t}, X_{2,t}, \dots X_{w,t}\right) \le 0\ ,\ \forall ic \in IC, \forall\ t \in T \tag{2-41}$$

$$X_{w,t} = h(X_{w,t-1})\ ,\quad \forall\ t \in T \tag{2-42}$$

The Lagrange function is shown in (2-43), where λ is the Lagrange multiplier. The KKT condition is represented by (2-44).

$$\begin{aligned} L = {} & \sum_t c\left(X_{1,t}, X_{2,t}, \dots X_{w,t}\right) + \sum_t \sum_{ec} \lambda_{ec,t} f_{ec}\left(X_{1,t}, X_{2,t}, \dots X_{w,t}\right) \\ & + \sum_t \sum_{ic} \lambda_{ic,t} g_{ic}\left(X_{1,t}, X_{2,t}, \dots X_{w,t}\right) + \sum_t \lambda_{w,t}\left(X_{w,t} - h(X_{w,t-1})\right) \end{aligned} \tag{2-43}$$

$$\nabla L = 0 \Rightarrow \begin{cases} \frac{\partial L}{\partial X_{1,t}} = 0, \quad \forall\ t \in T \\ \dots \\ \frac{\partial L}{\partial X_{w,t}} = 0, \quad \forall\ t \in T \\ \frac{\partial L}{\partial \lambda_{ec,t}} = 0, \ \forall ec, \forall\ t \in T \\ \frac{\partial L}{\partial \lambda_{ic,t}} = 0, \quad \forall ic, \forall\ t \in T \\ \frac{\partial L}{\partial \lambda_{w,t}} = 0, \quad \forall\ t \in T \end{cases} \tag{2-44}$$

In our proposed approximation method, the original problem (T hours) is divided into q subproblems. The jth subproblem for period T_j is shown in (2-45)-(2-50). By adding constraints (2-49) and (2-50), the subproblems are decoupled with each other.

$$\min \quad \sum_{t\in T_j} c(X_{1,t}, X_{2,t}, \dots X_{w,t}) \tag{2-45}$$

$$\text{s.t. } f_{ec}\left(X_{1,t}, X_{2,t}, \dots X_{w,t}\right) = 0\,, \quad \forall ec \in E, \forall\, t \in T_j \tag{2-46}$$

$$g_{ic}\left(X_{1,t}, X_{2,t}, \dots X_{w,t}\right) \le 0\,, \quad \forall ic \in IC, \forall\, t \in T_j \tag{2-47}$$

$$X_{w,t} = h\left(X_{w,t-1}\right), \quad \forall\, t \in T_j \tag{2-48}$$

$$X_{w,(\mathrm{j}-1)*\mathrm{t}_{total}/q} = \hat{X}_{w,(\mathrm{j}-1)*\mathrm{t}_{total}/q} \tag{2-49}$$

$$X_{w,\mathrm{j}*\mathrm{t}_{total}/q} = \hat{X}_{w,\mathrm{j}*\mathrm{t}_{total}/q} \tag{2-50}$$

The Lagrange function of j[th] subproblem is shown in (2-51). If estimated state variable $\hat{X}_{w,t}$ is sufficiently close to the optimal solution of $X^*_{w,t}$, the last two terms in (2-51) will disappear. Then (2-51) is in the same form of (2-43) but only a part of hours of the original problem. The KKT condition of each subproblem is $\nabla L_j = 0$. We can put KKT conditions of all subproblems together, which is exactly the same as (2-44).

$$\begin{aligned} L_j = {} & \sum_{t\epsilon T_j} c\left(X_{1,t}, X_{2,t}, \dots X_{w,t}\right) + \sum_{t\epsilon T_j}\sum_{ec} \lambda_{ec,t} f_{ec}\left(X_{1,t}, X_{2,t}, \dots X_{w,t}\right) \\ & + \sum_{t\epsilon T_j}\sum_{ic} \lambda_{i,t} g_{ic}\left(X_{1,t}, X_{2,t}, \dots X_{w,t}\right) + \sum_{t\in T_j} \lambda_{w,t}\left(X_{w,t} - h\left(X_{w,t-1}\right)\right) \\ & + \lambda^1_{w,j}\left(X_{w,(\mathrm{j}-1)*\mathrm{t}_{total}/q} - \hat{X}_{w,(\mathrm{j}-1)*\mathrm{t}_{total}/q}\right) + \lambda^2_{w,j}\left(X_{w,\mathrm{j}*\mathrm{t}_{total}/q} - \hat{X}_{w,\mathrm{j}*\mathrm{t}_{total}/q}\right) \end{aligned} \tag{2-51}$$

Therefore, we prove that the KKT conditions of the original problem and the simplified problem in the proposed approximation are the same given that $\hat{X}_{w,t} \approx X^*_{w,t}$ for the starting hour and the ending hour of each subproblem. Same KKT condition means the proposed approximation method will have the same local optimum as the original problem.

2.4 Numerical examples

The IEEE-118 bus system is used for demonstration, which has 187 lines and 54 generators. There is a wind plant at bus 26 with a capacity of 496.8 MW and a solar plant at bus

100 with a capacity of 422.8 MW. The total installed renewable generation capacity is 15.3% of the daily peak load. The daily load curve and renewable generation curves are created with reference to ERCOT data (Feb.27, 2017). The peak load is 6029.4MW, which appears at hour 20. BESS is installed with renewable plants at bus 26 and bus 100.

A laptop with 2.4GHz CPU and 16GB RAM is used for case stud. BONMIN solver in GAMS with a 1% relative gap is used to solve the MINLP problem. We select this solver because it is an open source solver, which is also used in solving AC-OTS problem in [35]. As for the initial condition of the optimization problem, we use the flat start for bus voltage magnitude ($V = 1$) and angle ($\delta = 0$) and all other variables are 0.

The details of BESS are shown in Table 2-1. The BESS in the system can provide 1.7% of the peak load if fully charged.

Table 2-1: Parameters of BESS: Reprinted with permission from [© 2017, IEEE]

E_e^{max}	E_e^{min}	$P_e^{in,max}$, $P_e^{out,max}$	$P_e^{in,min}$, $P_e^{out,min}$	η_e^{in}, η_e^{out}	Q_e^{max}	Q_e^{min}
150 MWh	30 MWh	50 MW	0	0.9	-30 MVAR	30 MVAR

A 24 hours case is tested in this section to demonstrate the proposed approximation method, which will also be compared with the other four methods. The number of allowed switching action per hour is set to 1 here for the purpose of computation efficiency. In principle, any number can be set and a trade-off between efficiency and performance should be considered by the operator. The results are shown in Table 2-2. And the details about the solution from the proposed scheme are shown in Table 2-3.

Table 2-2: 24 hours test with 1% relative gap: Reprinted with permission from [© 2017, IEEE]

Strategy	Time	Load shedding	Cost	Saving
ACOPF	1m18s	30.3 MWh	89464.8	NA
ACOPF with BESS	1m21s	0	84203.5	5.90%
AC-OTS	2m34s*	4.8 MWh	80847.2	9.63%
AC-OTS with BESS	Stop after 16h41m37s	0	78351.2	12.42%
The proposed approximation method for AC-OTS with BESS	24m16s **	0	78410.5	12.36%

Table 2-3: Results from the proposed scheme: Reprinted with permission from [© 2017, IEEE]

Stage	Period	Cost	Time	Load shedding
Stage 1 (Step 1)	hour 1-24	NA	1m21s	0
Stage 2 (Step 2-Step 4)	hour:1-6	14947.5	22m55s	0
	hour:7-12	16322.7	13m15s	0
	hour:13-18	15620.8	11m56s	0
	hour:19-24	31519.5	11m9s	0
	total	78410.5	24m16s**	0

* The result of the AC-OTS is calculated for each hour separately and then combined all together. Solving the 24 hours AC-OTS together will be very slow since a large number of binary variables are considered in the B&B algorithm.

** Parallel computing is used.

It can be observed from Table 2-2 that the ACOPF itself cannot avoid involuntary load shedding. The daily operational cost is 89464.8. If batteries are implemented in renewable sites, load shedding could be completely avoided and the operational cost is decreased to 84203.5. When OTS is used instead of BESS, load shedding cannot be eliminated but reduced to 4.8 MWh. Although the existence of load shedding, the operational cost is lower than the ACOPF and the

ACOPF with BESS. As for the AC-OTS with BESS, the computation time exceeds the time limit (60000s) and the program stops after 16 hours 41 minutes 37 seconds. The best integer solution yields an operational cost of 78351.2 and there still is a 4.6% gap compared with the best possible solution. This computational time is apparently inefficient for a practical daily scheduling problem.

And our proposed approximation method is much more efficient and almost the same optimality is achieved although approximation is used to decouple the original problem. The operational cost in the proposed scheme is 78410.5, which is as good as 78351.2 in the original problem (the AC-OTS with BESS). In Table 2-3, we can see the details of solving the problem. In stage 1, the optimal SOC of BESS is estimated with OTS disabled. It is an NLP optimization and can be solved in 1 minute 21 seconds. Then in stage two, the 24 hours case is divided into 4 subproblems and solved simultaneously with the estimated SOC added as additional constraints for the starting and ending hours. It takes up to 22 minutes 55 seconds to solve all subproblems in this case. Therefore, we can finish calculation in 24 minutes 16 seconds in parallel computing, which is much more efficient than solving the original problem directly (16 hours 41 minutes 37 seconds).

2.5 Summary

Transmission congestion occasionally occurs in the power system daily operation due to the integration of large-scale renewable generations. In Section 2, the basic DC-OTS and AC-OTS are introduced with the corresponding solution strategy. In addition, a co-optimization of the AC-OTS and BESS is proposed to offer further flexibility to reduce congestion and therefore operate system economically. The proposed optimization model is a MINLP problem. It is generally very time-consuming to solve such a problem in the B&B algorithm since a lot of binary variables are included. To improve the computational speed, an approximation method is developed while

keeping the same level of optimality. Numerical results on the IEEE-118 bus system show the effectiveness of the proposed method.

3. STOCHASTIC OPTIMIZATION FOR OPTIMAL TRANSMISSION SWITCHING: BASIC MODELING AND NUMERICAL ANALYSIS

In Section 2, the deterministic optimization for OTS is discussed. However, with the increasing penetration of renewable generations installed in the grid, grid uncertainties increase significantly. In the decision-making process, the uncertainties must be taken into consideration for OTS actions. Therefore, the stochastic optimization methods for OTS is presented in Section 3, where the grid uncertainties are considered carefully to make a switching decision. The fundamentals of SP are illustrated first and followed by the mathematical formulations for the stochastic OTS. The deterministic equivalent form and the two-stage formulation of the stochastic OTS are shown respectively. Then, the solution strategies that could be used to solve the stochastic OTS problems are discussed and the proposed decomposition approach is explained in detail. Numerical analysis of the stochastic OTS is given on systems of different size.

The symbols used in Section 3 are listed as follows.

Sets:

$s \in S$ Set of all scenarios

$g \in G$ Set of all conventional generators.

$r \in R$ Set of all renewable generators.

$b \in B$ Set of all buses.

$k \in L$ Set of all lines

$\Omega_{g,b}$ Set of conventional generators connected to bus b

$\Omega_{r,b}$ Set of renewable generators connected to bus b

$\Omega_{m=b}$ Set of lines with one end connected to bus *b*.

Parameters:

π_s	Probability of scenario s.
C_g	Linear generation cost of generator *g*.
C_{shed}^{p}	Linear penalty cost of real power load shedding.
C_{shed}^{q}	Linear penalty cost of reactive power load shedding.
V_b^{max}, V_b^{min}	Max. and min. voltage of bus *b*.
P_g^{max}, P_g^{min}	Max. and min. generation of generator *g*.
Q_g^{max}, Q_g^{min}	Max. and min. reactive power of generator *g*.
$P_{r,s}^{max}$, $P_{r,s}^{min}$	Max. and min. generation of renewable generator *r* in scenario *s*.
$Q_{r,s}^{max}$, $Q_{r,s}^{min}$	Max. and min. reactive power of renewable generator *r* in scenario *s*.
t_{kmn}	Transformer tap ratio of line *k* (from *m* to *n*). $t_{kmn} = 1$ for a non-transformer branch
$g_{kmn} + jb_{kmn}$	Admittance of line *k* (from *m* to *n*).
B_{kmn}^{shunt}	Shunt capacitance of line *k* (from *m* to *n*).
S_{kmn}^{max}	Thermal limit of line *k* (from *m* to *n*).
$G_b + jB_b$	Fixed shunt admittance of bus *b*.
c_{kmn}	Binary index. $c_{kmn} = 1$ if *m* is the tap side of the transformer; $c_{kmn} = 0$ if *n* is the tap side or line *k* is a non-transformer branch.
$P_{b,s}^{load}, Q_{b,s}^{load}$	Real and reactive load of bus *b* in scenario *s*.
N	Number of allowed switching actions.

M	Large number. Select as 1000.
$VSLI_{\text{limit}}$	Limit for *VSLI*.
Lb	Known lower bound on the expected recourse cost

Variables:

$P_{g,s}$	Generation of generator *g* in scenario *s*.
$P_{r,s}$	Generation of renewable generator *r* in scenario *s*.
$LSp_{b,s}$	Real load shedding at bus *b* in scenario *s*.
$LSq_{b,s}$	Reactive load shedding at bus *b* in scenario *s*.
$V_{b,s}, \delta_{b,s}$	Voltage magnitude and angle of bus b in scenario *s*.
$Q_{g,s}$	Reactive power of generator *g* in scenario *s*.
$Q_{r,s}$	Reactive power of renewable generator *r* in scenario *s*.
$P_{kmn,s}$	Real power flow of line *k* through *m* to *n* in scenario *s*.
$Q_{kmn,s}$	Reactive power flow of line *k* through *m* to *n* in scenario *s*.
z_k	Binary variable of line status. 0 for in service, 1 for out of service.
$R_{g,s}^{spin}$	Spinning reserve of generator *g* in scenario s.
$R_{g,s}^{up}, R_{g,s}^{down}$	Up and down regulation reserve of generator *g* in scenario s.
$VSLI_{kmn,s}$	VSLI index for line *k* through *m* to *n* in scenario *s*.

3.1 Fundamentals of SP

The basics of SP [36] is introduced in this section. Since the real world is uncertain, it is imperative to consider uncertainty in decision-making. SP is a framework for optimization problems that involve data uncertainties. A deterministic LP formulation is shown in (3-1)-(3-4), where x, y are the decision variables and $c^T,\ q^T, A, D, T, W, H$ are parameters. When there are

no uncertain parameters involved, decision variables x, y can be decided at the same stage in the deterministic optimization.

$$\min \quad c^T x + q^T y \tag{3-1}$$

$$\text{s.t.} \quad Ax \geq D \tag{3-2}$$

$$Tx + Wy \geq H \tag{3-3}$$

$$x \geq 0, y \geq 0 \tag{3-4}$$

When the parameter H is a random variable denoted by $H(\tilde{\omega})$, the two-stage stochastic LP formulation with fixed recourse is shown in (3-5)-(3-10). The basic idea of two-stage SP is that optimal decisions should be based on data available at the time the decisions are made and cannot depend on future observations. x is called the here-and-now variable since it must be decided without knowing the real value of $H(\omega)$, but knowing its probability distribution. y is the wait-and-see variable because we can wait until the random parameter is found and decide y to take recourse actions.

$$\min \quad c^T x + E[f(x, \tilde{\omega})] \tag{3-5}$$

$$\text{s.t.} \quad Ax \geq D \tag{3-6}$$

$$x \geq 0 \tag{3-7}$$

For each realization ω of $\tilde{\omega}$:

$$f(x, \omega) = \min \quad q^T y \tag{3-8}$$

$$\text{s.t.} \quad Wy \geq H(\omega) - Tx \tag{3-9}$$

$$y \geq 0 \tag{3-10}$$

We can also write (3-5)-(3-10) in the deterministic equivalent form with the discrete probability density function of the random scenarios s as shown in (3-11)-(3-14). It can be seen

that the uncertainty of the random parameter is considered explicitly in (3-11)-(3-14) and evaluated through an expectation function in the objective function. Therefore, the SP formulation (3-11)-(3-14) will yield a more cost-efficient solution when uncertain parameters are involved in decision-making.

$$\min \quad c^T x + \sum_s \pi_s q^T y_s \tag{3-11}$$

$$\text{s.t.} \quad Ax \geq D \tag{3-12}$$

$$Tx + Wy_s \geq H_s, \quad \forall s \tag{3-13}$$

$$x \geq 0, y_s \geq 0, \quad \forall s \tag{3-14}$$

3.2 Mathematical formulations for stochastic OTS

The framework of implementing OTS is shown in Figure 3-1. In OTS problems, the switching decision is usually decided in the day-ahead scheduling stage [5], [9] and then conducted in the online operation. It is because that the OTS problem is very time consuming [2], [11], which is not appropriate for online calculation. However, in the day-ahead scheduling stage, only the forecasted values for loads and renewable generations are known for the next day. Note that there always exist forecast errors for loads and renewable generations, especially for wind [37] and solar [38] generations. Therefore, the optimal switching plan, i.e. the optimal system topology, should be decided in the day-ahead stage considering grid uncertainties, which aims to minimize the expected operational cost of the system in the online operation. The main focus of this section is how to calculate the optimal switching plan under uncertainties as shown in the dashed line area.

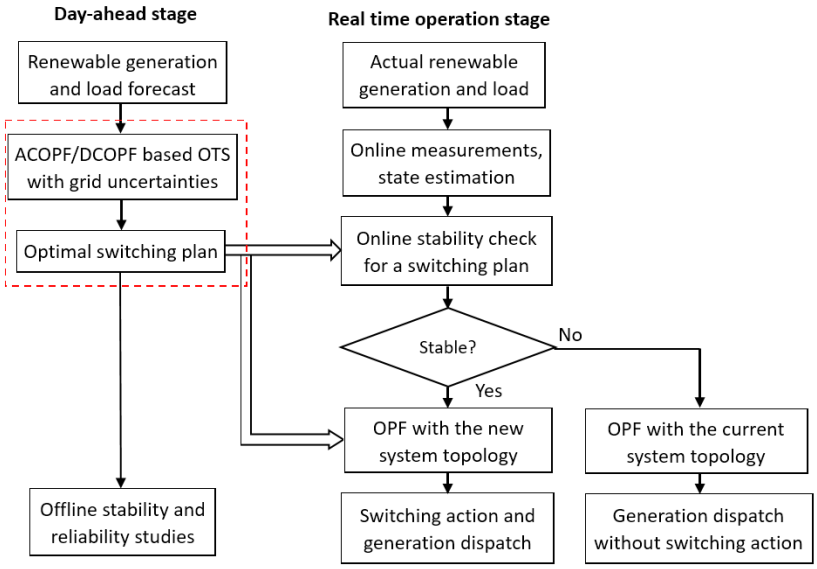

Figure 3-1: The framework of OTS implementation in power systems

In an OTS problem, loads and renewable generations are the parameters with uncertainties. The empirical distributions of loads and renewable generations can be obtained by using power system historical data [39]. Thus, this section uses SP, which is a risk-neutral method, to deal with grid uncertainties in the decision-making of OTS. In the proposed SP formulations, line status is the here-and-now decision variable since it must be decided in the day-ahead stage before the actual loads and renewable generations are known. Other decision variables such as conventional generation outputs are the wait-and-see decision variables because the generation outputs could be adjusted in the online economic dispatch and the automatic generation control.

3.2.1 The SP formulation for the AC-OTS

The basic SP formulation for AC-OTS is shown in (3-15)-(3-32) in the deterministic equivalent form. The objective is to minimize the expected operational cost (3-15), which is made up of generation cost and load shedding penalty cost. And a simplified linear generation cost is

used in (3-15), which is also commonly used in previous related studies such as [2]. Constraint (3-16) is the bus voltage limit. Real and reactive power generation limits are shown in (3-17)-(3-18) for conventional generators. Constraints (3-19)-(3-20) present the real and reactive generation limits for renewable sources. Line flows are calculated using AC power flow equations in (3-21)-(3-22), where $\delta_{mn,s}$ stands for $(\delta_{m,s} - \delta_{n,s})$. Transformer branch is taken into consideration and a binary index c_{kmn} is used to indicate the tap side of the transformer. Equation (3-23) is the line flow constraint. When a line is in service ($z_k = 0$), the corresponding line flow is constrained by the line capacity. And when a line is out of service ($z_k = 1$), the constraint (3-23) is no longer valid for the line. Constraints (3-24)-(3-25) represent the power balance equations, which contain conventional generators, renewable generators and load shedding. Allowed load shedding is shown in (3-26) and (3-27). And the number of switching actions allowed is presented in (3-28). The line switching decision should be feasible and cost-efficient for all scenarios. And line status is modeled as a binary variable as shown in (3-29). The system-wide regulation and spinning reserve are shown in (3-30)-(3-32). The up/down regulation reserve is set to be 2% of the total load [30] by constraints (3-30)-(3-31). And in (3-32), the total spinning reserve is required to be sufficient for any generator loss in a single contingency.

$$\min \quad \mathrm{TC} = \sum_s \pi_s \left(\sum_{g\in G} C_g P_{g,s} + \sum_{b\in B} C^p_{shed} LSp_{b,s} + \sum_{b\in B} C^q_{shed} LSq_{b,s}\right) \tag{3-15}$$

$$\text{s.t.} \qquad V_b^{min} \le V_{b,\,s} \le V_b^{max},\ \forall b, s \tag{3-16}$$

$$P_g^{min} + R_{g,s}^{down} \le P_{g,\,s} \le P_g^{max} - R_{g,s}^{up} - R_{g,s}^{spin},\ \forall g, s \tag{3-17}$$

$$Q_g^{min} \le Q_{g,s} \le Q_g^{max},\ \forall g, s \tag{3-18}$$

$$P_{r,s}^{min} \le P_{r,\,s} \le P_{r,s}^{max},\ \forall r, s \tag{3-19}$$

$$Q_{r,s}^{min} \le Q_{r,\,s} \le Q_{r,s}^{max},\ \forall r, s \tag{3-20}$$

$$P_{kmn,s} = -\frac{V_{m,s}V_{n,s}}{t_{kmn}}\left(g_{kmn}\,cos\left(\delta_{mn,s}\right) + b_{kmn}\,sin\left(\delta_{mn,s}\right)\right)$$

$$+V_{m,s}^2 g_{kmn}(1 - c_{kmn}) + \left(\frac{V_{m,s}^2 g_{kmn}}{t_{kmn}^2}\right)c_{kmn},\ \forall k, s \tag{3-21}$$

$$Q_{kmn,s} = -\frac{V_{m,s}V_{n,s}}{t_{kmn}}\left(g_{kmn}\,sin(\delta_{mn.s}) - b_{kmn}\,cos\left(\delta_{mn,s}\right)\right)$$

$$-V_{m,s}^2\left(b_{kmn} + \frac{B_{kmn}^{shunt}}{2}\right)(1 - c_{kmn}) - V_{m,s}^2\left(\frac{b_{kmn}}{t_{kmn}^2} + \frac{B_{kmn}^{shunt}}{2}\right)c_{kmn},\ \forall k, s \tag{3-22}$$

$$\left((1 - z_k) * P_{kmn,\,s}\right)^2 + \left((1 - z_k) * Q_{kmn,s}\right)^2 \le ((1 - z_k) * S_{kmn}^{max})^2,\ \forall k, s \tag{3-23}$$

$$\sum_{g\in\Omega_{g,b}} P_{g,s} + \sum_{r\in\Omega_{r,b}} P_{r,s} = \sum_{k\in\Omega_{m=b}}(1 - z_k) * P_{kbn,s}$$

$$+\left(P_{b,s}^{load} - LSp_{b,s}\right) + V_{b,s}^2 G_b,\quad \forall b, s \tag{3-24}$$

$$\sum_{g\in\Omega_{g,b}} Q_{g,s} + \sum_{r\in\Omega_{r,b}} Q_{r,s} = \sum_{k\in\Omega_{m=b}}(1 - z_k) * Q_{kbn,s}$$

$$+\left(Q_{b,s}^{load} - LSq_{b,s}\right) - V_{b,s}^2 B_b,\quad \forall b, s \tag{3-25}$$

$$0 \le LSp_{b,s} \le P_{b,s}^{load},\quad \forall b, s \tag{3-26}$$

$$0 \le LSq_{b,s} \le Q_{b,s}^{load},\quad \forall b, s \tag{3-27}$$

$$\sum_k z_k \le N \tag{3-28}$$

$$z_k \in \{0,1\},\quad \forall k \tag{3-29}$$

$$\sum_g R_{g,s}^{up} \ge 0.02\sum_b P_{b,s}^{load},\ \forall s \tag{3-30}$$

$$\sum_g R_{g,s}^{down} \ge 0.02\sum_b P_{b,s}^{load},\ \forall s \tag{3-31}$$

$$\sum_g R_{g,s}^{spin} \ge P_{g,\,s} + R_{g,s}^{spin},\ \forall g, s \tag{3-32}$$

Some extra constraints can also be added into the optimization problem. For example, in this section, the voltage stability constraints are presented in (3-33)-(3-34), where voltage stability load index (VSLI) [40] is incorporated to prevent voltage collapse in OTS actions.

$$VSLI_{kmn,s} = \frac{(1-z_k)*4*\left(V_{m,s}V_{n,s}\cos(\delta_{mn.s})-V_{n,s}^2\cos^2(\delta_{mn.s})\right)}{V_{m,s}^2},\ \forall k,s \quad (3\text{-}33)$$

$$\max\left(VSLI_{kmn,s}\right) \le VSLI_{\text{limit}},\ \ \forall s \quad (3\text{-}34)$$

3.2.2 The SP formulation for the DC-OTS

The deterministic equivalent form of the stochastic DC-OTS is shown in (3-35)-(3-47). It is an extension of the previous deterministic DC-OTS [6]. The differences from the stochastic AC-OTS formulation described in section 3.2.1 are: 1) the AC power flow equations are replaced by the DC power flow equations; 2) constraints related to voltage magnitude and voltage stability are removed; 3) a big M is used in the flow calculation in (3-38)-(3-39) and the flow constraint (3-40) is modified accordingly [2]. After the problem (3-35)-(3-47) is solved, the obtained switching solution will be validated in the ACOPF with the fixed network.

$$\text{min}\quad \text{TC} = \sum_s \pi_s\left(\sum_{g\in G} C_g P_{g,s} + \sum_{b\in B} C_{shed}^p LSp_{b,s}\right) \quad (3\text{-}35)$$

$$\text{s.t.}\quad P_g^{min} + R_{g,s}^{down} \le P_{g,\,s} \le P_g^{max} - R_{g,s}^{up} - R_{g,s}^{spin}, \forall g,s \quad (3\text{-}36)$$

$$P_{r,s}^{min} \le P_{r,\,s} \le P_{r,s}^{max},\ \forall r,s \quad (3\text{-}37)$$

$$b_{kmn}\left(\delta_{m,s} - \delta_{n,s}\right) - P_{kmn,s} + (z_k)M \ge 0,\ \forall k,s \quad (3\text{-}38)$$

$$b_{kmn}\left(\delta_{m,s} - \delta_{n,s}\right) - P_{kmn,s} - (z_k)M \le 0,\ \forall k,s \quad (3\text{-}39)$$

$$-(1-z_k)S_{kmn}^{max} \le P_{kmn,s} \le (1-z_k)S_{kmn}^{max}\ \ \forall k,s \quad (3\text{-}40)$$

$$\sum_{g\in\Omega_{g,b}} P_{g,s} + \sum_{r\in\Omega_{r,b}} P_{r,s} = \sum_{k\in\Omega_{m=b}} P_{kbn} + \left(P_{b,s}^{load} - LSp_{b,s}\right) + G_b,\ \forall b,s \quad (3\text{-}41)$$

$$0 \le LSp_{b,s} \le P_{b,s}^{load},\quad \forall b,s \quad (3\text{-}42)$$

$$z_k \in \{0,1\},\quad \forall k \quad (3\text{-}43)$$

$$\sum_k z_k \le N \quad (3\text{-}44)$$

$$\sum_g R_{g,s}^{up} \ge 0.02\sum_b P_{b,s}^{load},\ \ \forall s \quad (3\text{-}45)$$

$$\sum_g R_{g,s}^{down} \geq 0.02 \sum_b P_{b,s}^{load}, \quad \forall s \tag{3-46}$$

$$\sum_g R_{g,s}^{spin} \geq P_{g,s} + R_{g,s}^{spin}, \quad \forall g, s \tag{3-47}$$

3.3 Solution strategies

In this section, two solution strategies are presented for solving the stochastic OTS problems by either solving the problems directly or in a decomposed way.

3.3.1 The branch and bound algorithm

The aforementioned deterministic equivalent forms of the stochastic AC-OTS and DC-OTS can be solved by using the B&B algorithm as stated in section 2.3.1. The only difference from the deterministic optimization is that more scenarios are involved and the size of the problem is increased. Therefore, a longer computation time is needed for solving the SP problems in the deterministic equivalent form.

3.3.2 The L-shaped algorithm

The Benders decomposition [41] based L-shaped algorithm [42] is a divide-and-conquer strategy, which is computationally efficient in solving large-scale stochastic MILP problems. Therefore, the L-shaped algorithm is used to solve the stochastic DC-OTS problem. Using the two-stage formulation, the stochastic DC-OTS problem can be represented by a master problem (first stage) and subproblems (second stage).

1) Subproblems

The subproblem for scenario *s* in the *j*th iteration is shown in (3-48)-(3-59). With the obtained switching solution from the master problem, the subproblems are merely DCOPF problems, which are simply LP problems.

$$\min \qquad obj_s^{(j)} = \sum_{g \in G} C_g P_{g,s}^{(j)} + \sum_{b \in B} C_{shed}^{p} LSp_{b,s}^{(j)} \tag{3-48}$$

s.t. $$P_g^{min} + R_{g,s}^{down\,(j)} \le P_{g,s}^{(j)} \le P_g^{max} - R_{g,s}^{up\,(j)} - R_{g,s}^{spin\,(j)},\ \forall g \tag{3-49}$$

$$P_r^{min} \le P_{r,s}^{(j)} \le P_r^{max},\ \forall r \tag{3-50}$$

$$b_{kmn}\left(\delta_{m,s}^{(j)} - \delta_{n,s}^{(j)}\right) - P_{kmn,s}^{(j)} + \left(z_k^{(j)}\right)M \ge 0,\ \forall k \tag{3-51}$$

$$b_{kmn}\left(\delta_{m,s}^{(j)} - \delta_{n,s}^{(j)}\right) - P_{kmn,s}^{(j)} - \left(z_k^{(j)}\right)M \le 0,\ \forall k \tag{3-52}$$

$$-(1 - z_k^{(j)})S_{kmn}^{max} \le P_{kmn,s}^{(j)} \quad \forall k \tag{3-53}$$

$$P_{kmn,s}^{(j)} \le (1 - z_k^{(j)})S_{kmn}^{max} \quad \forall k \tag{3-54}$$

$$\sum_{g\in\Omega_{g,b}} P_{g,s}^{(j)} + \sum_{r\in\Omega_{r,b}} P_{r,s}^{(j)} = \sum_{k\in\Omega_{m=b}} P_{kbn,s}^{(j)} + \left(P_b^{load} - LSp_{b,s}^{(j)}\right) + G_b, \quad \forall b \tag{3-55}$$

$$0 \le LSp_{b,s}^{(j)} \le P_b^{load}, \quad \forall b \tag{3-56}$$

$$\sum_g R_{g,s}^{up\,(j)} \ge 0.02 \sum_b P_b^{load} \tag{3-57}$$

$$\sum_g R_{g,s}^{down\,(j)} \ge 0.02 \sum_b P_b^{load} \tag{3-58}$$

$$\sum_g R_{g,s}^{spin\,(j)} \ge P_{g,s}^{(j)} + R_{g,s}^{spin\,(j)},\ \forall g \tag{3-59}$$

2) Master problem

The master problem in the *j*th iteration is shown in (3-60)-(3-64). The objective (3-60) is to minimize the expected recourse cost $\eta^{(j)}$. Equation (3-61) is the Benders optimality cut. It should be pointed out that the subproblems are infeasible only when the sum of minimum generations is greater than the system load. However, this situation will not happen in any real power system (the sum of minimum generations is usually far smaller than the system load). Therefore, the subproblem is always feasible [43]. Thus, the subproblems are always feasible and there is no need to add the Benders feasibility cut in the master problem. An L2 cut [44] is added in the master problem to accelerate the convergence of the algorithm as shown in (3-62). The

transmission line status is model as binary variables in (3-63) and the total allowed switching actions are shown in (3-64).

$$\min \qquad MP^{(j)} = \eta^{(j)} \tag{3-60}$$

$$\text{s.t.} \qquad (\boldsymbol{\beta}^{(j)})^T \boldsymbol{z}_{\boldsymbol{k}}^{(j)} + \eta^{(j)} \geq \alpha^{(j)} \tag{3-61}$$

$$\eta^{(j)} \geq \left(\sum_s \pi_s obj_s^{(j)} - Lb\right)\left(\sum_{k\in S^{(v)}} z_k^{(j)} - \sum_{k\notin S^{(v)}} z_k^{(j)} - \left|S^{(v)}\right| + 1\right) + Lb \tag{3-62}$$

$$z_k^{(j)} \in \{0,1\}, \qquad \forall k \tag{3-63}$$

$$\sum_k z_k^{(j)} \leq N \tag{3-64}$$

where $\boldsymbol{z}_{\boldsymbol{k}}^{(j)} = \begin{bmatrix} z_1^{(j)} \\ z_2^{(j)} \\ \vdots \\ z_k^{(j)} \end{bmatrix}$, $\boldsymbol{\beta}^{(j)} = \begin{bmatrix} \beta_1^{(j)} \\ \beta_2^{(j)} \\ \vdots \\ \beta_k^{(j)} \end{bmatrix}$, $S^{(v)} = \{k | z_k^{(v)} = 1\}$, $v = 1, 2 \ldots j-1$.

The subproblems (3-48)-(3-59) can be written in the matrix form (3-65)-(3-66). Suppose $\boldsymbol{y}_{\boldsymbol{s}}^{(j)}$ is a $n_y \times 1$ vector and $\boldsymbol{x}^{(j)}$ is a $n_x \times 1$ vector, then $\boldsymbol{q}^{(j)}$ is a $n_y \times 1$ vector, $\boldsymbol{W}$ is a $n_y \times n_y$ matrix, $\boldsymbol{r}_{\boldsymbol{s}}$ is a $n_y \times 1$ vector and $\boldsymbol{T}_{\boldsymbol{s}}$ is a $n_y \times n_x$ matrix.

$$\min \qquad obj_s^{(j)} = (\boldsymbol{q}^{(j)})^T \boldsymbol{y}_{\boldsymbol{s}}^{(j)} \tag{3-65}$$

$$\text{s.t.} \qquad \boldsymbol{W}\boldsymbol{y}_{\boldsymbol{s}}^{(j)} \geq \boldsymbol{r}_{\boldsymbol{s}} - \boldsymbol{T}_{\boldsymbol{s}}\boldsymbol{x}^{(j)} : \boldsymbol{\lambda}_{\boldsymbol{s}}^{(j)} \tag{3-66}$$

where $\boldsymbol{y}_{\boldsymbol{s}}^{(j)} = \begin{bmatrix} y_{s,1}^{(j)} \\ y_{s,2}^{(j)} \\ \vdots \\ y_{s,n_y}^{(j)} \end{bmatrix}$ is the vector for second stage variables, $\boldsymbol{x}^{(j)} = \begin{bmatrix} x_1^{(j)} \\ x_2^{(j)} \\ \vdots \\ x_{n_x}^{(j)} \end{bmatrix}$ is the vector for first stage variables and $\boldsymbol{\lambda}_{\boldsymbol{s}}^{(j)} = \begin{bmatrix} \lambda_{s,1}^{(j)} \\ \lambda_{s,2}^{(j)} \\ \vdots \\ \lambda_{s,n_y}^{(j)} \end{bmatrix}$ is the dual of the constraint (3-66).

Then $\alpha^{(j)}$ and $\boldsymbol{\beta}^{(j)}$ could be calculated by (3-67)-(3-68).

$$\alpha^{(j)} = \sum_s \pi_s (\boldsymbol{\lambda}_s^{(j)})^T \boldsymbol{r}_s \tag{3-67}$$

$$\boldsymbol{\beta}^{(j)} = \sum_s \pi_s (\boldsymbol{\lambda}_s^{(j)})^T \boldsymbol{T}_s \tag{3-68}$$

3) Procedures of the L-shaped algorithm

The procedures of the L-shaped algorithm are shown in the following steps.

Step 1) Initialization. $j = 0$, $LB = -\infty$, $UB = +\infty$ and start with all lines in service $z_k^{(1)} = 0$.

Step 2) Check if $UB - LB > \varepsilon|UB|$ is satisfied. If yes, set $j = j + 1$ and go to **Step 3)**. Otherwise, stop the iteration and the optimal switching plan is z_k^*.

Step 3) Solve the decomposed subproblems with the fixed system topology $z_k^{(j)}$. Generate the optimality cut for iteration j. If $\sum_s \pi_s obj_s^{(j)} < UB$, update the $UB = \sum_s \pi_s obj_s^{(j)}$ and record the incumbent switching plan by $z_k^* = z_k^{(j)}$.

Step 4) Add the generated optimality cut into the master problem and solve the master problem. Update $LB = \max\left(LB, MP^{(j)}\right)$, set $z_k^{(j+1)}$ to the z_k value at the solution of the master problem and go to **Step 2)**.

3.4 Numerical analysis

In the numerical study, the deterministic OTS and stochastic OTS methods are compared. And the AC-OTS and DC-OTS are also analyzed in the stochastic OTS problems. The modified IEEE-118 bus system [45] is used for numerical analysis. A wind farm (bus 26, 496.8 MW) and a solar plant (bus 100, 500 MW) are included in the system. One midnight hour is selected for the stochastic OTS study and 50 scenarios with random uncertainties are created.

A laptop with 2.4GHz CPU and 16GB RAM is used for the case study. All optimization problems are solved in GAMS. BONMIN solver with a 1% relative gap is used to solve the

stochastic AC-OTS problem (MINLP). We select this solver because it is an open source solver, which is also used in solving AC-OTS problem in [35]. CPLEX is used to solve the deterministic DC-OTS (MILP) and the master problem (MILP) and the subproblems (LP) in the stochastic DC-OTS. CPLEX is a widely used commercial solver in solving LP and MILP problems. It is also used in DC-OTS studies like [2]. The AC feasibility check (NLP) is performed by CONOPT, which is a commercial solver proved to be suitable for ACOPF problems [11]. As for the initial condition of the optimization problems, we use the flat start for bus voltage magnitude ($V = 1$) and angle ($\delta = 0$) and all other variables are 0.

3.4.1 Creating random scenarios

The following distributions are used for uncertain parameters, namely wind generation, solar generation and load. 50 random scenarios are generated using these distributions and all scenarios have equal probabilities (0.02) in our case study. The specific data used could be found in [45].

1) Wind generation

Wind speed profile is modeled by the Weibull distribution best with $k_w = 2$, $c \approx 1.128 v_{mean}$ [39] as shown in (3-69). And the wind power generation from wind speed v is shown in (3-70).

$$f(v) = \frac{k_w}{c}\left(\frac{v}{c}\right)^{k_w-1} e^{-(v/c)^{k_w-1}} \tag{3-69}$$

$$P_{wind} = \begin{cases} 0, & (v < v_{ci}) \cup (v \geq v_{co}) \\ P_w^r \cdot \frac{v - v_{ci}}{v_r - v_{ci}}, & v_{ci} \leq v \leq v_r \\ P_w^r, & v_r \leq v \leq v_{co} \end{cases} \tag{3-70}$$

where v_{ci} is the cut-in speed, v_{co} is the cut-out speed, v_r is the rated wind speed., P_w^r is the rated wind generation.

2) Solar generation

The best function to model the stochastic behavior of solar irradiance s_g is the Beta distribution [39] as shown in (3-71). The relationship between irradiance s_g and the solar power generation in [39] can be simplified by assuming a constant temperature. A linear approximation is shown in (3-72).

$$f(s_g) = \begin{cases} \frac{\Gamma(\alpha_{solar}+\beta_{solar})}{\Gamma(\alpha_{solar})\times\Gamma(\beta_{solar})} \times {s_g}^{\alpha_{solar}-1} \times (1-s_g)^{\beta_{solar}-1}, 0 \le s_g \le 1 \\ 0, \qquad otherwise \end{cases} \tag{3-71}$$

$$P_{solar} = P_{solar}^{r} \cdot s_g \tag{3-72}$$

where μ_{solar} is the hourly average of forecasted irradiance, ${\sigma_{solar}}^2$ is the variance of solar irradiance obtained by historical data processing, $\beta_{solar} = (1-\mu_{solar})\left(\frac{\mu_{solar}(1+\mu_{solar})}{{\sigma_{solar}}^2} - 1\right)$, $\alpha_{solar} = \frac{\mu_{solar}\beta}{1-\mu_{solar}}$.

3) Load

The uncertainty of load is modeled by the normal distribution [39] in (3-73). And the actual load is decided by (3-74).

$$f_n(l) = \frac{1}{\sigma_l\sqrt{2\pi}} e^{-(1-\mu_l)^2/2{\sigma_l}^2} \tag{3-73}$$

$$S_{load} = (1+l)S_{load}^{f} \tag{3-74}$$

where S_{load}^{f} is the forecasted load, $\mu_l = 0$ and $\sigma_l = 0.5$ are used in our case study.

3.4.2 Comparison between different methods

The widely used deterministic DC-OTS [2] is shown in Table 3-1 as the benchmark, where the mean values of the load and renewable forecasts are used in the deterministic study. The DC-OTS is solved by the B&B algorithm and followed by an AC feasibility check.

Table 3-1: Numerical results for the deterministic DC-OTS

Scenarios	No. of switching	Switching plan	Expected DC cost	Expected AC cost	Time
3	1	NA	1184.8	4219.8	16s
5	1	Line 114	1253.0	3610.9	22s
10	1	Line 114	1745.6	7870.5	36s
15	1	Line 114	1640.1	6237.9	46s
20	1	Line 114	1607.3	6363.9	56s
30	1	Line 114	1582.4	6154.0	1m30s
50	1	Line 114	1658.3	6507.5	2m18s
5	2	Line 70,114	1253.0	3584.0	9m10s
5	3	Line 133,136,167	1253.0	3362.8	2h23m23s
10	2	Line 87,114	1722.4	7782.1	6m45s
10	3	Line 114,133,137	1698.9	7893.0	2h32m34s

The numerical results for the proposed stochastic optimization formulations for OTS problems are shown in Table 3-2 and Table 3-3. The results in Table 3-2 are gained by solving the stochastic AC-OTS directly in the deterministic equivalent form. And the results in Table 3-3 are gained by solving the stochastic DC-OTS using the L-shaped algorithm (maximum iterations=1000) and then conducting an AC feasibility check.

Table 3-1 and Table 3-3 show that the expected DC costs are usually lower than the expected AC costs due to the DC simplification. And switching solutions in the stochastic DC-OTS are similar to the results in the deterministic DC-OTS for single switching action, which finally leads to similar expected AC costs. However, the results in the stochastic DC-OTS and the deterministic DC-OTS are significantly different for multiple switching actions. In some multiple switching cases, the expected AC cost in the stochastic DC-OTS will have an extreme spike. As for the two stochastic methods, Table 3-2 and Table 3-3 show that the two proposed stochastic OTS methods will lead to different switching plans in all cases. The expected AC cost in the

stochastic AC-OTS is the lowest one among the three methods in most cases except for the cases with 10 and 15 scenarios when single switching is allowed. But the differences in these two cases are very small. Thus, the stochastic AC-OTS shows a superb performance in minimizing the expected AC cost over the other two methods. The reasons behind the discrepancies are the inherent assumptions of the DCOPF and the advantages of SP. The advantages of SP are already discussed in Section 3.1. As for the DCOPF, it ignores the voltage magnitude and the reactive power issues. The switching plans are calculated with the assumptions that the voltage magnitudes are fixed at 1 p.u. and line flows are calculated by linearized equations. Thus, despite the obtained switching plan is the global optimum in the deterministic or stochastic DC-OTS, it is not a global optimum when checked in the ACOPF and it is usually worse than the local optimum achieved by the stochastic AC-OTS. When the number of allowed switching increases, the DCOPF assumptions will be violated more, which results in a spike in the expected cost.

Table 3-2: Numerical results for the stochastic AC-OTS

Scenarios	No. of switching	Switching plan	Expected AC cost	Time
3	1	Line 104	3364.9	13s
5	1	Line 104	3086.8	17s
10	1	Line 116	8072.7	12m53s
15	1	Line 116	6397.4	22m38s
20	1	Line 116	6115.0	5m23s
30	1	Line 116	5759.5	11m20s
50	1	Line 116	6248.9	13m12s
5	2	Line 97,104	2873.7	34s
5	3	Line 97,101, 104	2727.0	41s
10	2	Line 87,116	7718.3	10m27s
10	3	Line 79, 87, 116	7241.5	15m8s

Table 3-3: Numerical results for the stochastic DC-OTS

Scenarios	No. of switching	Switching plan	Expected DC cost	Expected AC cost	Time
3	1	Line 114	1285.2	4105.6	2m44s
5	1	Line 113	1472.8	3285.9	3m46s
10	1	Line 114	4373.4	7870.5	6m8s
15	1	Line 114	3480.8	6237.9	9m
20	1	Line 114	3063.0	6363.9	15m13s
30	1	Line 114	2625.2	6154.0	15m2s
50	1	Line 114	2748.6	6507.5	25m39s
5	2	Line 2,113	1472.8	3593.9	38m17s
5	3	Line 3,113, 184	1472.7	10249.1	37m58s
10	2	Line 133,134	4448.0	8359.5	51m10s
10	3	Line 11,92, 114	4373.4	19276.1	57m53s

In Table 3-1-Table 3-3, the deterministic DC-OTS is generally faster than the two stochastic OTS approaches due to the simplicity, but sometimes it is much slower because of the fact that the B&B algorithm needs to enumerate all combinations to find the optimal solution in the worst case. As for the two stochastic methods, the stochastic AC-OTS is faster than the stochastic DC-OTS in most cases except for two cases. When the number of scenarios increases or multiple switching actions are allowed, the stochastic AC-OTS shows the great advantage in computation time over the DCOPF based stochastic method. For instance, 15 minutes and 8 seconds is needed for the case with 10 scenarios and 3 allowed switching actions in the stochastic AC-OTS, while the computation time increases to 57 minutes and 53 seconds in the stochastic DC-OTS. It is a counterintuitive observation that the simplified formulation is even slower, which also contradicts the previous deterministic OTS study [11]. The reason causing the counterintuitive results lies in the very basics of the B&B algorithm. In the stochastic DC-OTS (a convex MILP problem), the B&B algorithm will keep searching until the global optimum is reached. On the contrary, the B&B algorithm will stop at a local optimum with the gap tolerance is satisfied in the

stochastic AC-OTS (a nonconvex MINLP problem). The size of the problem will increase when the number of scenarios increases. And the possible combinations increase exponentially when more switching actions are allowed. In these situations, it is highly possible that finding the global optimum costs a much longer time in the stochastic DC-OTS when compared with finding a local optimum in the stochastic AC-OTS. And the obtained global optimum is not the true global optimum when checked in the ACOPF.

3.4.3 A detailed case study

The case with 5 scenarios and single allowed switching is shown here to compare the two proposed stochastic methods in detail. The generation difference in the solutions obtained by the stochastic AC-OTS and DC-OTS is shown in Table 3-4.

Table 3-4: Generation difference between the two stochastic OTS

	$s=1$	$s=2$	$s=3$	$s=4$	$s=5$	Cost ($/MW)
Gen. 6	1.1	0	0	3.9	0	1.0520
Gen. 19	0	-70.5	0	0	0	3.4480
Gen. 20	0	0	0.1	0	0	0.4670
Gen. 24	-15.2	0	0	-19.8	5.5	0.6060
Gen. 25	0	-379.5	0	0	-20.5	0.5880
Gen. 27	0	420.9	0	0	0	0.2493
Gen. 38	14.1	0	0	15.1	0	7.1420
Gen. 44	0	31.1	0	0	14.3	2.0000

The generation difference is in MW and the positive number means the calculated generation in the stochastic AC-OTS is higher. There is a major difference in the scenario 2, where

the cheap generator 27 can produce more power instead of the expensive generator 25 in the stochastic AC-OTS. In the scenario 1, 4 and 5, cheap generations could be utilized more in the stochastic DC-OTS, but the amount of difference is not significant. There is no real power load shedding for this hour in both stochastic OTS methods. The reactive power load shedding only appears in scenario 2. The stochastic AC-OTS will yield a solution with 38.4 MVAR load shedding while the value in the stochastic DC-OTS is 47.4 MVAR, which results in a higher penalty cost. Thus, the stochastic AC-OTS can lead to a lower expected cost since it can improve the utilization rate of cheap generations in some scenarios and reduce the involuntary load shedding effectively.

3.5 Summary

With the increasing penetration of renewable generations installed in the modern power systems, the grid uncertainties cannot be ignored when making decisions for OTS operations. In Section 3, the fundamentals of SP are introduced for decision-making. Two SP formulations for OTS problems are proposed and compared with the previous deterministic DC-OTS formulation. Numerical analysis of the three methods is performed on the IEEE-118 bus system. In most case studies, the stochastic AC-OTS achieves the lowest expected AC cost and is faster than the stochastic DC-OTS. A counterintuitive observation is found that the DC simplification does not always lead to a faster calculation in the stochastic OTS problems. The searching process for the global optimum in the B&B algorithm requires a long time and the obtained switching solution is often non-optimal when validated in the AC feasibility check.

4. STOCHASTIC OPTIMIZATION FOR OPTIMAL TRANSMISSION SWITCHING: A RELIABLE DECOMPOSITION APPROACH

In the last section, the basic modeling and numerical analysis of stochastic optimization are introduced for OTS problems. Although the stochastic optimization methods mentioned in the last section have many advantages, they have some drawbacks in terms of accuracy or scalability. In Section 4, a reliable decomposition approach for the stochastic AC-OTS is developed to obtain accurate results efficiently. A brief introduction is shown in the beginning of this section. The limitations of the existing SP methods and the advantages of the proposed approach are discussed. The mathematical formulations of the novel decomposition approach are illustrated next and followed by the proposed generalized Benders decomposition (GBD). Finally, numerical results on the IEEE RTS, the IEEE-118 bus system and the synthetic SouthCarolina500 system confirm the validity of the decomposition approach.

The symbols used in Section 4 are listed as follows.

Sets:

$s \in S$ Set of all scenarios

$g \in G$ Set of all conventional generators.

$r \in R$ Set of all renewable generators.

$b \in B$ Set of all buses.

$k \in L$ Set of all lines mn, where m is the "from" bus.

$\Omega_{g,b}$ Set of conventional generators connected to bus b

$\Omega_{r,b}$ Set of renewable generators connected to bus b

$\Omega_{m=b}$ Set of lines with one end connected to bus b.

S_{ca} Set of candidate lines in OTS

Parameters:

π_s Probability of scenario s.

c_g Linear generation cost of generator g.

$C_{shed}^{p}, C_{shed}^{q}$ Linear penalty cost of real and reactive load shedding.

V_b^{max}, V_b^{min} Max. and min. voltage of bus b.

P_g^{max}, P_g^{min} Max. and min. generation of generator g.

Q_g^{max}, Q_g^{min} Max. and min. reactive power of generator g.

$P_{r,s}^{max}$, $P_{r,s}^{min}$ Max. and min. generation of renewable generator r in scenario s.

$Q_{r,s}^{max}$, $Q_{r,s}^{min}$ Max. and min. reactive power of renewable generator r in scenario s.

t_{kmn} Transformer tap ratio of line k (from m to n). $t_{kmn} = 1$ for a non-transformer branch

$g_{kmn} + jb_{kmn}$ Admittance of line k (from m to n).

B_{kmn}^{shunt} Shunt capacitance of line k (from m to n).

c_{kmn} Binary index. $c_{kmn} = 1$ if m is the tap side of the transformer; $c_{kmn} = 0$ if n is the tap side or line k is a non-transformer branch.

S_{kmn}^{max} Thermal limit of line k (from m to n).

$G_b + jB_b$ Fixed shunt admittance of bus b.

$P_{b,s}^{load}, Q_{b,s}^{load}$ Real and reactive load of bus b in scenario s.

N Number of allowed switching actions.

M	Large number. $M = \max(S_{kmn}^{max})$.

Variables:

$P_{g,s}, Q_{g,s}$	Real power and reactive power generation of generator *g* in scenario *s*.
$P_{r,s}, Q_{r,s}$	Real power and reactive power of renewable generator *r* in scenario *s*.
$LSp_{b,s}, LSq_{b,s}$	Real and reactive load shedding at bus *b* in scenario *s*.
$V_{b,s}, \delta_{b,s}$	Voltage magnitude and angle of bus b in scenario *s*.
$P_{kmn,s}, Q_{kmn,s}$	Real and reactive power flow of line *k* through *m* to *n* in scenario *s*.
z_k	Binary variable of line status. 0 for in service, 1 for out of service.
$R_{g,s}^{up}, R_{g,s}^{down}$	Up and down regulation reserve of generator g in scenario s.
$R_{g,s}^{spin}$	Spinning reserve of generator g in scenario s.
$W_{mn,s}^{R}, W_{mn,s}^{I}$	The real part and imaginary part of term $V_{m,s}V_{n,s}^{*}$. $W_{mn,s}^{R} = W_{nm,s}^{R}, W_{mn,s}^{I} = -W_{nm,s}^{I}$.
$W_{b,s}$	$W_{b,s} = \lvert V_{b,s}\rvert^2$.

4.1 Introduction

4.1.1 The limitations of the existing stochastic OTS methods

In previous literature [19], a stochastic OTS method is proposed with the piece-wise linear power flow equations. In Section 3, the stochastic DC-OTS and AC-OTS are proposed to obtain the optimal switching plans. However, both of them have their own limitations in solving the OTS problem with uncertainties involved.

The stochastic DC-OTS developed in Section 3 and the stochastic OTS in [19] can be solved by the L-shaped algorithm, which is a scalable decomposition approach. However, the use of the DCOPF or the piece-wise linear power flow equations will sacrifice the accuracy of results.

The AC-OTS is proven to be more accurate [11]-[12]. It is due to the fact that the AC-OTS accounts for voltage and reactive power issues in the physical power system and thus yields a more realistic switching plan and the corresponding generation dispatch.

On the other hand, the AC-OTS is a nonconvex MINLP problem, which causes huge challenges in SP. SP problems can be formulated in the deterministic equivalent form and then solved directly. Usually, a large number of scenarios are needed to represent the uncertainties in SP problems. The drawback of using the deterministic equivalent is that the problem size will become extremely large when many scenarios are considered, which requires a large memory to store and in general makes an SP problem intractable. The L-shaped algorithm [46] based on the GBD [47] can overcome the aforementioned drawback by using the divide-and-conquer strategy. The GBD requires that the problem is convex when fixing the complicating variables [47]. Otherwise, the GBD may not converge [48]. Besides, the complicating variables and other variables should be separable so that the infimum functions in the optimality cut and the feasibility cut of the GBD can be calculated rather simply [47]. However, these two requirements are not satisfied by the existing formulations for the AC-OTS in [6], [11]-[12], and thus the GBD cannot be applied directly.

4.1.2 An overview of the proposed approach

In this section, a reliable decomposition approach, which includes a new two-stage SP formulation and a new GBD based algorithm, is proposed. This new approach is aimed to handle the stochastic AC-OTS problem efficiently. As discussed in Section 4.1.1, we have two technical issues to overcome for the stochastic AC-OTS:

1) **Scalability issue**: The aforementioned stochastic AC-OTS is solved directly in the B&B algorithm. When the number of scenarios increases, the problem size becomes very huge, which is very slow to solve.
2) **Memory issue**: When the number of scenarios is large, a large memory must be used to store data and results for the aforementioned stochastic AC-OTS. Sometimes, the required memory could be so large that is beyond the existing hardware.

The new approach has overcome those issues because the optimization problem is solved in a decomposed way using a master problem and subproblems, where Lagrange duality theory [49] is applied to gain information from subproblems in order to revise the master problem solution [46]-[47]. According to the weak duality theory [49], the dual problem actually gives the lower bound of the primal problem. Based on that, we can use Lagrange duality theory to generate the optimality cuts from the subproblems and use them in the master problem to revise the solution. The detailed description of the theory can be found in [46]-[47], [49] and the applications in our OTS study will be explained in Section 4.2.

In the new approach, different scenarios can be calculated separately. That is why the optimization problem can be solved fast and we do not need a large memory to store everything. An overall picture of the proposed method is shown in Figure 4-1.

As shown in Section 4.1.1, the GBD requires the separable condition and the convex condition [47] in mathematical perspective. In the new two-stage SP formulation, we satisfy the two mathematical requirements as follows:

1) **The separable condition**: It is satisfied by replacing the power flow equations by an equivalent form, where a big M is used. It will be shown in detail in Section 4.2.1.

2) **The convex condition:** It is satisfied by applying the SOC relaxation [54] to convexify the ACOPF as shown in Section 4.2.2.

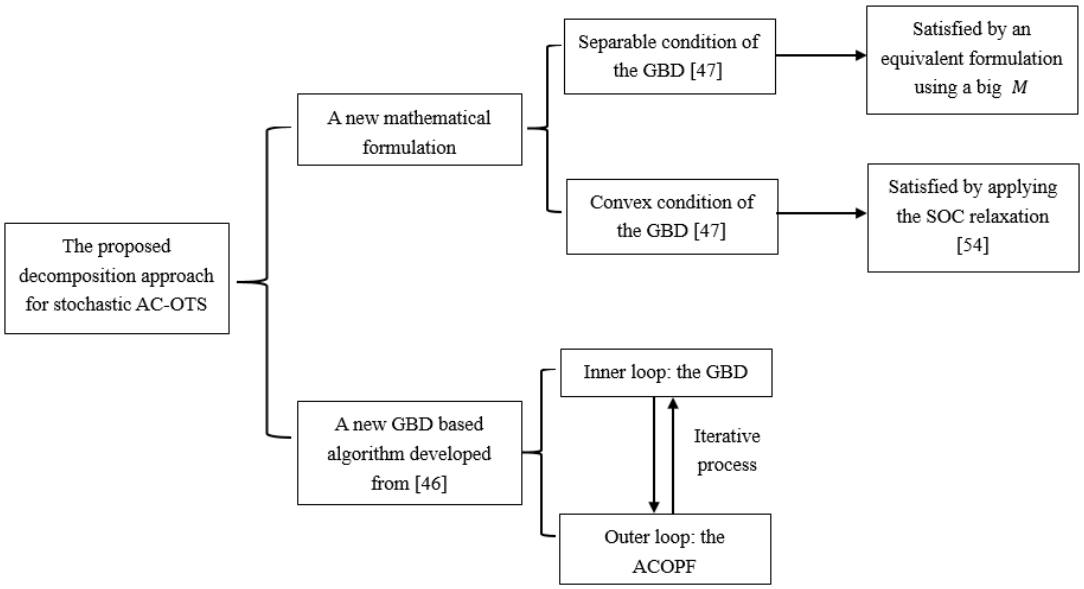

Figure 4-1: The overall picture of the proposed decomposition approach

The proposed GBD based algorithm is from [46], which will be shown in Section 4.3. Note that the proposed GBD based algorithm is a simplified form of its original version in [46]. This modification is to fit our optimization problem in OTS for a better efficiency. And this algorithm cannot deal with the original stochastic AC-OTS formulation in Section 3.2.1. A new SP formulation that satisfies the convex condition and the separable condition, as discussed above, is required. There are two loops in the proposed GBD based algorithm:

1) **Inner loop**: The GBD is used in the inner loop to calculate the candidate switching plans using the proposed stochastic AC-OTS formulation (Section 4.2.2). The convergence of the GBD is guaranteed.

2) **Outer loop**: The candidate switching plans will be validated in the outer loop in the ACOPF and decide whether it is necessary to go back to the inner loop.

Though this iterative process, the optimal switching plan will be obtained accurately and efficiently.

4.1.3 Contributions of this work

The main contributions are summarized as follows:

- In order to meet the rigorous mathematical requirements of the GBD, a novel SP formulation for the AC-OTS under uncertainties is first proposed, in which the complicating variables are separable from other variables. Based on the formulation, a new two-stage SP formulation is developed with a convex relaxation of the ACOPF constraints. The finite convergence of the GBD is guaranteed by using the proposed two-stage SP formulation.
- A GBD based algorithm is proposed to solve the SP problem of the AC-OTS under uncertainties. In the inner loop of the proposed algorithm, the GBD is used to solve the novel two-stage SP formulation, which can guarantee the finite convergence. And in the outer loop, the ACOPF is run to evaluate the obtained switching plans from the inner loop. The optimal switching plan and the expected system cost will be found in the iterative calculation without any sacrifice of accuracy.
- A comprehensive numerical study is conducted to evaluate the proposed decomposition approach for the AC-OTS under uncertainties. The proposed approach is compared with a series of existing methods, where the proposed method shows a good accuracy and scalability in solving the SP problems of the AC-OTS.

4.2 Novel SP formulations for AC-OTS under uncertainties

Since we want to take advantage of the GBD to solve the SP problem for the AC-OTS under uncertainties, we must keep in mind that the following two important requirements of the GBD [47]. A nonlinear SP problem is shown in (4-1)-(4-3).

$$\min \quad f(x, y_s) \tag{4-1}$$

$$\text{s.t.} \quad g_s(x, y_s) \leq 0, \quad \forall s \tag{4-2}$$

$$x \in X,\ y_s \in Y, \quad \forall s \tag{4-3}$$

Convex condition: the problem (4-1)-(4-3) is a convex problem when the complicating variable x is set at a fixed value.

Separable condition: the complicating variable x and other variables y_s are separable, which means (4-4) is satisfied.

$$f(x, y_s) = f_1(x) + f_2(y_s), \quad g_s(x, y_s) = g_{1,s}(x) + g_{2,s}(y_s) \tag{4-4}$$

With the two conditions satisfied, the finite convergence of the GBD is proven in [47]. And the infimum in the optimality cut and the feasibility cut can be computed efficiently [47].

The standard SP form for the AC-OTS is shown in section 3.2.1, which is derived from the previous deterministic AC-OTS studies. However, this nonconvex and non-separable form cannot be used in the GBD. In this section, a new separable SP formulation for the AC-OTS under uncertainties is proposed in the deterministic equivalent form. Based on the formulation, a novel separable two-stage SP form with a convex relaxation is developed.

4.2.1 The separable SP formulation for the AC-OTS problems

The separable SP formulation for the AC-OTS problems is proposed in (4-5)- (4-29). Note that the formulation is still nonconvex with the exact ACOPF used.

1) Objective function

The objective function (4-5) is to minimize the expected operational cost in the online operation, which is made up of the generation cost and the load shedding penalty cost.

$$\min \quad \sum_s \pi_s \begin{bmatrix} \sum_{g\in G} C_g P_{g,s} + \sum_{b\in B} C^p_{shed} LSp_{b,s} \\ + \sum_{b\in B} C^q_{shed} LSq_{b,s} \end{bmatrix} \tag{4-5}$$

2) Bus voltage constraints

Constraint (4-6) is the voltage magnitude constraint and (4-7) is the constraint for the maximum voltage angle difference.

$$V_b^{min} \le V_{b,s} \le V_b^{max}, \ \forall b, s \tag{4-6}$$

$$-\frac{\pi}{2} \le \delta_{m,s} - \delta_{n,s} \le \frac{\pi}{2}, \ \forall k, s \tag{4-7}$$

3) Generation constraints

Real and reactive power generation limits are shown in (4-8)-(4-9) for conventional generators. Constraints (4-10)-(4-11) present the real and reactive generation limits for renewable sources.

$$P_g^{min} + R_{g,s}^{down} \le P_{g,s} \le P_g^{max} - R_{g,s}^{up} - R_{g,s}^{spin}, \ \forall g, \ s \tag{4-8}$$

$$Q_g^{min} \le Q_{g,s} \le Q_g^{max}, \ \forall g, \ s \tag{4-9}$$

$$P_{r,s}^{min} \le P_{r,s} \le P_{r,s}^{max}, \ \forall r, \ s \tag{4-10}$$

$$Q_{r,s}^{min} \le Q_{r,s} \le Q_{r,s}^{max}, \ \forall r, \ s \tag{4-11}$$

4) Line switching constraints

Line status is modeled as a binary variable in (4-12). And the number of allowed switching actions is shown in (4-13). In OTS problems, it is usual to consider a subset of transmission lines as the candidate set instead of all lines considering computational efficiency [12], past operating

experience [50] and safety reasons [51]. In our model, binary variables are only defined for the lines in the candidate set S_{ca}. The reduced number of binary variables will accelerate the computation in the numerical study.

$$z_k \in \{0,1\}, \qquad \forall k \in S_{ca} \tag{4-12}$$

$$\sum_{k\in S_{ca}} z_k \le N \tag{4-13}$$

5) Line flow calculations

The line flow calculations for the lines in the candidate set S_{ca} are shown in (4-14)-(4-17), where transformer branches are considered by using a binary index c_{kmn}. A big M is used to ensure the bus voltages will not be constrained by (4-14)-(4-17), when a line is switched off. (4-18)-(4-19) show the line flow calculations for the lines that are not in the candidate set.

$$P_{kmn,s} \ge -\frac{1}{t_{kmn}}\left(g_{kmn}\Re\{V_{m,s}V_{n,s}^*\} + b_{kmn}\Im\{V_{m,s}V_{n,s}^*\}\right) + |V_{m,s}|^2 g_{kmn}(1-c_{kmn})$$
$$+|V_{m,s}|^2\left(\frac{g_{kmn}}{t_{kmn}^2}\right)c_{kmn} - z_k * M, \quad \forall s, \forall k \in S_{ca} \tag{4-14}$$

$$P_{kmn,s} \le -\frac{1}{t_{kmn}}\left(g_{kmn}\Re\{V_{m,s}V_{n,s}^*\} + b_{kmn}\Im\{V_{m,s}V_{n,s}^*\}\right) + |V_{m,s}|^2 g_{kmn}(1-c_{kmn})$$
$$+|V_{m,s}|^2\left(\frac{g_{kmn}}{t_{kmn}^2}\right)c_{kmn} + z_k * M, \quad \forall s, \forall k \in S_{ca} \tag{4-15}$$

$$Q_{kmn,s} \ge -\frac{1}{t_{kmn}}\left(g_{kmn}\Im\{V_{m,s}V_{n,s}^*\} - b_{kmn}\Re\{V_{m,s}V_{n,s}^*\}\right)$$
$$-|V_{m,s}|^2\left(b_{kmn} + \frac{B_{kmn}^{shunt}}{2}\right)(1-c_{kmn})$$
$$-|V_{m,s}|^2\left(\frac{b_{kmn}}{t_{kmn}^2} + \frac{B_{kmn}^{shunt}}{2}\right)c_{kmn} - z_k * M, \quad \forall s, \forall k \in S_{ca} \tag{4-16}$$

$$Q_{kmn,s} \le -\frac{1}{t_{kmn}}\left(g_{kmn}\Im\{V_{m,s}V_{n,s}^*\} - b_{kmn}\Re\{V_{m,s}V_{n,s}^*\}\right)$$
$$-|V_{m,s}|^2\left(b_{kmn} + \frac{B_{kmn}^{shunt}}{2}\right)(1-c_{kmn})$$

$$-\left|V_{m,s}\right|^2\left(\frac{b_{kmn}}{t_{kmn}^2}+\frac{B_{kmn}^{shunt}}{2}\right)c_{kmn}+z_k*M,\ \forall s,\forall k\in S_{ca} \tag{4-17}$$

$$\begin{aligned}P_{kmn,s}=&-\frac{1}{t_{kmn}}\left(g_{kmn}\Re\left\{V_{m,s}V_{n,s}^*\right\}+b_{kmn}\Im\left\{V_{m,s}V_{n,s}^*\right\}\right)\\&+\left|V_{m,s}\right|^2g_{kmn}(1-c_{kmn})\\&+|V_{m,s}|^2\left(\frac{g_{kmn}}{t_{kmn}^2}\right)c_{kmn},\ \ \forall s,\forall k\notin S_{ca}\end{aligned} \tag{4-18}$$

$$\begin{aligned}Q_{kmn,s}=&-\frac{1}{t_{kmn}}\left(g_{kmn}\Im\left\{V_{m,s}V_{n,s}^*\right\}-b_{kmn}\Re\left\{V_{m,s}V_{n,s}^*\right\}\right)\\&-|V_{m,s}|^2\left(b_{kmn}+\frac{B_{kmn}^{shunt}}{2}\right)(1-c_{kmn})\\&-\left|V_{m,s}\right|^2\left(\frac{b_{kmn}}{t_{kmn}^2}+\frac{B_{kmn}^{shunt}}{2}\right)c_{kmn}\ ,\ \forall s,\forall k\notin S_{ca}\end{aligned} \tag{4-19}$$

where $\Re$, $\Im$ stand for the real and imaginary part of the complex number.

6) Line flow constraints

The line flow limits are shown in (4-20). When a line in the candidate set S_{ca} is in service ($z_k=0$), the line flow is constrained by (4-20). When a line in the candidate set is out of service ($z_k=1$), constraints (4-21)-(4-22) will force the line flow to be zero.

$$\left(P_{kmn,s}\right)^2+\left(Q_{kmn,s}\right)^2\le(S_{kmn}^{max})^2,\quad \forall k,\ s \tag{4-20}$$

$$-(1-z_k)S_{kmn}^{max}\le P_{kmn,s}\le(1-z_k)S_{kmn}^{max},\forall s,\forall k\in S_{ca} \tag{4-21}$$

$$-(1-z_k)S_{kmn}^{max}\le Q_{kmn,s}\le(1-z_k)S_{kmn}^{max},\forall s,\forall k\in S_{ca} \tag{4-22}$$

7) Power balance constraints

Constraints (4-23)-(4-24) represent the power balance equations, which include the conventional generation, the renewable generation and the load shedding.

$$\sum_{g\in\Omega_{g,b}}P_{g,s}+\sum_{r\in\Omega_{r,b}}P_{r,s}=\sum_{k\in\Omega_{m=b}}P_{kbn,s}+\left(P_{b,s}^{load}-LSp_{b,s}\right)+V_{b,s}^2G_b,\ \forall b,\ s \tag{4-23}$$

$$\sum_{g\in\Omega_{g,b}} Q_{g,s} + \sum_{r\in\Omega_{r,b}} Q_{r,s} = \sum_{k\in\Omega_{m=b}} Q_{kbn,s} + \left(Q_{b,s}^{load} - LSq_{b,s}\right) - V_{b,s}^2 B_b,\ \forall b,\ s \quad (4\text{-}24)$$

8) Load shedding constraints

Load shedding limits are shown in (4-25) and (4-26). Here we take the same assumption that real and reactive load could be shed independently [52].

$$0 \le LSp_{b,s} \le P_{b,s}^{load}, \quad \forall b,\ s \quad (4\text{-}25)$$

$$0 \le LSq_{b,s} \le Q_{b,s}^{load}, \quad \forall b,\ s \quad (4\text{-}26)$$

9) Reserve constraints

The system-wide regulation and spinning reserve are shown in (4-27)-(4-29). The up/down regulation reserve is set to be 2% of the total load by constraints (4-27)-(4-28). And in (4-29), the total spinning reserve is required to be sufficient for any generator loss in a single contingency.

$$\sum_g R_{g,s}^{up} \ge 0.02 \sum_b P_{b,s}^{load}, \quad \forall s \quad (4\text{-}27)$$

$$\sum_g R_{g,s}^{down} \ge 0.02 \sum_b P_{b,s}^{load}, \quad \forall s \quad (4\text{-}28)$$

$$\sum_g R_{g,s}^{spin} \ge P_{g,s} + R_{g,s}^{spin}, \quad \forall g,\ s \quad (4\text{-}29)$$

4.2.2 The proposed two-stage SP formulation

Based on the SP formulation in section 4.2.1, a novel separable SP formulation with a convex relaxation is developed following the standard two-stage formulation [46], [53].

1) Subproblems (convex NLP)

Using a fixed network topology $z_k^{(j)}$ obtained from the master problem, we consider the subproblems that associate all scenarios for the topology, which naturally decompose the complicated problem into subproblems that can be calculated separately. The subproblem for scenario s is shown in (4-30)-(4-53). All variables are with a superscription (j) for the Benders' iteration. The objective function (4-30) is to minimize the sum of the generation adjustment cost,

the real load shedding adjustment cost and the reactive load shedding cost. The superscript SC stands for the scheduled value calculated from the master problem. The second-order cone relaxation [54] with a tight relaxation gap is applied to convexify the ACOPF equations as shown in (4-43)-(4-53). The original ACOPF is nonconvex because of the existence of the cosine and sine functions in $\Re\left\{V_{m,s}^{(j)}V_{n,s}^{*(j)}\right\}$ and $\Im\left\{V_{m,s}^{(j)}V_{n,s}^{*(j)}\right\}$ terms and the nonlinear term $|V_{b,s}^{(j)}|^2$. Here we use new variables $W_{mn,s}^{R(j)}$, $W_{mn,s}^{I(j)}$ and $W_{b,s}^{(j)}$ to replace $\Re\left\{V_{m,s}^{(j)}V_{n,s}^{*(j)}\right\}$, $\Im\left\{V_{m,s}^{(j)}V_{n,s}^{*(j)}\right\}$ and $|V_{b,s}^{(j)}|^2$ respectively and change related constraints accordingly. Thus, the ACOPF is convexified. And other equations are the same as in Section 4.2.1. The subproblem is a convex NLP problem with a fixed network topology. It should be pointed out that the subproblem is infeasible only when the sum of minimum generations is greater than the system load. However, this situation will not happen in any real power system (the sum of minimum generations is usually far smaller than the system load). Therefore, the subproblem is always feasible [43].

$$\min\ Obj_s^{(j)} = \sum_{g\in G} C_g\left(P_{g,s}^{(j)} - P_g^{SC(j)}\right) + \sum_{b\in B} C_{shed}^{p}\left(LSp_{b,s}^{(j)} - LSp_b^{SC(j)}\right) + \sum_{b\in B} C_{shed}^{q} LSq_b^{(j)} \tag{4-30}$$

s.t.

$$P_g^{min} + R_{g,s}^{down(j)} \le P_{g,s}^{(j)} \le P_g^{max} - R_{g,s}^{up(j)} - R_{g,s}^{spin(j)},\ \forall g,\ s \tag{4-31}$$

$$Q_g^{min} \le Q_{g,s}^{(j)} \le Q_g^{max},\ \forall g,\ s \tag{4-32}$$

$$P_{r,s}^{min} \le P_{r,s}^{(j)} \le P_{r,s}^{max},\ \forall r,\ s \tag{4-33}$$

$$Q_{r,s}^{min} \le Q_{r,s}^{(j)} \le Q_{r,s}^{max},\ \forall r,\ s \tag{4-34}$$

$$\left(P_{kmn,s}^{(j)}\right)^2 + \left(Q_{kmn,s}^{(j)}\right)^2 \le (S_{kmn}^{max})^2,\quad \forall k,\ s \tag{4-35}$$

$$-\left(1 - z_k^{(j)}\right)S_{kmn}^{max} \le P_{kmn,s}^{(j)} \le \left(1 - z_k^{(j)}\right)S_{kmn}^{max},\ \forall s, \forall k \in S_{ca} \tag{4-36}$$

$$-\left(1-z_k^{(j)}\right)S_{kmn}^{max} \le Q_{kmn,s}^{(j)} \le \left(1-z_k^{(j)}\right)S_{kmn}^{max}, \forall s, \forall k \in S_{ca} \quad (4\text{-}37)$$

$$0 \le LSp_{b,s}^{(j)} \le P_{b,s}^{load}, \quad \forall b, s \quad (4\text{-}38)$$

$$0 \le LSq_{b,s}^{(j)} \le Q_{b,s}^{load}, \quad \forall b, s \quad (4\text{-}39)$$

$$\sum_g R_{g,s}^{up(j)} \ge 0.02 \sum_b P_{b,s}^{load}, \quad \forall s \quad (4\text{-}40)$$

$$\sum_g R_{g,s}^{down(j)} \ge 0.02 \sum_b P_{b,s}^{load}, \quad \forall s \quad (4\text{-}41)$$

$$\sum_g R_{g,s}^{spin(j)} \ge P_{g,s}^{(j)} + R_{g,s}^{spin(j)}, \quad \forall g, s \quad (4\text{-}42)$$

$$P_{kmn,s}^{(j)} \ge -\frac{1}{t_{kmn}}\left(g_{kmn}W_{mn,s}^{R(j)} + b_{kmn}W_{mn,s}^{I(j)}\right) + W_{m,s}^{(j)}g_{kmn}(1-c_{kmn})$$

$$+W_{m,s}^{(j)}\left(\frac{g_{kmn}}{t_{kmn}^2}\right)c_{kmn} - z_k^{(j)} * M, \forall s, \forall k \in S_{ca} \quad (4\text{-}43)$$

$$P_{kmn,s}^{(j)} \le -\frac{1}{t_{kmn}}\left(g_{kmn}W_{mn,s}^{R(j)} + b_{kmn}W_{mn,s}^{I(j)}\right) + W_{m,s}^{(j)}g_{kmn}(1-c_{kmn})$$

$$+W_{m,s}^{(j)}\left(\frac{g_{kmn}}{t_{kmn}^2}\right)c_{kmn} + z_k^{(j)} * M, \forall s, \forall k \in S_{ca} \quad (4\text{-}44)$$

$$Q_{kmn,s}^{(j)} \ge -\frac{1}{t_{kmn}}\left(g_{kmn}W_{mn,s}^{I(j)} - b_{kmn}W_{mn,s}^{R(j)}\right) - W_{m,s}^{(j)}\left(b_{kmn} + \frac{B_{kmn}^{shunt}}{2}\right)(1-c_{kmn})$$

$$-W_{m,s}^{(j)}\left(\frac{b_{kmn}}{t_{kmn}^2} + \frac{B_{kmn}^{shunt}}{2}\right)c_{kmn} - z_k^{(j)} * M\,, \forall s, \forall k \in S_{ca} \quad (4\text{-}45)$$

$$Q_{kmn,s}^{(j)} \le -\frac{1}{t_{kmn}}\left(g_{kmn}W_{mn,s}^{I(j)} - b_{kmn}W_{mn,s}^{R(j)}\right) - W_{m,s}^{(j)}\left(b_{kmn} + \frac{B_{kmn}^{shunt}}{2}\right)(1-c_{kmn})$$

$$-W_{m,s}^{(j)}\left(\frac{b_{kmn}}{t_{kmn}^2} + \frac{B_{kmn}^{shunt}}{2}\right)c_{kmn} + z_k^{(j)} * M\,, \forall s, \forall k \in S_{ca} \quad (4\text{-}46)$$

$$P_{kmn,s}^{(j)} = -\frac{1}{t_{kmn}}\left(g_{kmn}W_{mn,s}^{R(j)} + b_{kmn}W_{mn,s}^{I(j)}\right) + W_{m,s}^{(j)}g_{kmn}(1-c_{kmn})$$

$$+W_{m,s}^{(j)}\left(\frac{g_{kmn}}{t_{kmn}^2}\right)c_{kmn}, \forall s, \forall k \notin S_{ca} \quad (4\text{-}47)$$

$$Q_{kmn,s}^{(j)} = -\frac{1}{t_{kmn}}\left(g_{kmn}W_{mn,s}^{I(j)} - b_{kmn}W_{mn,s}^{R(j)}\right) - W_{m,s}^{(j)}\left(b_{kmn} + \frac{B_{kmn}^{shunt}}{2}\right)(1-c_{kmn})$$

$$-W_{m,s}^{(j)}\left(\frac{b_{kmn}}{t_{kmn}^2}+\frac{B_{kmn}^{shunt}}{2}\right)c_{kmn}\ ,\forall s,\forall k\notin S_{ca} \tag{4-48}$$

$$\sum_{g\in\Omega_{g,b}}P_{g,s}^{(j)}+\sum_{r\in\Omega_{r,b}}P_{r,s}^{(j)}=\sum_{k\in\Omega_{m=b}}P_{kmn,s}^{(j)}+\left(P_{b,s}^{load}-LSp_{b,s}^{(j)}\right)+W_{b,s}^{(j)}G_b\quad\forall b,s \tag{4-49}$$

$$\sum_{g\in\Omega_{g,b}}Q_{g,s}^{(j)}+\sum_{r\in\Omega_{r,b}}Q_{r,s}^{(j)}=\sum_{k\in\Omega_{m=b}}Q_{kmn,s}^{(j)}+\left(Q_{b,s}^{load}-LSq_{b,s}^{(j)}\right)-W_{b,s}^{(j)}B_b,\ \forall b,s \tag{4-50}$$

$$W_{mn,s}^{R(j)}\tan(\delta_{min})\le W_{mn,s}^{I(j)}\le W_{mn,s}^{R(j)}\tan(\delta_{max})\ ,\ \forall k,s \tag{4-51}$$

$$(V_b^{min})^2\le W_{b,s}^{(j)}\le(V_b^{max})^2,\qquad\forall b,s \tag{4-52}$$

$$(W_{mn,s}^{R(j)})^2+(W_{mn,s}^{I(j)})^2\le W_{m,s}^{(j)}W_{n,s}^{(j)},\qquad\forall k,\ s \tag{4-53}$$

where $\delta_{min}=-\frac{\pi}{2}$, $\delta_{max}=\frac{\pi}{2}$.

2) Master problem (MILP)

The master problem (4-54)-(4-69) is a MILP problem. A DC-OTS is adopted to help the master problem find good switching plans and accelerate the GBD. Please note that the use of the DC-OTS will not affect the accuracy of the AC-OTS problem with uncertainties since the obtained switching plans will be validated in the ACOPF, as explained in the coming Section 4.3.

The decision variables of the master problem are:

$$x=\{\eta^{(j)},z_k^{(j)},\ P_g^{SC(j)},\ LSp_b^{SC(j)},P_r^{SC(j)},P_{kmn}^{SC(j)},\delta_m^{SC(j)}\}$$

where $\eta^{(j)}$ represents the expected recourse cost in the subproblems. The system topology $z_k^{(j)}$ is the key variable since $z_k^{(j)}$ will be fixed in the subproblems. The variables $P_g^{SC(j)}$, $LSp_b^{SC(j)}$, $P_r^{SC(j)}$, $P_{kmn}^{SC(j)}$, $\delta_m^{SC(j)}$ are only used to accelerate the GBD and their values will not affect the total system cost in the two-stage SP problem when we combine (4-54) and (4-30), as shown in (4-72) in the coming Section 4.3.

Note that the focus of the master problem is to find good switching plans $z_k^{(j)}$. The objective (4-54) is to minimize the sum of the scheduled generation cost, the scheduled real load shedding cost and the expected recourse cost in the subproblems. The mean forecasted loads ($\overline{P_{b,s}^{load}}$) and renewable generations ($\overline{P_{r,s}^{min}}, \overline{P_{r,s}^{max}}$) are used in a DC-OTS as shown in (4-55)-(4-66). Equation (4-67) is the optimality cut. The feasibility cut is not needed since the subproblem is always feasible as mentioned. And (4-68) imposes a lower bound on $\eta^{(j)}$ to accelerate the convergence. A canonical cut (4-69) is added to avoid repeated binary combinations for transmission lines.

$$\min MP^{(j)} = \sum_{g\in G} C_g P_g^{SC(j)} + \sum_{b\in B} C_{shed}^{p} LSp_b^{SC(j)} + \eta^{(j)} \quad (4\text{-}54)$$

s.t.
$$P_g^{min} \le P_g^{SC(j)} \le P_g^{max}, \ \forall g \quad (4\text{-}55)$$

$$\overline{P_{r,s}^{min}} \le P_r^{SC} \le \overline{P_{r,s}^{max}}, \ \forall r \quad (4\text{-}56)$$

$$-(1 - z_k^{(j)})S_{kmn}^{max} \le P_{kmn}^{SC(j)} \le (1 - z_k^{(j)})S_{kmn}^{max}, \ \forall k \in S_{ca} \quad (4\text{-}57)$$

$$-S_{kmn}^{max} \le P_{kmn}^{SC(j)} \le S_{kmn}^{max}, \ \forall k \notin S_{ca} \quad (4\text{-}58)$$

$$b_{kmn}\left(\delta_m^{SC(j)} - \delta_n^{SC(j)}\right) - P_{kmn}^{SC(j)} + \left(z_k^{(j)}\right)M \ge 0, \forall k \in S_{ca} \quad (4\text{-}59)$$

$$b_{kmn}\left(\delta_m^{SC(j)} - \delta_n^{SC(j)}\right) - P_{kmn}^{SC(j)} - \left(z_k^{(j)}\right)M \le 0, \forall k \in S_{ca} \quad (4\text{-}60)$$

$$P_{kmn}^{SC(j)} = b_{kmn}\left(\delta_m^{SC(j)} - \delta_n^{SC(j)}\right), \forall k \notin S_{ca} \quad (4\text{-}61)$$

$$\sum_{g\in\Omega_{g,b}} P_g^{SC(j)} + \sum_{r\in\Omega_{r,b}} P_r^{SC(j)} = \sum_{k\in\Omega_{m=b}} P_{kbn}^{SC(j)} + \left(\overline{P_{b,s}^{load}} - LSp_b^{SC(j)}\right) + G_b \quad \forall b \quad (4\text{-}62)$$

$$0 \le LSp_b^{SC(j)} \le \overline{P_b^{load}}, \quad \forall b \quad (4\text{-}63)$$

$$-\frac{\pi}{2} \le \delta_m^{SC(j)} - \delta_n^{SC(j)} \le \frac{\pi}{2}, \ \forall k \quad (4\text{-}64)$$

$$z_k^{(j)} \in \{0,1\}, \quad \forall k \in S_{ca} \quad (4\text{-}65)$$

$$\sum_{k\in S_{ca}} z_k^{(j)} \le N \quad (4\text{-}66)$$

$$\eta^{(j)} \geq Obj^{(v)} + \sum_{k\in S_{ca}} \left\{ \sum_{t=1}^{4} \left(\lambda_{t,k}^{(v)} S_{kmn}^{max} \left(z_k^{(j)} - z_k^{(v)} \right) \right) \right\}$$

$$+ \sum_{k\in S_{ca}} \left\{ \sum_{t=1}^{4} \left(\mu_{t,k}^{(v)} M \left(z_k^{(j)} - z_k^{(v)} \right) \right) \right\}, \ \forall v \tag{4-67}$$

$$\eta^{(j)} \geq \eta_{min} \tag{4-68}$$

$$\sum_{k\in S^{(v)}} z_k^{(j)} - \sum_{k\notin S^{(v)}} z_k^{(j)} \leq \left| S^{(v)} \right| - 1, \ \forall v \tag{4-69}$$

where $Obj^{(v)} = \sum_s \pi_s Obj_s^{(v)}$, equations (4-70)-(4-71) are used to calculate $\lambda_{t,k}^{(v)}$ and $\mu_{t,k}^{(v)}$, $S^{(v)} = \{k | z_k^{(v)} = 1\}, v = 1, \dots j-1$.

$$\lambda_{t,k}^{(v)} = \sum_s \pi_s \lambda_{t,k,s}^{(v)}, \quad t = 1,2,3,4 \tag{4-70}$$

$$\mu_{t,k}^{(v)} = \sum_s \pi_s \mu_{t,k,s}^{(v)}, \quad t = 1,2,3,4 \tag{4-71}$$

where $\lambda_{t,k,s}^{(v)}$ are the duals of constraints (4-36)-(4-37) in the subproblem s and $\mu_{t,k,s}^{(v)}$ are the duals of relaxed form of constraints (4-43)-(4-46) in the subproblem s.

4.3 The proposed solution strategy

In Section 4.2, a novel two-stage SP formulation is proposed and can be solved in the GBD. However, the solution to the two-stage SP problem is an approximated solution since the convex relaxation is applied. The obtained switching plans should be validated in the original ACOPF. Accordingly, a general GBD based algorithm [46] with an inner loop and an outer loop is proposed as follows to solve the SP problem of the AC-OTS under uncertainties. The flowchart is shown in Figure 4-2.

In the inner loop, the proposed two-stage SP formulation, which includes both the master problem and the subproblems, is solved in the GBD to get a beneficial switching plan. Please note that the switching plan is calculated in the convexified ACOPF as shown in the subproblems (convex NLP). As shown in Section 4.2.2, the SOC relaxation [16], [54] is used to make the

subproblems convex. A series of new variables are used to replace the voltage related terms in the subproblems and the voltage related constraint (4-53) is relaxed with an inequality sign instead of an equality sign. So, the relaxed power flow equations may lead to a solution which has different voltage magnitude when compared with the original ACOPF. As a result, the calculated switching plan may not be the best solution for the actual system due to the convexification. Therefore, this beneficial switching plan must be checked again in the outer loop using the ACOPF (nonconvex NLP).

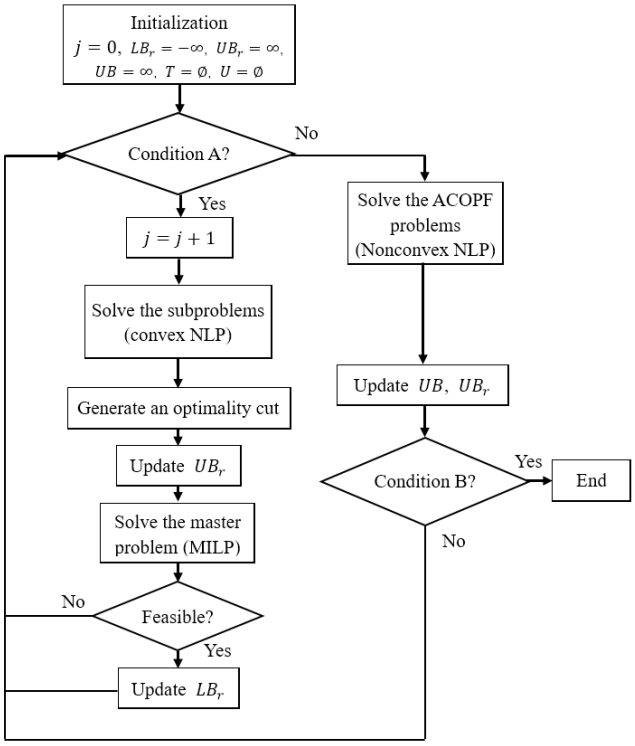

Figure 4-2: Flowchart of the proposed algorithm

In the outer loop, the ACOPF is run with the fixed system topology to calculate the actual generation dispatch and the associated cost of the system. It is to validate if the obtained switching

plan is the optimal solution and whether we need to go back to the inner loop to further improve the switching plan. If the switching plan is not the optimal one, we need to keep a record of this switching plan and exclude it from the following calculation in the inner loop. Through the iterative process in the inner loop and the outer loop, the optimal switching plan will be found with guaranteed convergence and no sacrifice on accuracy. Apparently, this new algorithm is better than the previous DC-OTS methods in [3], [6], [18] because we keep checking the switching plan and improving it iteratively instead of a single DC-OTS calculation followed by the AC validation.

Note that the proposed algorithm is a scenario-based decomposition method, where the subproblems for different scenarios can be computed separately in either a sequential or a parallel/distributed computing. The memory required is much less than it in solving an SP problem in the deterministic equivalent form. Thus, the proposed decomposition approach can deal with a large number of scenarios in the SP problems of the AC-OTS. The detailed procedures of the proposed algorithm are shown in the following steps:

Step 1) Set $j = 0$, $LB_r = -\infty$, $UB_r = \infty$, $UB = \infty$, $T = \emptyset$, $U = \emptyset$ and start with all lines in service $z_k^{(1)} = 0$.

Step 2) Check if Condition A is satisfied. If yes, set $j = j + 1$ and go to **Step 2)**. Otherwise, go to **Step 5)**

Condition A: $j = 0$, or (the master problem in (j) iteration is feasible and $LB_r < UB_r$ and $LB_r < UB$)

Step 3) Solve the decomposed subproblems with the fixed system topology $z_k^{(j)}$. Set $T = T \cup \{j\}$. Generate the optimality cut for iteration j as shown in (4-67). Calculate the $TC^{(j)}$ as

shown in (4-72). If $TC^{(j)} < UB_r$, update the $UB_r = TC^{(j)}$ and record the incumbent switching plan by $j^* = j$, $z_k^* = z_k^{(j)}$.

$$TC^{(j)} = \sum_s \pi_s \left[\sum_{g \in G} C_g P_{g,s}^{(j)} + \sum_{b \in B} C_{shed}^{p} LSp_{b,s}^{(j)} + \sum_{b \in B} C_{shed}^{q} LSq_{b,s}^{(j)} \right] \quad (4\text{-}72)$$

Step 4) Solve the master problem. If it is feasible, update LB_r by (4-73), set $z_k^{(j+1)}$ to the z_k value at the solution of the master problem and go to **Step 2)**. Otherwise, go to **Step 2)** without updating LB_r.

$$LB_r = \max \left(LB_r, MP^{(j)} \right) \quad (4\text{-}73)$$

Step 5) Run the ACOPF with the obtained beneficial switching plan z_k^* for all scenarios to get the expected system operational cost $\overline{Cost}_{AC}$. Set $U = U \cup \{j^*\}$.

Step 6) If $\overline{Cost}_{AC} < UB$, set $UB = \overline{Cost}_{AC}$ and update optimal switching plan $z_k^{opt} = z_k^*$ and the associated generation dispatch $P_{g,s}^{opt}$, $P_{r,s}^{opt}$. If $T \setminus U = \emptyset$, set $UB = +\infty$. If not, pick $i \in T \setminus U$ so that $TC^{(i)} = \min_{j \in T \setminus U}(TC^{(j)})$. Update $UB_r = TC^{(i)}$, $j^* = i$, $z_k^* = z_k^{(i)}$.

Step 7) Check if Condition B is satisfied. If yes, the optimal switching plan is found and stop the calculation. The final solution is $\{z_k^{opt}, P_{g,s}^{opt}, P_{r,s}^{opt}\}$ and the expected system cost is shown by UB. Otherwise, go to **Step 2)**.

Condition B: $UB_r \geq UB$ and (the master problem in (j) iteration is infeasible or $LB_r \geq UB$)

4.4 Numerical results

The numerical study is conducted on the IEEE RTS, the IEEE-118 bus system and the synthetic SouthCarolina500 system [55] to demonstrate the proposed decomposition approach. GAMS software is used to solve the optimization problems. MINLP problems are solved by BONMIN with a 0 relative gap. LP and MILP problems are solved by CPLEX and NLP problems

are solved by CONOPT. The reasons for selecting the aforementioned solvers are already explained in Section 3.4. A desktop with Intel I7-4770 3.4GHz CPU and 16GB memory is used for computation.

4.4.1 Creating scenarios for testing

Different scenarios, including different values of loads and renewable generations, are created randomly. And each scenario is assigned with equal probability. For example, when 100 scenarios are used, each scenario has a probability of 0.01 and when 20 scenarios are used, each scenario has a probability of 0.05.

4.4.2 Methods used for comparison in the numerical study

The proposed decomposition approach (**Method 7)** is compared with the following 7 other relevant methods (**Method 0-Method 6)** to demonstrate the merits of the new method. These 7 methods are either from previous literature or developed in this dissertation. They all have their unique features so that they are compared here with our new approach.

Method 0: The stochastic ACOPF without OTS. This the traditional method and can serve as the benchmark.

Method 1: The deterministic DC-OTS [6], [11] with mean values of loads and renewable generations used.

Method 2: The deterministic AC-OTS (Section 2.1.2) with mean values of loads and renewable generations used.

Method 3: The SP formulation for the DC-OTS under uncertainties (Section 3.2.2) and solved directly in the B&B algorithm.

Method 4: The SP formulation for the AC-OTS under uncertainties (Section 3.2.1) and solved directly in the B&B algorithm.

Method 5: The proposed separable SP formulation (Section 4.2.1) for the AC-OTS problem and solved directly in the B&B algorithm.

Method 6: The SP formulation for the DC-OTS problem (Section 3.2.2) and solved in the L-shaped decomposition algorithm (Section 3.3.2).

Method 7: The SP formulation for the AC-OTS problem and solved in the proposed decomposition approach.

The features of the aforementioned methods are summarized here. **Method 0** is a basic stochastic ACOPF without OTS. This is a traditional method to consider grid uncertainties in power system operation. It serves as the benchmark in our case study. **Method 1** is the deterministic DC-OTS developed in [6], [11]. This method is the most popular one in the OTS studies. **Method 2,** which is similar to [16], is the deterministic AC-OTS developed in Section 2.1.2 of this dissertation. It can consider the voltage and reactive power issues in OTS in the deterministic formulation. **Method 3** is the SP formulation for the DC-OTS developed in Section 3.2.2. It can consider grid uncertainties in the SP for OTS problems in linearized power flow equations. **Method 4** is the SP formulation for the AC-OTS, which is developed in Section 3.2.1. It shows a great improvement when compared with DC-OTS approaches. **Method 5** is the proposed separable SP formulation in Section 4.2.1. It only satisfies the separable condition of the GBD and does not satisfy the convex condition. This formulation is actually an intermediate formulation along the way to develop the **Method 7**. Note that this separable form is also carried out to **Method 7**. And **Method 5** is equivalent to **Method 4** in the mathematical sense but with a different formulation. As we test before in GAMS using the same solver, a different formulation may lead to a different performance in terms of speed and accuracy. That is why we also list it here to evaluate its performance for comparison. **Method 6** is the SP formulation for the DC-OTS

problem in Section 3.2.2. This formulation satisfies the separable condition and the convex condition because the DCOPF is used and thus it is a MILP problem. It is solved in the L-shaped decomposition method instead of the B&B algorithm in **Method 3**. The L-shaped algorithm is based on the Benders decomposition as shown in Section 3.3.2. This is a decomposition method used in [18] for stochastic OTS instead of solving the SP problem directly in the B&B algorithm. **Method 6** is a scalable method that can deal with a large number of scenarios. However, the DCOPF is used to satisfy the separable condition and the convex condition, which may affect the accuracy of the result. Thus, it is meaningful to compare this decomposition method with the proposed method to show whether the new method is indeed better. **Method 7** is our newly proposed decomposition method, which is an AC-OTS based decomposition approach for solving the OTS problem under grid uncertainties. In the proposed decomposition method, the new formulation that satisfies both the convex condition and the separable condition of the GBD is used. Note that sequential computing of subproblems is used in the proposed **Method 7** for our case studies. Parallel/distributed computing can further accelerate the computation.

4.4.3 Case studies on the IEEE-118 bus system

To evaluate the proposed approach comprehensively, we need to consider two key factors, namely accuracy and scalability. Four case studies on the IEEE-118 system, where different deviations of uncertainties are presented, are shown first to demonstrate the accuracy of the proposed approach in stochastic AC-OTS problems. Later on, the scalability of the proposed approach will be analyzed in the coming Section 4.4.4.

There are 118 buses, 186 branches and 54 generators in the IEEE-118 bus system. Four generators (at bus 26, 54, 87 and 100) are replaced by renewable generations. The wind capacity is 696.6 MW and the solar capacity is 700 MW. The renewable generations take up 18.6% of the

total generation capacity in the system.

1) Case 1

In Case 1, 10 scenarios with a small deviation are created and used. The mean variance of real power load is 0.0057, which is calculated using (4-74). The number of allowed switching actions is set to be 2. 10 candidate lines are provided in this case.

$$\overline{var(P_l)} = \frac{1}{N_L}\sum_{i=1}^{N_L} var(P_i) \tag{4-74}$$

where $\overline{var(P_l)}$ is the mean variance of real power load, N_L is the number of loads and $var(P_i)$ is the variance of real power load at bus i.

The results of **Method 0**-**Method 7** (**M0**-**M7**) are summarized in Table 4-1. The detailed generator output differences in different OTS methods are not shown here since a similar study has been done in Section 3.4.3. In general, a good switching plan will reduce transmission congestion in the system and cheap generation can be utilized more. Note that the obtained switching plan from each method is tested for all scenarios in the ACOPF to check the AC feasibility and obtain the actual expected cost.

Table 4-1: Numerical results of Case 1

10 scenarios, $\overline{var(P_l)} = 0.0057$, mean system load=5375.16 MW						
Type	Method	Estimated expected cost	Time(s)	Switching plan	Actual expected cost	Cost saving
Deterministic	M1	2331.01	2	Line 123, 125	11715.61	2476.90 (17.45%)
	M2	10052.29	23	Line 123, 124	11319.72	2872.79 (20.24%)
Stochastic	M0	14192.51	6	NA	14192.51	0.00
	M3	2642.19	5	Line 123, 125	11715.61	2476.90 (17.45%)
	M4	11319.72	320	Line 123, 124	11319.72	2872.79 (20.24%)
	M5	11319.72	3540	Line 123, 124	11319.72	2872.79 (20.24%)
	M6	2642.19	76	Line 123, 125	11715.61	2476.90 (17.45%)
	M7	11319.72	1315	Line 123, 124	11319.72	2872.79 (20.24%)

The savings of using OTS are very significant in this case. The saving can be up to 20.24% here. In **M0**, 10 scenarios are calculated in the ACOPF one by one without OTS. The expected cost in the benchmark case is 14192.51. The actual expected costs from other methods are compared with this expected cost in the benchmark. It can be seen that OTS in all methods (**M1**-**M7**) can lead to a significant cost saving in this case, ranging from 17.45% to 20.24%. Among those seven methods, **M2**, **M4**, **M5** and **M7** can give the best switching plan (Line 123 and 124) and thus the best cost saving (2872.79/hour). **M1**, **M3** and **M6** yield a different switching plan (Line 123 and 125), which results in a smaller cost saving (2476.90/hour).

In this case, deterministic OTS methods (**M1** and **M2**) perform well because all scenarios are similar with only a small deviation. Using an averaged case in those deterministic OTS methods is fairly good for decision-making. However, this is not going to happen when random scenarios have a big deviation, which will be shown in the next 3 cases.

It is also worth mentioning that the deterministic OTS methods (**M1** and **M2**) and stochastic DC-OTS methods (**M3** and **M6**) cannot estimate the expected cost accurately in OTS problems. There are some discrepancies between the estimated expected cost and the actual expected cost in those 4 methods, especially in **M1**, **M3** and **M6**. This is due to the DC simplifications and the underestimation of the variance of uncertain parameters, which may also affect the calculated switching plans. The drawbacks of those methods will be demonstrated in the following 3 cases.

2) Case 2

In Case 2-Case 4, scenarios with a big deviation are used to test the aforementioned OTS methods. In Case 2, 5 scenarios ($\overline{var(P_l)} = 0.1915$) are created and used. The number of allowed switching actions is set to be 2 and 15 candidate lines are provided. The results are shown in Table

4-2.

Table 4-2: Numerical results of Case 2

5 scenarios, $\overline{var(P_i)} = 0.1915$, mean system load= 5447.04 MW						
Type	Method	Estimated expected cost	Time (s)	Switching plan	Actual expected cost	Cost saving
Deterministic	M1	2134.46	2	Line 38, 102	47042.33	-4913.02 (-11.66%)
	M2	3887.67	8	Line 105, 106	41572.59	556.72 (1.32%)
Stochastic	M0	42129.31	4	NA	42129.31	0.00
	M3	26953.35	3	Line 37, 102	40252.95	1876.36 (4.45%)
	M4	39889.48	123	Line 100, 102	39889.48	2239.83 (5.32%)
	M5	39984.01	3635	Line 100, 102	39889.48	2239.83 (5.32%)
	M6	26953.35	119	Line 37, 102	40252.95	1876.36 (4.45%)
	M7	39811.74	2446	Line 102, 103	39811.74	2317.56 (5.50%)

With a big deviation exists in the scenarios, not all OTS methods can lead to a cost saving. A bad switching plan (Line 38 and 102) is calculated in **M1**, which make the actual expected cost even higher than the benchmark without OTS. Among **M2**-**M7**, **M7** can get the best switching plan (Line 102 and 103), which results in the best cost saving (2317.56 /hour). And a different switching plan (Line 100 and 102) is obtained in **M4** and **M5**, which leads to a very similar saving (2239.83/hour) as in **M7**. **M4**-**M5** and **M7** are equivalent in the mathematical sense. However, **M4** and **M5** deal with the SP problem with all scenarios together rather than in a decomposed way as in **M7**, which makes **M4** and **M5** easy to converge to a different local optimum. The savings in **M4**, **M5** and **M7** are about four times of the saving in **M2**, which shows the advantage of the stochastic AC-OTS over the deterministic AC-OTS. Note that the savings in **M4**, **M5** and **M7** are only slightly better than the savings in **M3** and **M6** in this case. The advantage of the stochastic AC-OTS over the stochastic DC-OTS will be illustrated better in the next case.

3) Case 3

In Case 3, 5 scenarios ($\overline{var(P_l)} = 0.1965$) are generated and used. The number of allowed switching actions is set to be 2 and 26 candidate lines are provided. The numerical results are shown in Table 4-3.

Table 4-3: Numerical results of Case 3

5 scenarios, $\overline{var(P_l)} = 0.1965$, mean system load= 5144.64 MW						
Type	Method	Estimated expected cost	Time (s)	Switching plan	Actual expected cost	Cost saving
Deterministic	M1	1757.79	2	Line 38, 102	28761.09	808.76 (2.74%)
	M2	2716.34	9	Line 105, 123	29362.09	207.76 (0.70%)
Stochastic	M0	29569.85	4	NA	29569.85	0.00
	M3	21978.97	3	Line 71, 102	31519.35	-1949.50 (-6.59%)
	M4	27933.07	305	Line 102, 103	27933.07	1636.79 (5.54%)
	M5	28089.87	>10800	Line 101, 102	28089.87	-156.80 (-0.53%)
	M6	21978.97	338	Line 71, 102	31519.35	-1949.50 (-6.59%)
	M7	27933.07	8890	Line 102, 103	27933.07	1636.79 (5.54%)

In Case 3, different methods have different performance. The two stochastic AC-OTS methods, **M4** and **M7**, can give the best switching plan (Line 102 and 103) and achieve the best cost saving (1636.79/hour). The other stochastic AC-OTS, **M5**, is too slow in this case. It cannot finish computing within 3 hours and it stops at a bad switching solution, which leads to a negative saving (-0.53%). Deterministic methods **M1** and **M2** give different switching plans, which can result in a cost saving of 808.76/hour and 207.76/hour respectively. We can see that **M1** and **M2** are not as good as **M4** and **M7** in this case. As for **M3** and **M6**, they yield the worst solution (-1949.50/hour saving) in this case. The actual expected cost is even much higher than the benchmark.

4) Case 4

In Case 4, 3 scenarios are used with 2 switching actions are allowed. 26 candidate lines are provided for this case. This case has the largest deviation in random scenarios ($\overline{var(P_l)} = 0.2374$). The numerical results are shown in Table 4-4.

Table 4-4: Numerical results of Case 4

3 scenarios, $\overline{var(P_l)} = 0.2374$, mean system load= 5301.83 MW						
Type	Method	Estimated expected cost	Time (s)	Switching plan	Actual expected cost	Cost saving
Deterministic	M1	1886.74	2	Line 38, 102	37850.62	628.05 (1.63%)
	M2	3221.93	7	Line 105, 106	37691.80	786.87 (2.04%)
Stochastic	M0	38478.67	3	NA	38478.67	0.00
	M3	27723.96	2	Line 95, 102	36876.67	1602.01 (4.16%)
	M4	36728.54	106	Line 83, 102	36728.54	1750.14 (4.55%)
	M5	36728.54	3385	Line 83, 102	36728.54	1750.14 (4.55%)
	M6	27723.96	124	Line 95, 102	36876.67	1602.01 (4.16%)
	M7	36728.54	5533	Line 83, 102	36728.54	1750.14 (4.55%)

In this case, OTS can reduce the operational cost in general in **M1**-**M7**. It can be seen that the **M4**, **M5** and **M7** give the best solution in terms of the switching plan (Line 83 and 102) and the cost saving (1750.14/hour). Stochastic DC-OTS methods, **M3** and **M6**, generate a different switching plan (Line 95 and 102) but a comparable cost saving (1602.01/hour) as in **M4**, **M5** and **M7**. As for deterministic methods **M1** and **M2**, they can only achieve a much lower cost saving when compared with the stochastic AC-OTS methods.

From the above 4 cases, we can conclude that:

1) OTS can reduce power system operational cost in general as seen in Case 1 and Case 4. However, the benefit of OTS may vary from case to case. For example, in Case 1,

we can reduce the operational cost through OTS significantly. The amount of saving can be up to 20.24%. However, in Case 4, the saving from OTS is lower. The maximum saving is 4.55%.

2) Bad switching solution (negative saving) could happen due to the DC approximations, where reactive power and voltage issues are ignored. In Case 2, a bad switching decision happens in the deterministic DC-OTS (**M1)** while the deterministic AC-OTS (**M2**) can give a beneficial switching plan. And in Case 3, the stochastic DC-OTS methods (**M3** and **M6**) give a bad switching plan while the stochastic AC-OTS methods (**M4** and **M7**) give a good switching plan.
3) The stochastic AC-OTS is better than the deterministic methods when there is a huge deviation in the random scenarios as indicated in Case 1-Case 4. When the deviation is small as in Case 1, using a deterministic method is good enough. However, a significant deviation is usually used in the OTS problems to represent the grid uncertainties comprehensively as shown in Case 2-Case 4. In these situations, the stochastic AC-OTS is much better than the deterministic methods.
4) The impact of variance in random scenarios could be demonstrated using Case 2 and Case 4. Although the variances are different, the averaged cases are similar. As a result, the two deterministic methods (**M1** and **M2**) generate the same switching plans in the two cases. However, from the stochastic AC-OTS (**M7**), we can see that the optimal switching plans are actually different in these two cases due to the variances. Thus, it can be seen that the variance will affect the optimal switching plan in OTS problems. Deterministic methods will underestimate the variance and yield sub-optimal switching plans.

5) The stochastic AC-OTS is better than the stochastic DC-OTS as shown in Case 1-Case 4. The DC method cannot consider the voltage and reactive power issues. As a result, the calculated switching plans are often sub-optimal as shown in Case 1-Case 2 and Case 4. More importantly, the generated switching plan may lead to a higher operational cost than the benchmark without OTS as shown in Case 3.
6) The two stochastic AC-OTS methods, **M4** and the proposed approach **M7** can always give the best solution in all four cases when compared with the other methods. The accuracy of the proposed approach **M7** is therefore demonstrated.

Note that the main purpose of this part is to show the accuracy of the proposed approach **M7**. It is as accurate as the original stochastic AC-OTS, **M4**. Although **M7** is slower than **M4** in the above cases, **M7** will have a much better performance in terms of speed when a large number of scenarios are involved. In fact, a large number of scenarios should be used to represent the uncertainties in a real SP problem. Therefore, a good scalability is very important. In the next part, we are going to investigate the scalability of the proposed approach **M7**.

4.4.4 Scalability analysis

A scalability analysis is shown in this part to demonstrate the merits of the proposed decomposition approach **M7** over other stochastic AC-OTS methods. Here, we only take the stochastic AC-OTS methods (**M4**, **M5**) for comparison because they can yield the same level of accuracy. The test results are shown in Table 4-5-Table 4-6. Note that this part is conducted on a desktop with Intel I7-6700 3.4GHz CPU and 32GB memory.

In Test 1, different numbers of scenarios are tested, where the proposed decomposition method **M7** shows the best capability of handling a large number of scenarios among the three methods. The computation time of **M7** increases linearly when the number of scenarios increases,

which means the per scenario computation time is almost constant. As a comparison, the computation time of **M4** and **M5** increases fast when more scenarios are involved. **M4** fails to get a switching plan within 3 hours when 150 scenarios are involved and **M5** fails to reach an optimal solution within 3 hours when 50 scenarios or more are involved. The **M7** can handle the 150 scenarios case and find the optimal switching plan in 8351 seconds.

Table 4-5: Test 1: Scalability analysis on the number of scenarios

Test 1: Candidate lines=10, allowed switching=1, the IEEE-118 bus system						
No. of Scenarios	M4		M5		M7	
	Total time (s)	Per scenario time (s)	Total time (s)	Per scenario time (s)	Total time (s)	Per scenario time (s)
10	151	15.1	902	90.2	581	58.1
20	316	15.8	2799	140.0	1148	57.4
50	671	13.4	>10800, feasible solution	>216	2910	58.2
100	1058	10.6	>10800, no solution	>108	5631	56.3
150	>10800, no solution	>72	>10800, no solution	>72	8351	55.7

The scalability of **M7** is also tested on the number of candidate lines, the number of allowed switching actions and the system size in Test 2-Test 4 as shown in Table 4-6-Table 4-8. **M7** has a good scalability on these aspects, but no significant improvement is found over **M4** and **M5** as expected since **M7** is a scenario-based decomposition approach. In Test 2 and Test 3, **M7** shows a linear time increment when the number of binary combinations of transmission line status increases due to the increase of candidate lines or allowed switching actions. In Test 4, when the system size increases, **M7** shows a quadratic computation time. This is caused by the nonlinear

increase of the number of variables as the number of buses increases, which makes more complexity of the problem.

Table 4-6: The results of Test 2 (different number of candidate lines)

	No. of candidate lines	Combinations	Time (s)
Test 2: scenarios=3, allowed switching =1, IEEE-118 bus system	10	10	118
	20	20	292
	30	30	466
	50	50	822

Table 4-7: The results of Test 3 (different number of allowed switching actions)

	No. of allowed switching	Combinations	Time (s)
Test 3: scenarios=3, candidate lines=10, IEEE-118 bus system	1	11	183
	2	56	920
	3	176	2795

Table 4-8: The results of Test 4 (different sizes of systems)

	System	Buses	Time (s)
Test 4: scenarios=3, allowed switching =1, candidate lines=10	IEEE RTS	24	24
	IEEE-118	118	183
	SouthCarolina500	500	1482

In summary, the proposed **M7** is the best approach among the existing methods because of the best optimality as shown in Table 4-1-Table 4-4, the significant improvement of the scalability on the number of scenarios as shown in Table 4-5 and the comparable good scalability on other aspects as shown in Table 4-6-Table 4-8.

4.5 Summary

In Section 4, a new separable SP formulation for the AC-OTS under uncertainties is proposed. Based on the formulation, a novel two-stage SP formulation with a convex relaxation is developed. The proposed two-stage SP formulation strictly follows the mathematical requirements of the GBD and thus can guarantee the finite convergence. And a GBD based algorithm is proposed to solve the SP problem of the AC-OTS using the proposed two-stage formulation in the inner loop and the ACOPF in the outer loop. Therefore, an optimal switching plan could be found efficiently without any sacrifice of accuracy for the AC-OTS problem under grid uncertainties. The numerical results confirm the effectiveness and scalability of the proposed decomposition approach.

5. TRANSIENT STABILITY ANALYSIS FOR TRANSMISSION SWITCHING ACTIONS*

In Section 2-4, the optimization approaches for OTS are shown in detail. However, the switching actions will introduce disturbances into the system that may cause transient instability. Thus, starting from Section 5, the transient stability issues of OTS are investigated to avoid any instability in real implementation. In Section 5, two major transient stability analysis methods, namely the numerical integration method using the state-of-the-art commercial power system simulation tools and the direct method using the transient energy function (TEF) theory, are presented. The advantages and disadvantages of them are discussed. The potential risk of transient instability caused by transmission switching actions is shown in numerical studies. And batteries and thyristor-controlled series compensation (TCSC) are proposed to enhance transient stability for transmission switching actions.

The symbols used in Section 5 are listed as follows.

x	Dynamic state variable, such as generator voltage and rotor angle
$\dot{x}$	The derivative of dynamic state variable x
y	Instantaneous variable, such as load bus voltage magnitude and angle
p	System configuration and operation parameter, such as loads
δ_i	Internal voltage angle of the ith generator
H_i	Inertia constant of the ith generator
δ_{COI}	Center of inertia

* © [2015] IEEE. Reprinted, with permission, from [T. Lan and G. M. Huang, Transmission Line Switching in Power System Planning with Large Scale Renewable Energy, 2015 First Workshop on Smart Grid and Renewable Energy (SGRE), 03/2015]

P_{mi}	Mechanical input power
J_i	Per unit moment of inertia of the ith generator. $J_i = 2H_i\omega_0$. ω_0 is the synchronous speed in electoral rad/s
ω_i	Per unit speed deviation of the ith machine with respect to the COI
θ_i^s	Angle of bus i at the post-disturbance stable equilibrium point
E_i	Internal voltage magnitude of the ith generator
G_{ij}	Conductance of branch ij
B_{ij}	Susceptance of branch ij
n	Number of generators in the system
V_{cr}	Critical energy of the system
V_{cl}	Initial energy of the system (at the instant of fault-clearing)
M	Energy margin
T_m	Mechanical torque
T_e	Electrical torque
K_{D1}	Damping factor
$\Delta\omega$	Rotor speed deviation
T_{extra}	Extra damping torque

5.1 Power system transient stability analysis

Transient stability is the ability of the power system to maintain synchronism when subjected to a severe disturbance such as a generator loss, a fault on transmission facilities or a loss of load [24]. Transmission switching is one of the actions that may introduce a large disturbance in a power system and thus transient stability study is essential. In this section, two

prevailing power system transient stability analysis methods are reviewed. The numerical integration method and the direct method have their own advantages and disadvantages and thus can be applied to different power system transient stability applications.

5.1.1 The numerical integration method

The dynamic behavior of a power system can be described by a set of differential-algebraic equations as shown in (5-1). The differential equation in (5-1) represents power system dynamics while the algebraic equation in (5-1) represents the power flow equation. For large power systems, it is impossible to obtain an analytical solution for the system dynamic behavior, i.e. the explicit expressions for variable x and y as functions of time. Instead, numerical integration methods, such as the Euler method, the Runge-Kutta method and the trapezoidal method, could be applied to obtain a numerical solution for the system dynamic response [24].

$$\begin{cases} \dot{x} = f(x, y, p) \\ 0 = g(x, y, p) \end{cases} \tag{5-1}$$

Currently, various commercial software is available for power system transient stability study using numerical integration methods. PSS/E [56], PowerWorld [57] and TSAT [58] are the state-of-the-art simulators for power system electromechanical transient study, while PSCAD [59] is the state-of-the-art simulator for power system electromagnetic transient study. One can choose an appropriate tool based on its needs in power system transient stability study. The numerical integration method can utilize the detailed dynamic models for power system transient stability studies, which has a good accuracy and has been used by the industry for many years.

5.1.2 The TEF method

The TEF method is a special case of the more general Lyapunov's second method or the direct method [24]. The TEF is one of the Lyapunov functions for nonlinear dynamic systems like power systems. To derive the TEF, we have the following assumptions and simplifications:

1) Generators are modeled by the classical model (constant voltage behind transient reactance);
2) Loads are modeled as constant impedance;
3) Generator transient reactance and load admittance are included in the node admittance matrix;
4) Generator outputs are fixed during the disturbance.

Then with the center of inertia (COI) of the system defined in (5-2), we can get the TEF as shown in (5-3).

$$\delta_{COI} = \frac{\sum_{i=1}^{n} H_i \delta_i}{\sum_{i=1}^{n} H_i} \tag{5-2}$$

$$\begin{aligned} V_{TEF} = {} & \frac{1}{2}\sum_{i=1}^{n} J_i \omega_i^2 - \sum_{i=1}^{n} P'_{mi}(\theta_i - \theta_i^s) \\ & - \sum_{i=1}^{n-1}\sum_{j=i+1}^{n}\left[C_{ij}\left(\cos\theta_{ij} - \cos\theta_{ij}^s\right) - \int_{\theta_i^s+\theta_j^s}^{\theta_i+\theta_j} D_{ij}\cos\theta_{ij}\, d(\theta_i+\theta_j)\right] \end{aligned} \tag{5-3}$$

where $C_{ij} = E_i E_j B_{ij}$, $D_{ij} = E_i E_j G_{ij}$, $P'_{mi} = P_{mi} - E_i^2 G_{ii}$, $\theta_i = \delta_i - \delta_{COI}$, $\theta_{ij} = \theta_i - \theta_j$.

There are four terms in the energy function as shown in (5-3):

1) $\frac{1}{2}\sum_{i=1}^{n} J_i \omega_i^2$ is the change in rotor kinetic energy of all generators in the system in the COI reference.
2) $\sum_{i=1}^{n} P'_{mi}(\theta_i - \theta_i^s)$ is the change in rotor potential energy of all generators relative to the COI.

3) $\sum_{i=1}^{n-1}\sum_{j=i+1}^{n}\left[C_{ij}\left(\cos\theta_{ij}-\cos\theta_{ij}^{s}\right)\right]$ is the change in stored magnetic energy of all branches.

4) $\sum_{i=1}^{n-1}\sum_{j=i+1}^{n}\left[\int_{\theta_i^s+\theta_j^s}^{\theta_i+\theta_j} D_{ij}\cos\theta_{ij}\,d(\theta_i+\theta_j)\right]$ is the change in dissipated energy of all branches.

The first term is called the kinetic energy and the last three terms together are called the potential energy of the system. When using the TEF theory for transient stability study, first we need to calculate the system critical energy V_{cr} using (5-3). This is the most difficult step in applying the TEF method. Some possible methods are [24]: the closest unstable equilibrium point (UEP) approach, the controlling UEP approach and the boundary of stability-region-based controlling UEP method. Then, the next step is to calculate the total system initial energy at the instant of fault-clearing V_{cl} using (5-3). This step requires that the numerical simulation runs to the instant of fault-clearing to obtain angle and speed information of all generators. At last, the energy margin is calculated as in (5-4). The system is stable if $M > 0$ and the system is unstable if $M < 0$.

$$M = V_{cr} - V_{cl} \tag{5-4}$$

5.1.3 Discussions

The numerical integration method can take precise generator models into consideration for power system stability studies and yield accurate results. Therefore, it is widely used in the power industry. However, one drawback is that it cannot provide direct control instructions for operators if unstable situations are identified. Operators usually need to rely on their past experience or the pre-defined contingency list to handle the situation and ensure system stability. On the other hand,

the numerical integration needs to be performed for the entire event to assess system transient stability.

As for the TEF method, it simplifies the transient stability assessment since the numerical integration is only needed until the fault clearing moment. Based on the information at that moment, the system energy margin can be calculated to assess transient stability. And it is convenient to use the TEF method to explain many situations in power system stability studies since it has the ability to show the factors that affect the system stability in a quantitative manner. However, the major concern is that the use of the simplified models will affect the accuracy significantly. And only conventional synchronous generators can be included in the classical TEF. Renewable generations are usually treated as negative load or converted to equivalent synchronous generators for the TEF calculation, which will also affect the accuracy of transient stability studies. Besides, finding the UEP is difficult since the standard power flow calculation usually finds a stable equilibrium point. Special efforts must be taken to find a good initial point in order to get the UEP in power flow calculation.

5.2 Transient stability enhancement using batteries and TCSC

In this section, batteries and TCSC are introduced for transient stability enhancement in line switching actions. The impacts of batteries and TCSC in power system dynamics are explained first and followed by numerical examples.

5.2.1 The impact of batteries and TCSC

TCSC and energy storage devices are used in improving transient stability during fault situation [60]-[62]. A line switching operation is not a fault situation but similarly related to damping torque and acceleration torque.

The equation of motion for a generator in per unit is shown in (5-5).

$$\Delta\dot{\omega} = \frac{1}{2H}(T_m - T_e - K_{D1}\Delta\omega) \tag{5-5}$$

With TCSC installed to the connecting branch or energy storage devices installed at the bus, the generator can have extra damping torque T_{extra} as shown in (5-6).

$$\Delta\dot{\omega} = \frac{1}{2H}(T_m - (T_e + T_{extra}) - K_{D1}\Delta\omega) \tag{5-6}$$

When the speed of generator goes up, we decrease the impedance of a connecting line to increase line flow or we charge the battery at this bus to keep $T_{extra} > 0$. When the speed of generator goes down, we increase the impedance of a connecting line to decrease line flow or we discharge the battery at this bus to keep $T_{extra} < 0$. In this way, the transient stability can be enhanced. It should be pointed out that batteries can be used for charging and discharging for a short while. But it is still very effective to damp the first swing when line switching happens.

5.2.2 Numerical examples

A simplified WSCC 9-bus system is used for demonstration as shown in Figure 5-1.

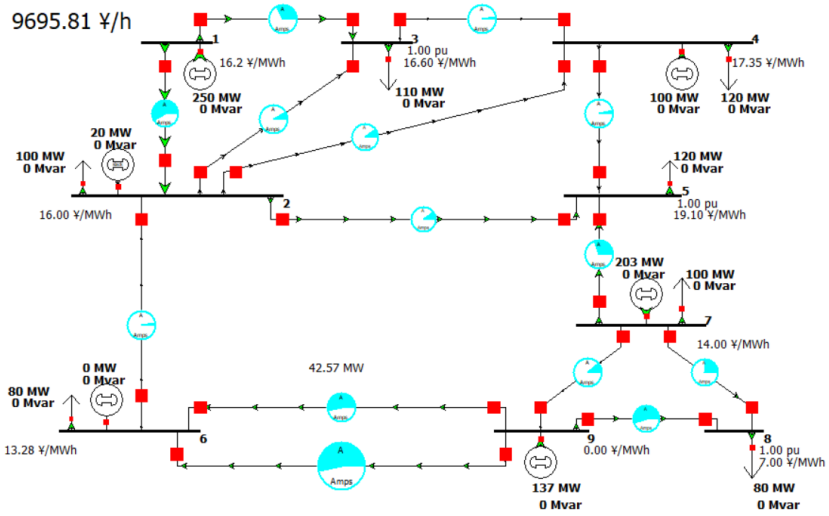

Figure 5-1: The simplified WSCC 9-bus system: Reprinted with permission from [© 2015, IEEE]

We use PSS/E to check the transient stability of the system during a line switching action. In the following cases, the target line (bus 1-bus 2) is switched off at t=5s to change the system topology. And then a redispatch happens at t=30s to obtain the new state.

The result shows transient instability arises in the original system. Figure 5-2 shows the relative angle between bus 1 and bus 2. Before the redispatch happens, the system is already unstable. Figure 5-2 indicates that the damping torque near the switching area is not sufficient. TCSC and energy storage devices such as batteries can provide more damping torque to enhance transient stability in concept as discussed in Section 5.2.1. In this case, the area where the line switching operation happens will be affected more in the transient process. Therefore, installing TCSC and batteries in the nearby area will be helpful.

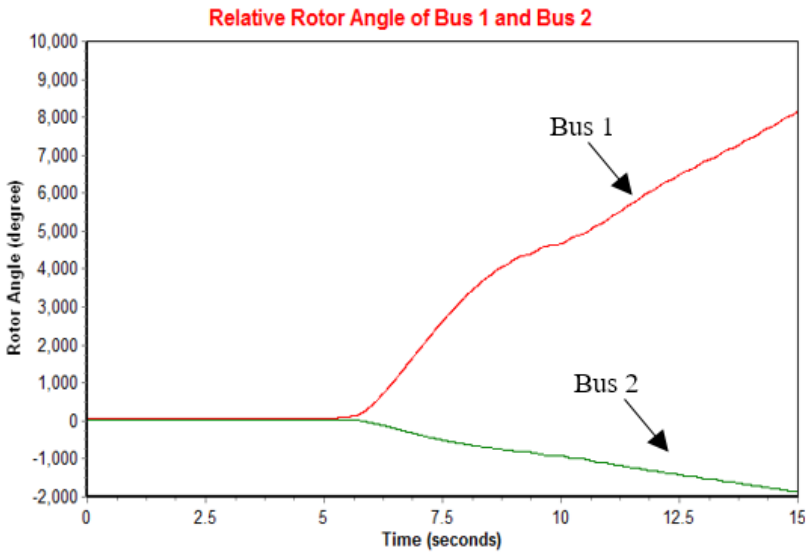

Figure 5-2: The relative rotor angle for the original system: Reprinted with permission from [© 2015, IEEE]

1) Transient stability enhancement using TCSC

TCSC is installed on the transmission line between bus 2 to bus 3. The reactance of the line can vary between 0.05 per unit and 1 per unit. Due to TCSC, the rotor angle difference between bus 1 and bus 2 does not become too large in the transient process as shown in Figure 5-3 indicating the system is stable now. And the reactance of the line with TCSC is shown in Figure 5-4. When the redispatch is applied to conventional generators at bus 2, bus 4 and bus 7 at t=30s, the system can move to the new state.

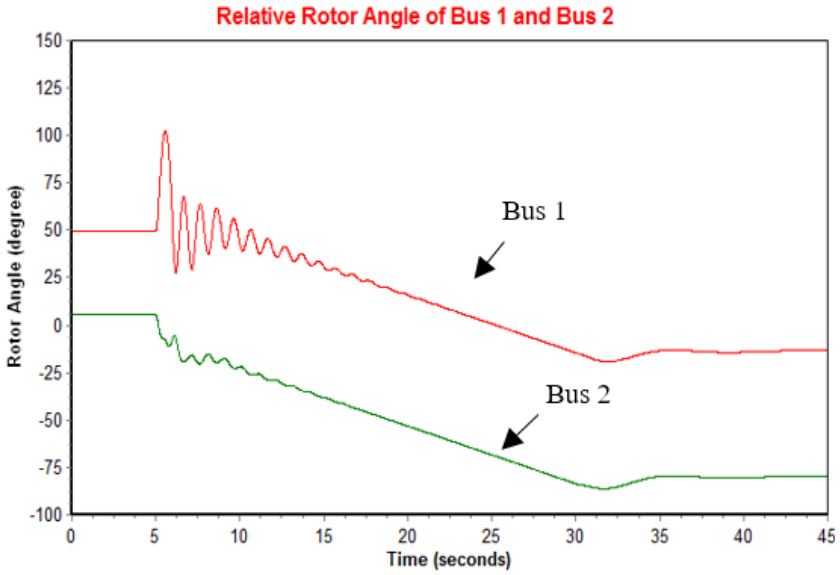

Figure 5-3: The relative rotor angle for the system with TCSC: Reprinted with permission from [© 2015, IEEE]

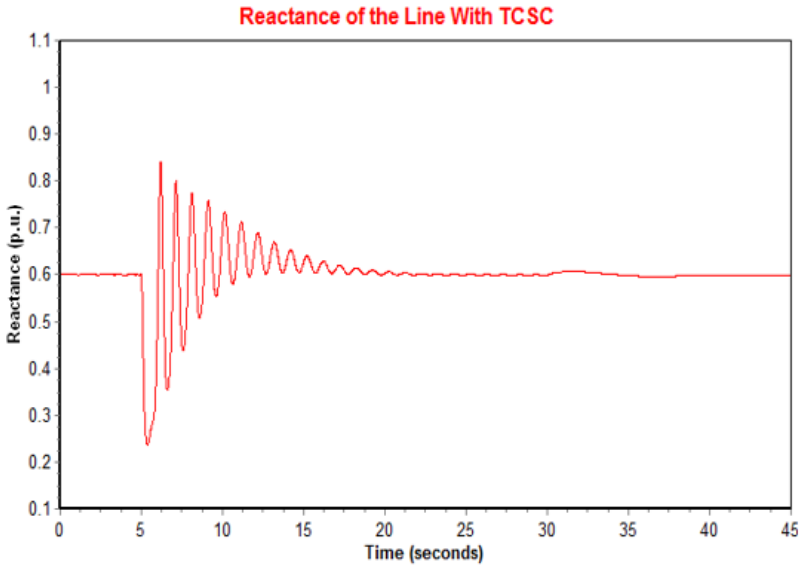

Figure 5-4: The reactance of the line with TCSC: Reprinted with permission from [© 2015, IEEE]

2) Transient stability enhancement using batteries

Large-scale energy storage devices can also provide extra damping torque for the generators by charging or discharging to keep the system stable. We choose to install a large-scale battery at bus 2 in the test system, instead of TCSC. Here, the battery provides 65MW for 5s after the line switching operation happens. Although it is a short period, results in Figure 5-5 show the battery will also make this system stable.

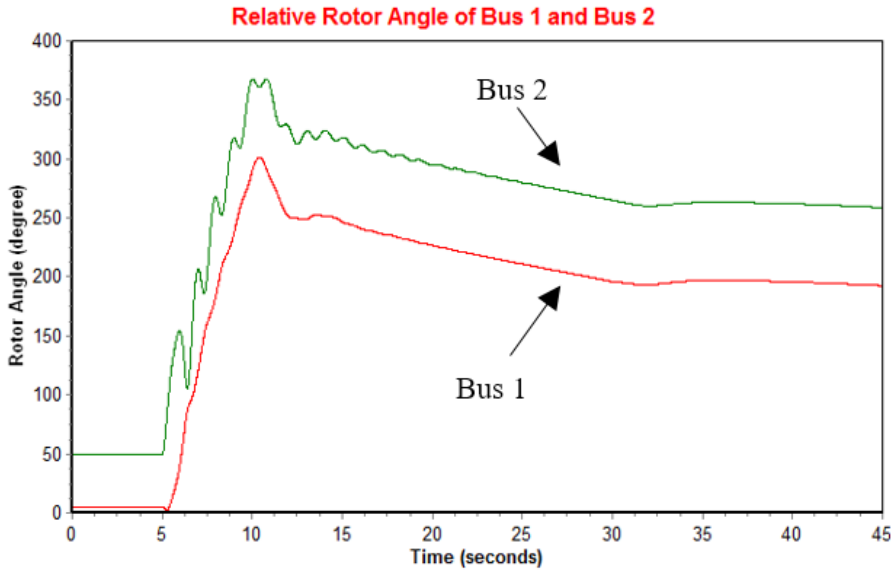

Figure 5-5: The relative rotor angle for the system with a battery: Reprinted with permission from [© 2015, IEEE]

5.3 Summary

In Section 5, we review two prevailing methods for power system transient stability study. The numerical integration method and the TEF method have their own advantages and disadvantages. Researchers should choose the proper method according to their research purpose. This section also shows the potential risk of transient instability in transmission switching actions. The numerical example shows a system could lose synchronism in a switching action and thus transient stability enhancement is needed. TCSC and batteries are used in Section 5 to enhance system transient stability significantly. The unstable switching action will be stabilized if TCSC or batteries are installed.

6. CSF BASED PREVENTIVE STABILIZING REDISPATCH FOR TRANSMISSION SWITCHING ACTIONS[*]

In Section 5, transient stability analysis is presented for transmission switching actions using well-established methods. However, the existing methods cannot give explicit instructions when instability is found in the transmission switching actions. In Section 6, a new transient stability index, critical switching flow (CSF), is designed and the corresponding preventive stabilizing redispatch scheme is developed to avoid unstable switching actions in the online operation. The overall scheme is shown first and followed by the detailed mathematical derivation of the new transient stability index. An offline Monte Carlo simulation algorithm is proposed to calculate the index and then the index will be used in the online preventive stabilizing redispatch scheme. Numerical examples will be shown in the IEEE-118 bus system.

The symbols used in Section 6 are listed as follows.

δ_1^{s1}	Rotor angle of generator 1 at the pre-switching stable equilibrium s1.
δ_1^{s2}	Rotor angle of generator 1 at the post-switching stable equilibrium s2.
δ_1^{u2}	Rotor angle of generator 1 at the post-switching controlling unstable equilibrium u2.
V_1, V_2	Internal voltages of generator 1 and 2.
B_1, B_2	Susceptance of line 1 and 2 in the equivalent reduced network.
M	Energy margin.
$\dot{M}$	Derivative of energy margin.

[*] © [2016] IEEE. Reprinted, with permission, from [T. Lan, W. Wang and G. M. Huang, A Critical Switching Flow Index for Transient Stability Assessment in Smart Grid Topology Control, 2016 IEEE Innovative Smart Grid Technologies (IGST), 09/2016] © [2018] IEEE. Reprinted, with permission, from [T. Lan, W. Wang and G. M. Huang, Transmission Grid Topology Control Using Critical Switching Flow Based Preventive Stabilizing Redispatch, IEEE Transactions on Power Systems, 05/2018]

$P'_{m,i}$	Generator i mechanical input minus its loading.
f_{12}	Total real power transferred from bus 1 to bus 2.
f_2	Real power flow on line 2.
f_{cr}	CSF of a switching target line.
f_{target}	Real power flow on a switching target line in the multi-machine system.
$f(v)$	Probability density function (PDF) of wind speed v.
P_{wind}	Wind power generation.
k	Shape parameter of the Weibull distribution.
c	Scale parameter of the Weibull distribution.
v_{mean}	Hourly average of forecasted wind speed from a time series.
v_{ci}	Cut-in speed of wind turbine.
v_o	Cut-out speed of wind turbine.
v_r	Rated wind speed.
P_w^r	Rated wind power generation.
$f(s)$	PDF of solar irradiance s.
α	Parameter of the Beta distribution.
β	Parameter of the Beta distribution.
P_s	Solar power generation.
P_s^r	Rated solar plant generation.
μ_s	Hourly average of forecasted irradiance.
${\sigma_s}^2$	Variance of solar irradiance, obtained by historical data processing.
$f_n(l)$	PDF of load uncertainty l.

S_{load}^{f}	Forecasted load (including real and reactive load).
μ_l	Mean value of load uncertainty l.
${\sigma_l}^2$	Variance of load uncertainty l.
S_{load}	Load with uncertainty.
$f(P)$	PDF of conventional generator output P.
L_c, U_c	Lower and upper bound of the output of a conventional generator.
P_a	Scheduled generation from day-ahead SCOPF using forecasted loads and renewable generations.
ΔP	The amount of allowed conventional generation adjustment.
P_{max}, P_{min}	Maximum and minimum output of a conventional generator.
$AS(0)$	Maximum rotor angle separation between any two machines at t=0s.
AS_{max}	Maximum rotor angle separation between any two machines at the same time in the whole simulation period.
$E(X)$	Expected value of variable X.
$SD(E(X))$	Standard deviation of mean value of X.
$Var(X)$	Variance of X.
N_s	Number of randomly generated cases in Monte Carlo simulation.
ΔN	Pre-chosen sample increment
USF_{min}	The minimum unstable switching flow found in two stages together.
ΔS	Safety margin.
$F_{i,max}^{c}$	Estimated maximum flow change by shifting the outputs of generation control pair i (generator i and the generator at the slack bus).

$\Delta P_{i,max}$ Maximum allowed generation shift between generation control pair i.

DF_i Generation shift distribution factor between generation control pair i.

n_g Number of generation control pairs involved in the redispatch scheme.

P_i Actual output of generator i.

$P_{i,a}$ Scheduled output of generator i from day-ahead SCOPF using forecasted data.

ΔP_i Control uncertainty of generator i.

$f_{original}$ Original flow on the switching target line.

$\Delta P_{i,ac}$ Actual generation shift between generation control pair i

6.1 Overall scheme for transmission switching actions

The framework of implementing transmission switching actions is shown in the top part of Figure 6-1. TC is incorporated in optimal day-ahead unit commitment and scheduling to calculate switching plans for each hour [5], [9]. The forecasted renewable generations and loads are used in the OPF with optimal switching. The calculated switching plan is then provided for real-time operation. In the operation stage, actual renewable generations and loads are ascertained. Using online measurements, the online stability check for the switching plan is performed. If the switching plan is stable, it will be permitted with corresponding generation dispatch to optimize the system by either reducing operational cost or solving a contingency. Otherwise, only generation dispatch will be implemented.

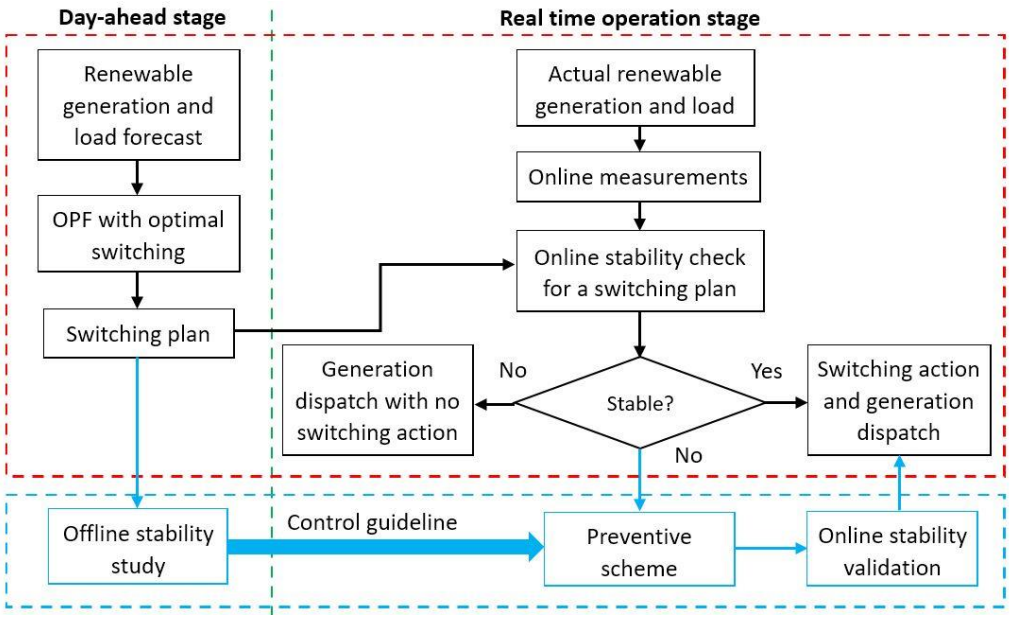

Figure 6-1: Framework of transmission switching in power system operation: Reprinted with permission from [© 2018, IEEE]

However, the switching plan may be unstable. If no additional control is applied, the operator has to abandon the beneficial switching plan. Our proposed online preventive scheme is to enable the beneficial switching plan while keeping the system stable. In the bottom part of Figure 6-1, the offline stability study is performed in the day-ahead stage based on the CSF index, which provides control guidelines for the online preventive scheme to enhance system stability in switching actions. The proposed preventive scheme is further validated in the online stability study before the actual switching action is made.

6.2 Derivation of the CSF index

As it is shown in the literature review, the existing transient stability indices are inappropriate for transmission switching actions. Therefore, a new index, CSF, is invented in this section for transmission switching actions.

6.2.1 Definition of CSF

In transmission switching applications, the line flow on a switching target line represents the amount of disturbance introduced into the system. The sudden disruption of the flow will cause power imbalance for some machines at the switching moment. As the line flow increases, power imbalance will be more severe, which makes the system less stable. Thus, there is a critical flow which sets the boundary between stable and unstable switching actions.

The definition of CSF is proposed as follows: CSF is the maximum real power flow allowed on a transmission line so that the system is stable when switching off the line. When a line flow is greater than CSF, the system has a risk of instability when switching off the line.

6.2.2 Existence of CSF

We use TEF in a two-machine system first to explain the existence of CSF and then extend the argument to multi-machine systems. Here, TEF [24] with reference to the center of inertial (COI) is used to calculate the energy margin of the system in transmission switching actions. To simplify our presentation, it is assumed: 1) transmission lines are lossless; 2) generators are modeled by classical model (constant voltage behind transient reactance) [24]-[26]; 3) loads are modeled as constant impedance [24]; 4) small amount of renewable generations are modeled as negative load [63]-[64].

1) Two-machine system

A two-machine system before and after a switching action is shown in Figure 6-2. The pre-switching system is at the original stable equilibrium point s1 and the post-switching system is at the new stable equilibrium point s2. We will investigate the relationship between the flow on a switching target line and system transient stability in the switching action.

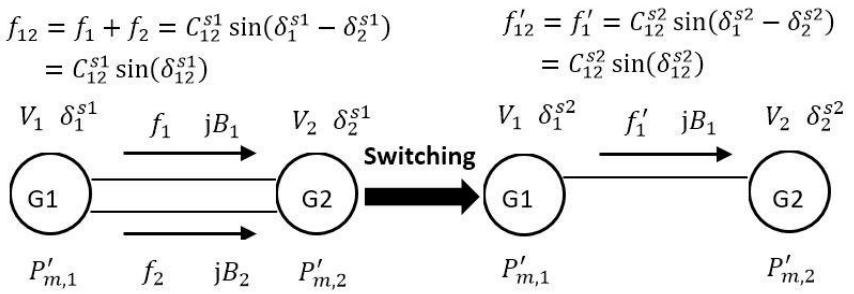

Figure 6-2: A two-machine system before and after a switching action: Reprinted with permission from [© 2018, IEEE]

Assuming bus 2 is the reference bus, the total flow between bus 1 and 2 and the flow on the switching target line are shown in (6-1) and (6-2). The energy margin M for the system under the switching action is shown in (6-3). M equals to the system critical energy minus the initial energy, which is a metric of system stability under given disturbance. When $M > 0$, the system is stable. And when $M < 0$, the system is unstable [24].

$$f_{12} = C_{12}^{s1} \sin(\delta_1^{s1}) = P'_{m,1} = C_{12}^{s2} \sin(\delta_1^{s2}) = C_{12}^{s2} \sin(\pi - \delta_1^{u2}) \tag{6-1}$$

$$f_2 = C_t \sin(\delta_1^{s1}) \tag{6-2}$$

$$\begin{aligned} M &= -C_{12}^{s1} \sin(\delta_1^{s1}) (\delta_1^{u2} - \delta_1^{s1}) + C_{12}^{s2} (\cos(\delta_1^{s1}) - \cos(\delta_1^{u2})) \\ &= -C_{12}^{s1} \sin(\delta_1^{s1}) \left(\pi - \arcsin\left(\frac{C_{12}^{s1}}{C_{12}^{s2}} \sin(\delta_1^{s1})\right) - \delta_1^{s1}\right) \\ &\quad + C_{12}^{s2} \left(\cos(\delta_1^{s1}) - \cos\left(\pi - \arcsin\left(\frac{C_{12}^{s1}}{C_{12}^{s2}} \sin(\delta_1^{s1})\right)\right)\right) \end{aligned} \tag{6-3}$$

where the values of the parameters are $C_{12}^{s1} = |(B_1 + B_2)V_1V_2|$, $C_{12}^{s2} = |B_1V_1V_2|$, $C_t = |B_2V_1V_2|$. δ_1^{s1} must be in the range $[0, \arcsin\left(\frac{C_{12}^{s2}}{C_{12}^{s1}}\right)]$ to ensure the existence of the post-switching equilibrium point s2.

We take the derivative of M to judge the relationship between system stability and the flow on the switching target line as shown in (6-4). As we know $\frac{\mathrm{d}\delta_1^{s1}}{\mathrm{d}f_2} = \frac{C_t}{\sqrt{(C_t)^2-(f_2)^2}} > 0$ from (6-2), we can look into the part $\frac{\mathrm{d}M}{\mathrm{d}\delta_1^{s1}} = \dot{M}(\delta_1^{s1})$ as shown in (6-5).

$$\frac{\mathrm{d}M}{\mathrm{d}f_2} = \frac{\mathrm{d}M}{\mathrm{d}\delta_1^{s1}} \times \frac{\mathrm{d}\delta_1^{s1}}{\mathrm{d}f_2} \tag{6-4}$$

$$\begin{aligned}\dot{M}(\delta_1^{s1}) = &-C_{12}^{s1}\left\{\pi - \delta_1^{s1} - \arcsin\left(\frac{C_{12}^{s1}\,sin(\delta_1^{s1})}{C_{12}^{s2}}\right)\right\}\cos(\delta_1^{s1}) \\ &+C_{12}^{s1}\sin(\delta_1^{s1})\left\{1 + \frac{C_{12}^{s1}\cos(\delta_1^{s1})}{C_{12}^{s2}\sqrt{1-(\frac{C_{12}^{s1}}{C_{12}^{s2}}\sin(\delta_1^{s1}))^2}}\right\} \\ &-C_{12}^{s2}\left\{\sin(\delta_1^{s1}) + \frac{{C_{12}^{s1}}^2\cos(\delta_1^{s1})\sin(\delta_1^{s1})}{{C_{12}^{s2}}^2\sqrt{1-(\frac{C_{12}^{s1}}{C_{12}^{s2}}\sin(\delta_1^{s1}))^2}}\right\}\end{aligned} \tag{6-5}$$

Define $k_c = \frac{C_{12}^{s2}}{C_{12}^{s1}} \in (0,1)$ and then (6-5) is simplified into (6-6).

$$\begin{aligned}\dot{M}(\delta_1^{s1}) = &-C_{12}^{s1}\left\{\pi - \delta_1^{s1} - \arcsin\left(\frac{\sin(\delta_1^{s1})}{k_c}\right)\right\}\cos(\delta_1^{s1}) \\ &-C_{12}^{s1}\sin(\delta_1^{s1})\,(1-\,k_c)\left\{\frac{1}{k_c}\sqrt{\frac{1-(\sin(\delta_1^{s1}))^2}{{k_c}^2-(\sin(\delta_1^{s1}))^2}} - 1\right\}\end{aligned} \tag{6-6}$$

From (6-1), we know $0 \le \delta_1^{s1} \le \arcsin(\,k_c) < \frac{\pi}{2}$. Then we have $\pi - \delta_1^{s1} - \arcsin\left(\frac{sin(\delta_1^{s1})}{k_c}\right) > 0$ and $\cos(\delta_1^{s1}) > 0$. Thus, the first term in (6-6) is less than 0. With $k_c \in (0,1)$, we can easily find the fact that $1-(\sin(\delta_1^{s1}))^2 > {k_c}^2 - (\sin(\delta_1^{s1}))^2$ and $\frac{1}{k_c}\sqrt{\frac{1-(\sin(\delta_1^{s1}))^2}{{k_c}^2-(\sin(\delta_1^{s1}))^2}} > 1$. So, the second term in (6-6) is also less than 0. Finally, we can find $\dot{M}(\delta_1^{s1})<0$ and $\dot{M}(f_2) < 0$.

$\dot{M}(f_2) < 0$ means when the flow on the switching target line becomes larger, M will be smaller no matter what machine inertia and line parameters are. Besides, from (6-3) we know $M(\arcsin(k_c)) < 0, M(0) > 0$ and M is a continuous function. Then, the sketch of M is shown in Figure 6-3. Since M is monotone decreasing, it is easy to find the only zero crossing point, which is the CSF f_{cr}.

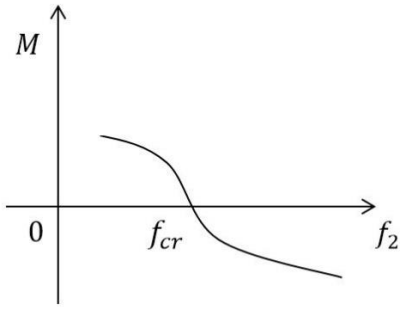

Figure 6-3: Relationship between the energy margin and the flow on the switching target line in a two-machine system: Reprinted with permission from [© 2018, IEEE]

Therefore, we build the relationship between the flow on the switching target line in the pre-switching system and system stability under a switching action. In the pre-switching system, if $f_2 > f_{cr}$, switching off the line will cause instability. And if $f_2 < f_{cr}$, switching off the line will be feasible.

2) Multi-machine systems

For a system with n machines, the relationship between the line flow on a switching target line and the nodal power injections can be expressed by a nonlinear function as shown in (6-7). The calculation of M is shown in (6-8) [24].

$$f_{target} = f\left(P'_{m,i}\right),\ i = 1,2 \dots n \tag{6-7}$$

$$M(f_{target}) = \sum_{i=1}^{n} P'_{m,i}\,(\delta_i^{s1} - \delta_i^{u2}) + \sum_{i=1}^{n-1}\sum_{j=i+1}^{n} C_{ij}^{s2}\left(\cos\left(\delta_{ij}^{s1}\right) - \cos\left(\delta_{ij}^{u2}\right)\right) \quad (6\text{-}8)$$

Although it is difficult to derive the analytical relationship between M and f_{target} in (6-7) and (6-8), we can make qualitative analysis for the system. It is assumed that the pre-switching system is at a stable equilibrium point and there exists a stable equilibrium point for the post-switching system. Note that:

1) $M(0) > 0$. If a line with zero flow is switched off, the power flow solution will not change. The pre-switching equilibrium point and the post-switching equilibrium point are the same. No disturbance is introduced and the switching action is stable.
2) $M(\infty) < 0$. If a line with a large enough flow is switched off, a large enough disturbance will be introduced into the system which can only endure a limited amount of disturbance, depending on the system inertia and control methods. The system will inevitably be unstable.
3) There exists at least one finite flow value x so that $M(\mathrm{x}) = 0$ as $M(f_{target})$ is a continuous function with $M(0) > 0$ and $M(\infty) < 0$.
4) Different M values may exist for a given line flow value. It is because that different net power injections at buses can lead to the same f_{target}. And the value of M is associated with net power injections. Therefore, the relationship between M and f_{target} is not one to one but a range characterized by an "enveloped function" that wraps all the possible values in the range.

The relationship between the energy margin M and f_{target} can be sketched in Figure 6-4. Instead of a single line in Figure 6-3, it is an enveloped function.

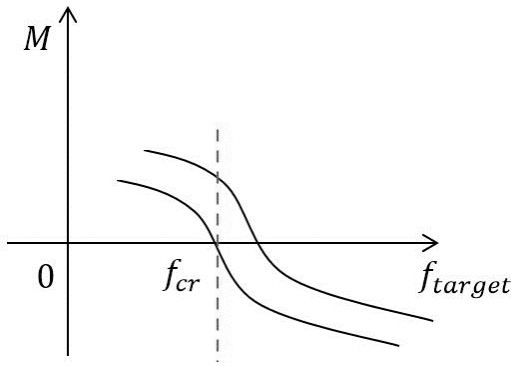

Figure 6-4: Relationship between the energy margin and the flow on the switching target line in a multi-machine system: Reprinted with permission from [© 2018, IEEE]

The CSF f_{cr} is determined at the first zero crossing point. In the region $0 \leq f_{target} < f_{cr}$, $M > 0$. And in the region $f_{target} > f_{cr}$, M may be greater or smaller than 0 showing the system has a risk of instability in the switching action. Selecting first zero crossing point as the CSF may be conservative, but it will lead to safer control guidelines for operation.

6.3 CSF calculation algorithm in the day-ahead stage

The existence of CSF is explained by TEF conceptually, but it is unrealistic to use TEF for actual CSF calculations since it uses simplified models and has inherent conservativeness [27]. In this section, a scalable two-stage Monte Carlo algorithm is proposed to obtain the statistically precise CSF of a line at an hourly basis considering the uncertainties of the system in the day-ahead stage. Detailed industrial models are used in the algorithm. The calculated CSF will indicate the boundary between stable and unstable switching actions and then provide control guidelines to avoid unstable switching actions in the preventive stabilizing redispatch scheme.

It should be pointed out that the calculated CSF here is under a specified range of uncertainties, which needs to be studied and determined. To differentiate from the conceptual CSF

developed in Section 6.2, which has $[0, \infty)$ range, we use the phrase "practical CSF" (PCSF) from now on. To consider the extreme case(s) with low probability that may be missed in the probabilistic study due to the randomness, a safety margin is included in PCSF to further ensure stability in transmission switching actions.

6.3.1 Generation and load distribution modeling

One can model the uncertainties of generations and loads by appropriate probability distributions based on historical data or the past operating experience. The following distributions used in our study are adopted from the research literature [39].

4) Wind generation

Wind speed profile is modeled by the Weibull distribution best with k=2, $c \approx 1.128 v_{mean}$ [39] as shown in (6-9). And the wind power generation from wind speed v is shown in (6-10).

$$f(v) = \frac{k}{c}\left(\frac{v}{c}\right)^{k-1} e^{-(v/c)^{k-1}} \tag{6-9}$$

$$P_{wind} = \begin{cases} 0, & (v < v_{ci}) \cup (v \geq v_{co}) \\ P_w^r \cdot \frac{v - v_{ci}}{v_r - v_{ci}}, & v_{ci} \leq v \leq v_r \\ P_w^r, & v_r \leq v \leq v_{co} \end{cases} \tag{6-10}$$

5) Solar generation

The best function to model the stochastic behavior of solar irradiance s is the Beta distribution [39] as shown in (6-11). The relationship between irradiance s and the solar power generation in [39] can be simplified by assuming a constant temperature. A linear approximation is shown in (6-12).

$$f(s) = \begin{cases} \frac{\Gamma(\alpha+\beta)}{\Gamma(\alpha)\times\Gamma(\beta)} \times s^{\alpha-1} \times (1-s)^{\beta-1}, 0 \leq s \leq 1 \\ 0, \quad otherwise \end{cases} \tag{6-11}$$

$$P_s = P_s^r \cdot s \tag{6-12}$$

where $\beta = (1-\mu_s)\left(\frac{\mu_s(1+\mu_s)}{{\sigma_s}^2}-1\right)$, $\alpha = \frac{\mu_s\beta}{1-\mu_s}$.

6) Load

The uncertainty of load is modeled by the normal distribution [39] in (6-13). And the actual load is decided by (6-14).

$$f_n(l) = \frac{1}{\sigma_l\sqrt{2\pi}} e^{-(1-\mu_l)^2/2{\sigma_l}^2} \tag{6-13}$$

$$S_{load} = (1+l)S_{load}^f \tag{6-14}$$

where $\mu_l = 0$ and $\sigma_l = 0.1$ are used in our case study.

7) Conventional generation

In the preventive stabilizing redispatch scheme, the operator may change the dispatch pattern of conventional generators to stabilize the subsequent switching action. The uncertainties of these control actions are modeled by the uniform distribution within a small range as shown in (6-15), showing the allowed generation adjustment in online operation. And the allowed generation adjustment should be more feasible for generators with high ramp up/down rates.

$$f(P) = \begin{cases} \frac{1}{U_c - L_c}, & L_c \le P \le U_c \\ 0\ , & otherwise \end{cases} \tag{6-15}$$

where $U_c = \min\{P_{max}, P_a + \Delta P\}$, $L_c = \max\{P_{min}, P_a - \Delta P\}$. In our case study, ΔP is selected as 30 MW as an example.

6.3.2 Two-stage PCSF calculation algorithm

In the offline PCSF calculation, we want to find the "enveloped function" caused by all potential scenarios to determine the worst scenario using limited but sufficient samples through statistical means. The proposed two-stage Monte Carlo algorithm is shown in Figure 6-5.

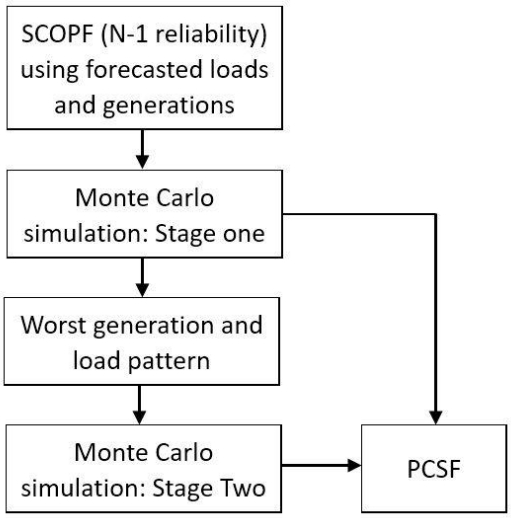

Figure 6-5: Flowchart of the two-stage Monte Carlo based test algorithm: Reprinted with permission from [© 2018, IEEE]

First, a base case with N-1 reliability is set up using forecasted generation and load data in the security constrained OPF (SCOPF). Planned outages are also considered in the SCOPF in the day-ahead scheduling. Then, in stage one, generation and load uncertainties are examined by applying the aforementioned distributions to the base case. The approximate enveloped function is obtained in this stage and the worst generation and load pattern (the case with the minimum unstable switching flow) is found as the first stage solution. It is worth mentioning that the first stage solution is only a less precise worst case found in a cruder scale of uncertainties and we need to refine the first stage solution by pinpointing a more precise worst case. In stage two, finer scaled uncertainties are applied to the first stage solution to create statistically sufficient samples to search for a higher precision boundary between stable and unstable switching actions. Finally, the worst case with the minimum unstable switching flow from both stages determines the PCSF value.

The calculation details of each stage for a line are shown in Figure 6-6. The two stages follow the same procedures but with different base cases and uncertainties used.

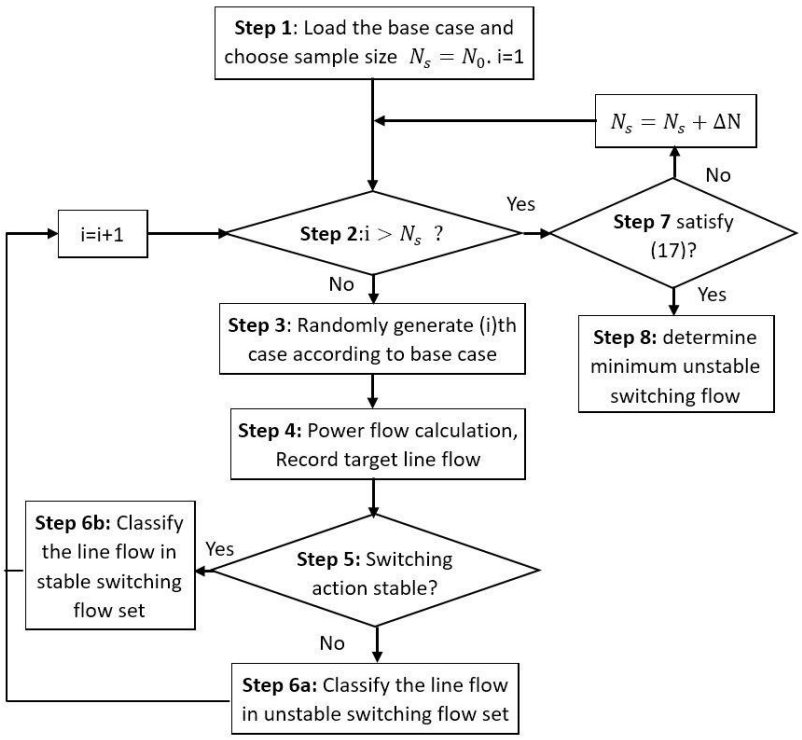

Figure 6-6: Flowchart of each stage of the Monte Carlo simulation: Reprinted with permission from [© 2018, IEEE]

Step 1) Load the base case and choose a sample size N_s. In stage one, the base case is the planned system (N-1 reliable) using the forecasted mean values of generations and loads in the day-ahead stage. In stage two, the base case is the solution of stage one.

Step 2) Check if i > N_s. If yes, which means enough cases are tested, go to **Step 7)**. Otherwise, go to **Step 3)**.

Step 3) Randomly generate the (i)th case with deviations from the base case. In stage one, distributions in Section 6.3.1 are used. In stage two, uniform distributions are applied to all generations and loads in the base case (the first stage solution) to generate samples within $\pm 5\%$ deviations.

Step 4) The flow on the switching target line is obtained and recorded through the power flow calculation.

Step 5) Run the offline stability check for a specified switching action in the randomized case by using (6-16) [65]. Actually (6-16) is an equivalent form of TSI [58]. If (6-16) is satisfied, which means the system is unstable, go to **Step 6a)**. Otherwise, the system is stable in the switching action and **Step 6b)** is followed.

$$AS_{max} - AS(0) > 2\pi \tag{6-16}$$

Step 6a) Classify the line flow into the unstable switching flow set.

Step 6b) Classify the line flow into the stable switching flow set.

Step 7) Check if the coefficient of variation (COV) is satisfied for convergence by using (6-17). If yes, go to **Step 8)**. If not, increase the sample size by a pre-chosen ΔN and continue the test.

$$\mathrm{COV} = \frac{SD(E(X))}{E(X)} = \frac{1}{E(X)}\sqrt{\frac{Var(X)}{N_s}} \leq 1\% \tag{6-17}$$

Step 8) After the COV criterion (6-17) is satisfied, the minimum unstable switching flow of the line is determined based on the worst scenario in the current stage. After finishing the calculations of the both stages, the PCSF is determined by (6-18) with a safety margin included. The selection of ΔS is a trade-off between cost and safety. A large ΔS requires

more flow adjustment but results in a better safety. System operators can choose an appropriate ΔS based on their regulations and accumulated experience.

$$\text{PCSF} = USF_{min} - \Delta S \tag{6-18}$$

6.3.3 Scalability and computational efficiency

All transmission lines in the system are tested one by one for the PCSF calculation in our demonstration. But in reality, system operators can focus on a subset of target lines needed to be switched, which will decrease computational burden greatly. Also, the proposed algorithm can be implemented in parallel computing to accelerate since independent sampling is used. Several computers can run the algorithm simultaneously to test more cases per unit time. Therefore, the proposed probabilistic algorithm is applicable to large realistic systems.

A series of numerical studies on systems of different sizes are performed to estimate the computational time of the proposed algorithm. The computation time is based on a laptop with 2.4GHz CPU and 16GB RAM. The IEEE RTS [66], the modified IEEE-118 bus system [67] and the Texas 2000 system [68] are tested. The first two systems are IEEE standard test systems and the last system is a synthetic system built from public information and a statistical analysis of the real power systems in Texas. The typical computational time without parallel computing for one PCSF calculation is shown in Table 6-1. And the relationship between system size and total computational time is depicted in Figure 6-7, where an approximately linear relationship is shown. The total computational time is increased when system size increases. When the proposed algorithm is applied to a realistic system, for example, the Texas 2000 system, it takes about 80 minutes to calculate the PCSF for a line without parallel computing. Table 6-2 shows the estimated computational time in the Texas 2000 system with different numbers of cases. The computational time is linearly related to the number of cases. Thus, when parallel computing is implemented

with shared memory, the computational time could be reduced to about $1/n_c$ of the original value with n_c computers, which makes the algorithm appropriate for the day-ahead stage calculation.

Table 6-1: Estimation of computational time without parallel computing: Reprinted with permission from [© 2018, IEEE]

System	Buses	Time of stage 1	Time of stage 2	Total
IEEE RTS	24	99.6 s	206.6 s	306.2 s
IEEE-118	118	229.0 s	252.9 s	481.9 s
Texas 2000	2007	2438.6 s	2367.6 s	4806.2 s

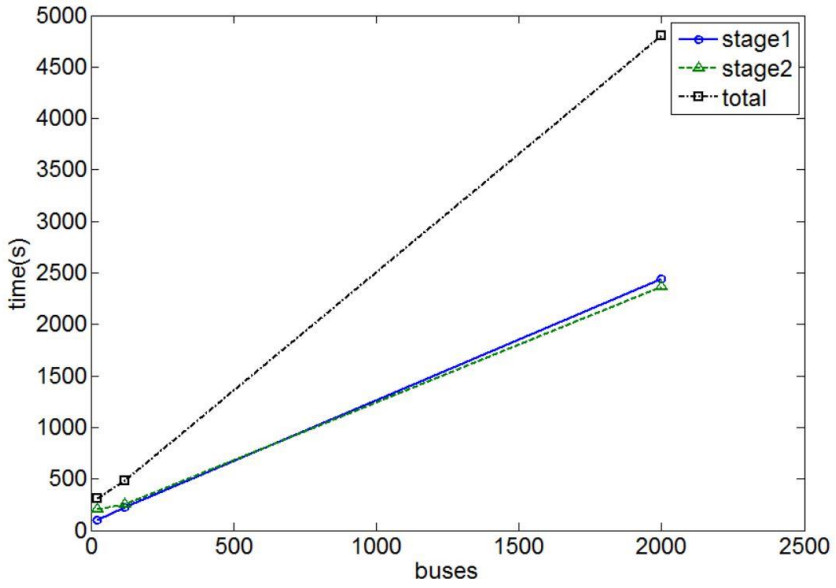

Figure 6-7: System size and computational time without parallel computing: Reprinted with permission from [© 2018, IEEE]

Table 6-2: Estimated computational time with different numbers of cases: Reprinted with permission from [© 2018, IEEE]

Texas 2000 system: Stage 1							
Cases	10	30	50	80	100	150	300
Time (s)	75.3	222.3	362.3	551.1	718.8	1060.8	2438.6

6.4 The preventive stabilizing redispatch scheme

Our proposed preventive stabilizing redispatch scheme is used when a switching plan is found unstable in the online stability check in the operation stage. An alternative stable trajectory will be provided if possible to achieve the same final optimal operating point. Figure 6-8 illustrates the principles of the proposed scheme in transmission switching actions. For simplicity, only a two-dimensional axis is used for illustration. The trajectory of the original switching plan is S_1-S_2-S_3. We wish to drive the system from the original operating point S_1 to a new operating point S_2 by a switching action and then redispatch the system to get to the final operating point S_3, which is obtained by the online 15 minutes economic dispatch with the new system topology. However, such a switching action is infeasible.

In the day-ahead stage shown in Section 6.3, many cases on a planned system with uncertainties are simulated to find the PCSF of the line, which is represented by the enveloped sample set in Figure 6-8. We can find an alternative trajectory S_1-S_1'-S_2'-S_3 indicated by the PCSF. First, a redispatch is done within the enveloped sample set according to the PCSF (S_1 to S_1'). Then, a stable switching action will drive the system to a new operating point (S_1' to S_2'), which is followed by a necessary redispatch again (S_2' to S_3). Thus, the proposed scheme will secure a stable trajectory to the final optimal operating point S_3. The generators involved in the intermediate

redispatch (S_1 to S_1') are chosen in the day-ahead stage based on network knowledge and physical constraints. The previous work [69] shows how to choose generation control pairs for active power control. In this dissertation, index $F_{i,max}^c$ is calculated in (6-19) for each generation control pair (generator i and the generator at the slack bus) to estimate the maximum line flow change by shifting the outputs of a generation control pair. Many sensitivity based methods are available to estimate flow change [69]-[70]. Generation shift distribution factor [70] is used here. And (6-20) is to ensure the redispatch is within the enveloped sample set from the offline study. Then all the generation control pairs are ranked in descending order according to the $F_{i,max}^c$ index. The first n_g generation control pairs are selected for the preventive stabilizing redispatch scheme since their dispatch changes can effectively reduce the flow on the switching target line.

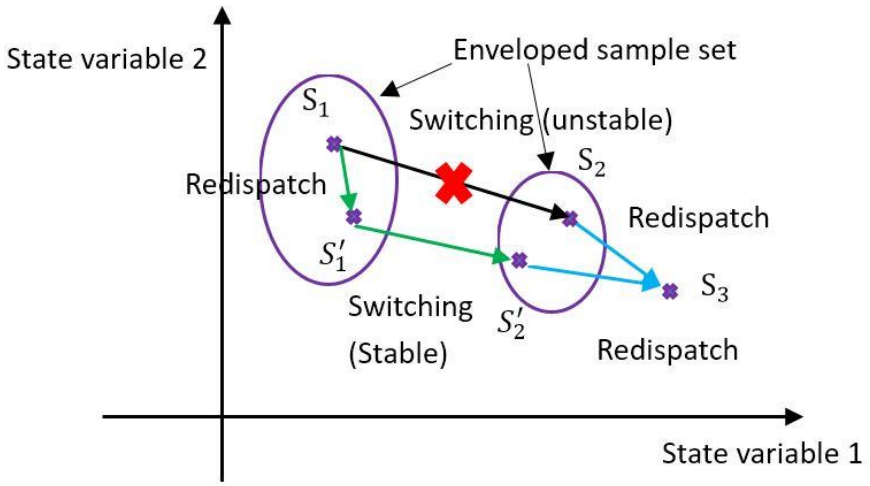

Figure 6-8: Online implementation based on the enveloped sample set: Reprinted with permission from [© 2018, IEEE]

$$F_{i,max}^c = \Delta P_{i,max} DF_i \tag{6-19}$$

$$\Delta P_{i,max} = \begin{cases} P_{i,a} + \Delta P_i - P_i, & if\ DF_i > 0 \\ P_{i,a} - \Delta P_i - P_i, & if\ DF_i < 0 \end{cases} \quad (6\text{-}20)$$

The detailed procedures of the scheme are as follows:

Step 1) Estimate if it is feasible to decrease the line flow to a value below the PCSF within the pre-studied enveloped sample set by using (6-21). If (6-21) is satisfied, **Step 2)** is followed. Otherwise, the switching plan is abandoned.

$$\sum_{i=1}^{n_g} F_{i,max}^{c} \geq f_{original} - \text{PCSF} \quad (6\text{-}21)$$

Step 2) Redispatch the selected n_g generation control pairs so that (6-22) is satisfied to make the new flow below the PCSF. The n_g generation control pairs are dispatched in descending order of $F_{i,max}^{c}$, i.e. the generation control pair with the largest $F_{i,max}^{c}$ is dispatched first. And it always takes full use of one generation control pair before the next one is used.

$$\sum_{i=1}^{n_g} \Delta P_{i,ac}\, DF_i = f_{original} - \text{PCSF} \quad (6\text{-}22)$$

where $\Delta P_{i,ac} > 0$ when $DF_i > 0$, $\Delta P_{i,ac} < 0$ when $DF_i < 0$.

Step 3) Compute the new AC power flow and check if the flow is below the PCSF. If not, repeat **Step 2)** until the new line flow is equal or smaller than the PCSF.

Step 4) Switch off the line and make a necessary redispatch to recover to the final optimal dispatch for the new system.

Please note that the preventive stabilizing redispatch scheme is only a temporary measure for line switching actions to avoid potential stability issues. Optimality of the system is not a concern since the final optimal dispatch value will be recovered at **Step 4)**. And the ramp up/down cost of generators in the redispatch scheme is not considered in this dissertation since the redispatch is temporary. If the ramp up/down cost in the ancillary service market is too high

compared to the saving from the optimal line switching, the operator can always abort the line switching action. This would not happen too often if the day ahead planning is done properly.

6.5 Numerical examples

Detailed numerical examples are shown on the modified IEEE-118 bus system [67]. Dynamic data is created with reference to PSS/E typical data and PJM dynamic data. There are 118 buses and 187 branches in the system. The total generation capacity is 8096.6 MW including 500 MW solar generation and 496.8 MW wind generation.

6.5.1 Offline calculation of PCSF

For one hour in the day-ahead stage, the planned system has a forecasted load of 5874.7 MW. The renewable forecasts are 422.4 MW and 496.8 MW for the solar and wind generation respectively. The PCSF results of 5 lines are shown in Table 6-3, where $N_s = 300$ and $\Delta N = 50$.

Table 6-3: PCSF determination in the day-ahead stage: Reprinted with permission from [© 2018, IEEE]

Line no.	Stage	Cases	Unstable switching flows	Stable switching flows	PCSF
65-68	1	350	506.9-780.6 MW (16 cases)	204.1-554.6 MW (334 cases)	480.2 MW
	2	300	489.5-563.9 MW (149 cases)	436.6-513.0 MW (151 cases)	
68-81	1	300	468.4-558.6 MW (21 cases)	238.0-492.3 MW (279 cases)	449.3 MW
	2	300	458.0-514.8 MW (170 cases)	421.8-469.9 MW (130 cases)	
77-82	1	300	297.6-390.4 MW (144 cases)	236.1-309.3 MW (156 cases)	288.2 MW
	2	300	293.8-317.7 MW (168 cases)	279.8-297.4 MW (132 cases)	
81-80	1	300	459.2-519.1 MW (16 cases)	238.4-478.0 MW (284 cases)	440.3 MW
	2	300	448.8-503.4 MW (152 cases)	417.5-459.7 MW (148 cases)	
92-89	1	300	328.4-389.7 MW (54 cases)	217.7-335.8 MW (246 cases)	318.9 MW
	2	300	325.1-346.3 MW (155 cases)	312.0-328.8 MW (145 cases)	

And a safety margin $\Delta S = 0.019 \times USF_{min}$ is included in the PCSF as an example to avoid all unstable switching actions and guarantee the success of the preventive stabilizing redispatch. The rest of the lines are free of transient instability in switching actions and no meaningful PCSF exists for them.

6.5.2 Offline validation of PCSF and the proposed scheme

To validate the above PCSF results and the proposed preventive stabilizing redispatch scheme in the day-ahead stage, a bigger sample set (1000 cases) that is independent of Section 6.5.1 is created and tested using the distributions in Section 6.3.1. It is to simulate all possible scenarios in the operation stage. The results are shown in Table 6-4. The calculated PCSF values are valid to avoid all unstable scenarios. Moreover, the proposed redispatch scheme is activated when there are sufficient resources to redispatch and decrease the flow on the switching target line to a value below the PCSF. The proposed scheme is activated in 371 out of 800 unstable switching cases in total. All the 371 activated cases are stabilized in switching actions. The proposed scheme will not be activated for the rest of unstable cases because of insufficient resources to redispatch.

Table 6-4: PCSF result validation: Reprinted with permission from [© 2018, IEEE]

Line No.	Cases	Unstable switching flows	Stable switching flows	PCSF	Preventive scheme activated
65-68	1000	507.3-713.3 MW (47 cases)	189.8-574.6 MW (953 cases)	480.2 MW	24
68-81	1000	453.3-584.9 MW (72 cases)	226.3-490.5 MW (928 cases)	449.3 MW	59
77-82	1000	296.8-389.5 MW (490 cases)	222.9-311.6 MW (510 cases)	288.2 MW	223
81-80	1000	454.7-552.3 MW (42 cases)	216.6-490.5 MW (958 cases)	440.3 MW	32
92-89	1000	327.7-393.1 MW (149 cases)	224.6-339.3 MW (851 cases)	318.9 MW	33

6.5.3 Online application of PCSF based preventive scheme

In this section, two online cases are shown in detail to illustrate the proposed preventive stabilizing redispatch based on the calculated PCSF from the day-ahead stage.

Case 1: In the day-ahead stage, a switching plan (line 81-80) with corresponding dispatch change is calculated for an hour, in which cheap generation can be fully utilized. Compared with dispatch only, the optimal switching and dispatch together can decrease the hourly operational cost from 2962.0 to 2603.8, which is a reduction of 12.1%.

In this online case, the total load is 5952.3 MW and renewable generations are 433.9 MW and 496.8 MW for the solar and wind respectively. The load is 1.3% more and solar generation is 2.7% more when compared with the forecasted values, which is covered by our offline study. Although the total deviation is not significant, the flow on line 81-80 has deviated from the planned mean value 362.6 MW to 464.5 MW in the online case due to area-wise significant deviations.

From our offline study, the PCSF of line 81-80 is found to be 440.3 MW in Table 6-3, which is smaller than the measured flow on line 81-80 (464.5 MW). Switching off line 81-80 is found unstable in the online stability check as shown in Figure 6-9. The proposed preventive stabilizing redispatch scheme is activated since there are enough resources to redispatch the system. Generators at bus 87, 92, 111 and 61 are chosen for the redispatch scheme to secure the switching action. The proposed control actions modify the original switching plan (S_1 to S_3 in Figure 6-8) as follows:

1) Redispatch the system at t=1s. Change generator outputs ($\Delta P_{111} = 38.5\ MW$ and $\Delta P_{61} = -43.1\ MW$) to decrease the line flow to 438.7 MW, which is smaller than the PCSF of the line. System operating point moves from S_1 to S_1' by the redispatch.

2) Switch off line 81-80 at t=10s. System operating point moves from S_1' to S_2' by the stable switching action.

3) Make a necessary redispatch again at t=30s to recover to the final optimal dispatch of the system, which is obtained with the new system topology (S_2'). System operating point moves from S_2' to S_3 by the redispatch.

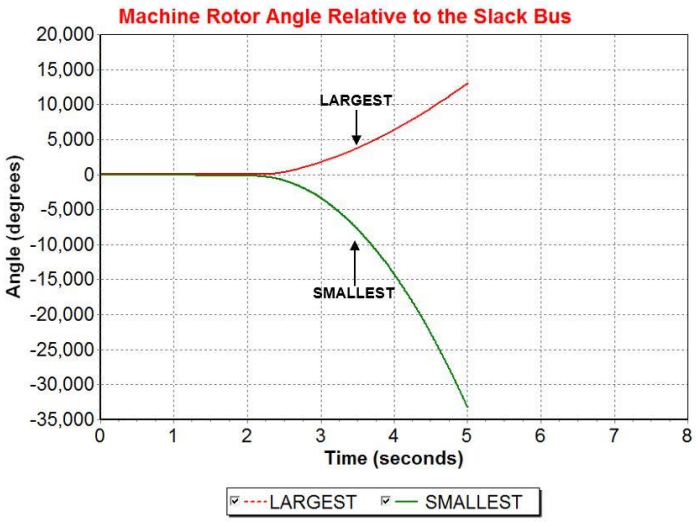

Figure 6-9: Case 1: loss of synchronism without the preventive stabilizing redispatch: Reprinted with permission from [© 2018, IEEE]

In contrast with Figure 6-9, the effectiveness of the proposed preventive stabilizing redispatch is shown in Figure 6-10, in which all generators remain synchronized resulting in finite rotor angle difference between connected buses.

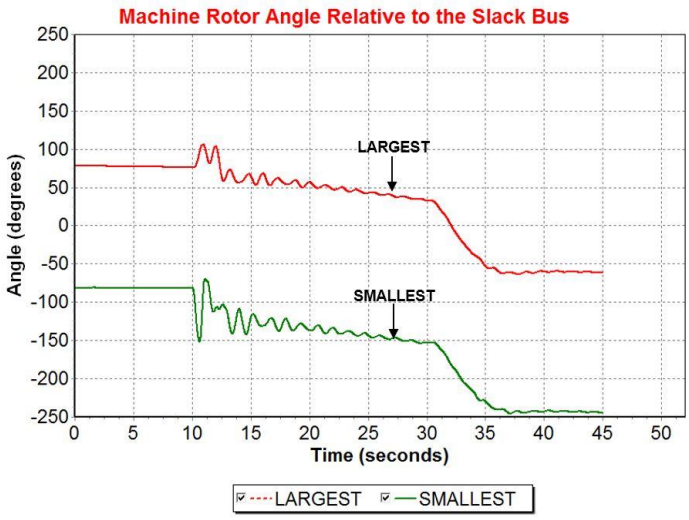

Figure 6-10: Case 1: synchronism intact with our proposed redispatch scheme: Reprinted with permission from [© 2018, IEEE]

Case 2: Another switching plan (line 68-81) is shown for the hour. Compared with dispatch only, the operational cost is reduced from 2962.0 to 2603.7.

In this online case, the total load is 6057.7 MW and solar and wind generations are 446.6 MW and 496.8 MW. The flow on line 68-81 has a significant deviation from 371.5 MW in the planned case to 528.5 MW here. The original switching action is unstable in the online stability check as shown in Figure 6-11. Our proposed redispatch scheme is applied with the same procedures followed as in Case 1. The line flow on the switching target line is reduced to 434.9 MW (below the PCSF value, 449.3 MW) by the redispatch ($\Delta P_{87} = 57.3$ MW, $\Delta P_{92} = 32.3$ MW, $\Delta P_{111} = 39.2$ MW, $\Delta P_{61} = -151.0$ MW). Then the switching action is stabilized and the final optimal operating point is recovered as shown in Figure 6-12.

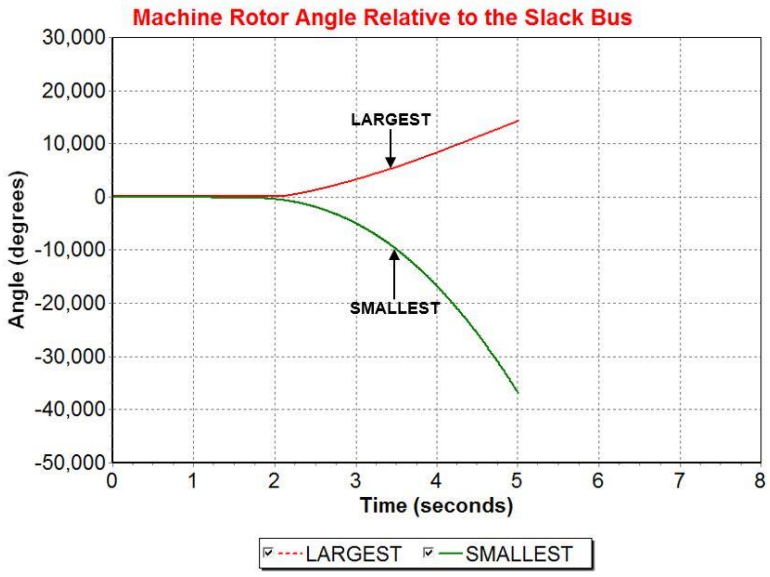

Figure 6-11: Case 2: loss of synchronism without the preventive stabilizing redispatch: Reprinted with permission from [© 2018, IEEE]

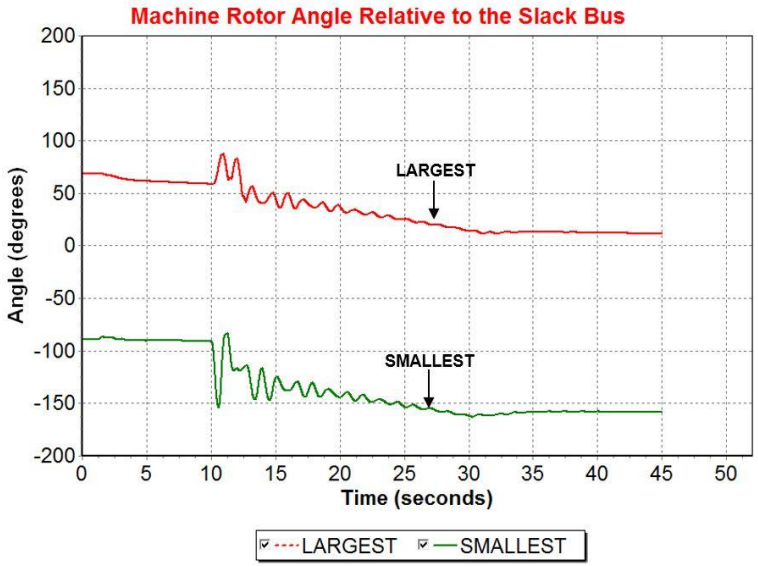

Figure 6-12: Case 2: synchronism intact with our proposed redispatch scheme: Reprinted with permission from [© 2018, IEEE]

6.6 Summary

Transmission switching actions have great potential to resolve power system economic operation and contingency problems. However, transient stability is a concern for such controls. In Section 6, a PCSF based preventive stabilizing redispatch scheme is proposed to enhance system stability in switching actions. The PCSF is calculated in the day-ahead stage using a two-stage Monte Carlo algorithm considering various uncertainties in the system. In the real time operation stage, when a switching plan is found unstable, the line flow on the switching target line is decreased to a value below the PCSF by the proposed scheme to stabilize the subsequent switching action. Numerical results demonstrate the effectiveness and scalability of the proposed scheme.

7. CYBER-SECURITY ANALYSIS FOR TRANSMISSION SWITCHING ACTIONS*

Cyber-security is a crucial factor for modern power systems as many applications heavily rely on the result of state estimation in energy management system (EMS). Therefore, it is necessary to assess and enhance cyber-security for new applications in power systems. As an emerging technology, transmission switching has been investigated in stability and reliability perspectives while the associated cyber-security issue has not been studied yet. In Section 7, the FDIA against power system state estimation is investigated for systems incorporated with transmission switching actions. The mathematical requirements of achieving successful FDIA are proposed. And the physical impact of the FDIA on power system stability is illustrated. Finally, a countermeasure scheme is proposed to prevent the FDIA from devastating the system in the transmission switching actions. Numerical examples are given on the IEEE 24 bus RTS.

The symbols used in Section 7 are listed as follows.

z	Measurement
h	Nonlinear measurements function
x	State variable
e	Random noise
$\hat{x}$	Estimated state variable
W	Weight matrix
$\hat{r}$	Residue

Δz	Measurement change
Δx	Change of state variable
$\hat{x}_a$	State variable under FDIA
$\hat{r}_a$	Residue under FDIA
z_a	Measurement under FDIA
P_{mk}, Q_{mk}	Real and reactive line flow
P_k, Q_k	Real and reactive power nodal injections
V_m	Voltage magnitude of bus m
δ_{mk}	Bus angle difference between bus m and k
g_{mk}+jb_{mk}	Line admittance
B_{mk}^{shunt}	Line shunt susceptance
t_{mk}	Transformer tap ratio ($t_{mk} = 1$ for non-transformer branch)
c	Binary index for transformer tap side ($c = 1$ if m is the tap side of transformer; $c = 0$ if k is the tap side of transformer)
S_m	Set of all buses connected to bus m
G_{ki}+jB_{ki}	Real and reactive part of element Y_{ki} in admittance matrix
Δz^{DC}	Calculated measurements change from DC power flow equations
ΔP_i	Submatrix of real power nodal injection change
ΔP_{ij}	Submatrix of real power flow change on transmission lines
H_{22}^{DC}, H_{42}^{DC}	Submatrix corresponding to ΔP_i and ΔP_{ij} respectively
$\Delta \delta^{DC}$	Change of bus angles in DC power flow equations
Δz^{Aug}	Matrix of measurement change in imperfect FDIA

H^{Aug}	Augmented H matrix
Δx^{DC}	Designed state variable changes in imperfect FDIA
H^{AC}	Jacobian matrix of $h(x)$
Δx^{AC}	Change of state variables in AC estimation under imperfect FDIA
$V = [V_1 \quad ... \quad V_n]^T$	Vector of bus voltage magnitudes
$\delta = [\ \delta_1 \quad ... \quad \delta_n]^T$	Vector of bus angles
$P = [P_1 \quad ... \quad P_n]^T$	Vector of nodal real power injections
$Q = [Q_1 \quad ... \quad Q_n]^T$	Vector of nodal reactive power injections
$P_L = [P_{12} \quad ... \quad P_{ij}]^T$	Vector of line real power flow measurements
$Q_L = [Q_{12} \quad ... \quad Q_{ij}]^T$	Vector of line reactive power flow measurements
P_{ij}	Real power flow from bus i to bus j
π_j, π_i	LMP at bus j and bus i
P_{ij}^S	Real power flow on line from bus i to bus j at planning stage
CSF_{ij}	CSF index for line from bus i to bus j
M	Pre-defined margin

7.1 Introduction

7.1.1 Power system state estimation in the energy management system

EMS is a collection of computerized tools used to monitor, control, and optimize the performance of modern power systems. And power system state estimation is the core of the EMS. Online measurements are collected from supervisory control and data acquisition (SCADA) system and phasor measurement unit (PMU). Then the system current operating states are

calculated in the state estimator based on the obtained measurements and various control actions will be applied accordingly.

It can be seen that modern power systems are complicated cyber-physical systems, in which many applications heavily rely on the result of state estimation in the EMS. Therefore, cyber-security has become a key factor in modern power grids. As stated in the literature review (Section 1.2.2), the FDIA could compromise both the AC estimation and the DC estimation and make significant influence on power systems. That is why we need to assess and enhance cyber-security for new applications, such as transmission switching actions.

7.1.2 Power system operation with transmission switching actions

1) Implementation of transmission switching actions

The framework of transmission switching is shown in Figure 7-1. OTS is incorporated in the unit commitment and scheduling at the day-ahead planning stage [9]. The calculated switching plan will be provided for the real-time operation. Offline stability study for switching actions is also performed at the day-ahead planning stage as stated in Section 5-6. And in the real-time operation, system states are obtained by state estimator based on online measurements. Then loading conditions are determined using the generation data and the calculated nodal power injections. The obtained system information from state estimation is then used in the online stability check for the proposed switching plan. If the online stability check is passed, the switching action will be carried out with the corresponding generation dispatch. Otherwise, only a generation dispatch will be carried out with no switching action.

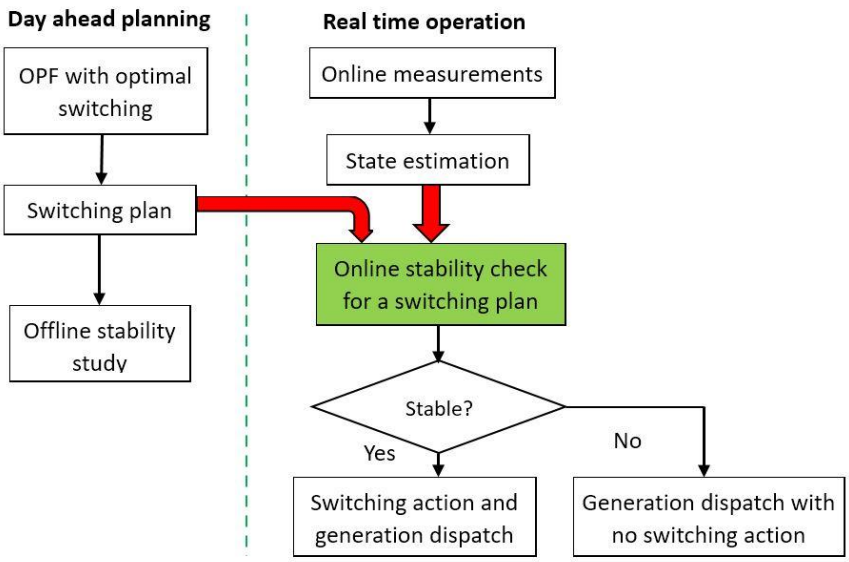

Figure 7-1: Relationship between switching actions and state estimation: Reprinted with permission from [© 2017, IEEE]

2) Impact of line flow on system transient stability

In Section 6, system transient stability is proven to be strongly related to the real power flow measurement on the switching target line. The suddenly disruption of the flow in a switching action will cause power imbalance for machines. As the line flow becomes heavier, power imbalance will be more severe and make the system less stable. When the disturbance is bigger than the critical amount that a physical system can endure, the system becomes unstable in the switching action.

Therefore, the integrity of data in state estimation will affect the accuracy of the online stability check (an unstable switching action seems to be stable) and moreover may affect the physical system stability in switching actions misled by the inaccurate stability check.

7.2 FDIA in transmission switching actions

The aim of the proposed FDIA is to decrease real the power flow measurement of a switching target line to alter the result of the online stability check for transmission switching actions, which undermines the physical system stability in the subsequent switching action. Meanwhile, residues under the FDIA must remain the same or the change of residues is small enough to pass the bad data detection.

7.2.1 FDIA against the AC state estimation

The AC state estimation is used to obtain accurate state variables for power system operation as shown in (7-1)-(7-2) by using the weighted least squares method. And the residue based bad data detection is used after the best estimate is given as shown in (7-3). A threshold is pre-defined in the largest normalized residual test [71] to identify bad data.

$$z = h(x) + e \tag{7-1}$$

$$\hat{x} = \arg\min(z - h(\hat{x}))^T W\,(z - h(\hat{x})) \tag{7-2}$$

$$\hat{r} = z - h(\hat{x}) \tag{7-3}$$

The residue under attack is given in (7-4) and the condition of an undetected FDIA is given in (7-5). Generally, it is difficult to achieve the undetected FDIA since both system parameters and current state variables are needed to conceal the attack perfectly.

$$\hat{r}_a = z + \Delta z - h(\hat{x}_a) = z + \Delta z - h(\hat{x} + \Delta x) = z + \Delta z - h(\hat{x} + \Delta x) + h(\hat{x}) - h(\hat{x})$$

$$= \hat{r} + \Delta z - h(\hat{x} + \Delta x) + h(\hat{x}) \tag{7-4}$$

$$\Delta z = h(\hat{x} + \Delta x) - h(\hat{x})\ or\ z_a = h(\hat{x}_a) + e \tag{7-5}$$

7.2.2 Perfect FDIA for transmission switching actions

Here is our proposed method to formulate a perfect FDIA to satisfy condition (7-5). In order to change the real power flow P_{mn} on the switching target line, the attacker could aim to

change the bus angle of either end of the switching target line to decrease angle difference between two buses while keeping all other state variables unchanged. As shown in Figure 7-2, we assume the attacker aims to change δ_m to decrease P_{mn}. Then the attacker must modify the line flow and nodal power injection measurements simultaneously to achieve the FDIA as shown in (7-6)-(7-9).

$$P_{mk} = -\frac{V_m V_k}{t_{mk}}(g_{mk}\, cos(\delta_{mk}) + b_{mk}\, sin(\delta_{mk})) + \left(\frac{V_m^2 g_{mk}}{t_{mk}^2}\right) c + V_m^2 g_{mk}(1-c),\ \forall k \in S_m \tag{7-6}$$

$$Q_{mk} = -\frac{V_m V_k}{t_{mk}}(g_{mk}\, sin(\delta_{mk}) - b_{mk}\, cos(\delta_{mk})) - V_m^2\left(\frac{b_{mk}}{t_{mk}^2} + \frac{B_{mk}^{shunt}}{2}\right) c - V_m^2\left(b_{mk} + \frac{B_{mk}^{shunt}}{2}\right)(1-c), \quad \forall k \in S_m \tag{7-7}$$

$$P_k = V_k \sum_{i \in S_k} V_i (G_{ki} \cos(\delta_{ki}) + B_{ki} \sin(\delta_{ki})) \quad \forall k \in (S_m \cup \{m\}) \tag{7-8}$$

$$Q_k = V_k \sum_{i \in S_k} V_i (G_{ki} \sin(\delta_{ki}) - B_{ki} \cos(\delta_{ki})) \quad \forall k \in (S_m \cup \{m\}) \tag{7-9}$$

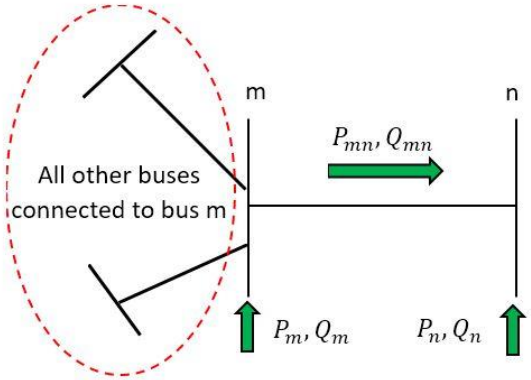

Figure 7-2: Undetected FDIA to decrease real line flow of switching target line: Reprinted with permission from [© 2017, IEEE]

7.2.3 Imperfect FDIA for transmission switching actions

Although the aforementioned FDIA can decrease real line flow perfectly without increasing residues, it is hard to get all the required system information. Therefore, in this part, we propose an imperfect FDIA scheme against the AC estimation using an attack vector constructed from the DC estimation equations.

The DC estimation is formulated by (7-10)-(7-11), in which a linearized constant H matrix is used. If attackers know the ith column of the H matrix and modify measurements accordingly as shown in (7-12), state x_i^{DC} will be changed while residues are kept unchanged in DC estimator [29].

$$z^{DC} = Hx^{DC} + e \tag{7-10}$$

$$\hat{x}^{DC} = (H^T W H)^{-1} H^T W z^{DC} \tag{7-11}$$

$$\Delta z^{DC} = H \Delta x^{DC} \tag{7-12}$$

Next, we will show that a valid attack vector for the AC estimation can be constructed from (7-12). Equation (7-12) can be shown in the matrix form in (7-13). Since DC power flow equations only use bus angle as state variables and ignore reactive power measurements, equation (7-13) is not an appropriate form of the attack vector against the AC estimation. We need to augment the matrix in (7-13) to construct a valid attack vector in the right form as shown in (7-14), in which bus angle and voltage are used as state variables and reactive power measurements are also included. Then (7-14) is plugged into (7-4) and we can get the residue of the AC estimation under the imperfect FDIA as shown in (7-15). First order Taylor expansion is done for $h(\hat{x} + \Delta x^{AC})$ at $x = \hat{x}$, which yields (7-16).

$$\Delta z^{DC} = \begin{bmatrix} \Delta P_i \\ \Delta P_{ij} \end{bmatrix} = \begin{bmatrix} H_{22}^{DC} \\ H_{42}^{DC} \end{bmatrix} \Delta \delta^{DC} \tag{7-13}$$

$$\Delta z^{Aug} = H^{Aug}\Delta x^{DC} = \begin{bmatrix} 0 & 0 \\ 0 & H_{22}^{DC} \\ 0 & 0 \\ 0 & H_{42}^{DC} \\ 0 & 0 \end{bmatrix} \begin{bmatrix} 0 \\ \Delta\delta^{DC} \end{bmatrix} = \begin{bmatrix} 0 \\ \Delta P_i \\ 0 \\ \Delta P_{ij} \\ 0 \end{bmatrix} \tag{7-14}$$

$$\hat{r}_a = z + H^{Aug}\Delta x^{DC} - h(\hat{x}_a) = z + H^{Aug}\Delta x^{DC} - h(\hat{x}_a) + h(\hat{x}) - h(\hat{x})$$

$$= \hat{r} + H^{Aug}\Delta x^{DC} - (h(\hat{x} + \Delta x^{AC}) - h(\hat{x})) \tag{7-15}$$

$$\hat{r}_a = \hat{r} + H^{Aug}\Delta x^{DC} - (h(\hat{x}) + \frac{\partial h}{\partial x}|_{x=\hat{x}}\Delta x^{AC} - h(\hat{x})) = \hat{r} + (H^{Aug}\Delta x^{DC} - \frac{\partial h}{\partial x}|_{x=\hat{x}}\Delta x^{AC})$$

$$= \hat{r} + (H^{Aug}\Delta x^{DC} - H^{AC}\Delta x^{AC}) \tag{7-16}$$

The H^{AC} is shown in (7-17). Note that in power flow equations, real power is more sensitive to bus angle while reactive power is more sensitive to bus voltage. Thus we can ignore the terms $\frac{\partial P}{\partial V}$, $\frac{\partial P_L}{\partial V}$, $\frac{\partial Q}{\partial \delta}$ and $\frac{\partial Q_L}{\partial \delta}$ in the Jacobian matrix. Then residue under the imperfect FDIA is shown in (7-18) by expanding (7-16) into the matrix form.

$$H^{AC} = \begin{bmatrix} H_{11}^{AC} & H_{12}^{AC} \\ H_{21}^{AC} & H_{22}^{AC} \\ H_{31}^{AC} & H_{32}^{AC} \\ H_{41}^{AC} & H_{42}^{AC} \\ H_{51}^{AC} & H_{51}^{AC} \end{bmatrix} = \begin{bmatrix} \frac{\partial V}{\partial V}\Big|_{x=\hat{x}} & \frac{\partial V}{\partial \delta}\Big|_{x=\hat{x}} \\ \frac{\partial P}{\partial V}\Big|_{x=\hat{x}} & \frac{\partial P}{\partial \delta}\Big|_{x=\hat{x}} \\ \frac{\partial Q}{\partial V}\Big|_{x=\hat{x}} & \frac{\partial Q}{\partial \delta}\Big|_{x=\hat{x}} \\ \frac{\partial P_L}{\partial V}\Big|_{x=\hat{x}} & \frac{\partial P_L}{\partial \delta}\Big|_{x=\hat{x}} \\ \frac{\partial Q_L}{\partial V}\Big|_{x=\hat{x}} & \frac{\partial Q_L}{\partial \delta}\Big|_{x=\hat{x}} \end{bmatrix} \approx \begin{bmatrix} I & 0 \\ 0 & \frac{\partial P}{\partial \delta} \\ \frac{\partial Q}{\partial V} & 0 \\ 0 & \frac{\partial P_L}{\partial \delta} \\ \frac{\partial Q_L}{\partial V} & 0 \end{bmatrix}\Bigg|_{x=\hat{x}} \tag{7-17}$$

$$\hat{r}_a \approx \hat{r} + \left(\begin{bmatrix} 0 & 0 \\ 0 & H_{22}^{DC} \\ 0 & 0 \\ 0 & H_{42}^{DC} \\ 0 & 0 \end{bmatrix} \begin{bmatrix} 0 \\ \Delta\delta^{DC} \end{bmatrix} - \begin{bmatrix} H_{11}^{AC} & 0 \\ 0 & H_{22}^{AC} \\ H_{31}^{AC} & 0 \\ 0 & H_{42}^{AC} \\ H_{51}^{AC} & 0 \end{bmatrix} * \begin{bmatrix} \Delta V^{AC} \\ \Delta\delta^{AC} \end{bmatrix} \right) = \hat{r} + \begin{bmatrix} -H_{11}^{AC}\Delta V^{AC} \\ H_{22}^{DC}\Delta\delta^{DC} - H_{22}^{AC}\Delta\delta^{AC} \\ -H_{31}^{AC}\Delta V^{AC} \\ H_{42}^{DC}\Delta\delta^{DC} - H_{42}^{AC}\Delta\delta^{AC} \\ -H_{51}^{AC}\Delta V^{AC} \end{bmatrix} \tag{7-18}$$

When we use the conditions of the DC flow approximation in H_{22}^{AC} and H_{42}^{AC} calculation, they become equal to H_{22}^{DC} and H_{42}^{DC}. And if the AC estimation actually yields similar angle

information as calculated by the DC power flow ($\Delta\delta^{DC} \approx \Delta\delta^{AC}$), which is highly possible as the DC approximation is a good approximation in power systems, (7-18) can be further simplified into (7-19).

$$\hat{r}_a \approx \hat{r} + \begin{bmatrix} -H_{11}^{AC}\Delta V^{AC} \\ 0 \\ -H_{31}^{AC}\Delta V^{AC} \\ 0 \\ -H_{51}^{AC}\Delta V^{AC} \end{bmatrix} \tag{7-19}$$

It can be seen from (7-19) that the residues for real power related measurements in the AC estimation under the imperfect FDIA are almost unchanged. On the contrary, the residues for voltage and reactive power related measurements will have bigger changes, which may be identified as bad data if the residues are beyond a pre-defined threshold. Therefore, the attacker may use the local system information in H^{Aug} and DC power flow equations to obtain a valid attack vector to change the real power flow on the switching target line. Despite bad data may be detected in the system, false data injection on real power related measurements will be concealed. Instead, other measurements may be identified and deleted in the state estimation.

7.3 Practical attacking scheme and countermeasure

7.3.1 Attacking strategy

Searching for switching target lines that are beneficial to the system cost is hard in an attacker's perspective with limited knowledge of the system. Therefore, we propose a practical scheme here, in which an attacker searches for beneficial lines according to an index based on the openly accessible locational marginal price (LMP) and the line flow measurements as shown in (7-20). If index α_{ij} is negative with large absolute value, which means real power flow is from the high LMP to the low LMP, switching off the line has the potential to reduce the system cost in OTS [7]. The index was originally proposed in [7] as a prescreening index for OTS problems.

$$\alpha_{ij} = (\pi_j - \pi_i)P_{ij} \tag{7-20}$$

After determination of a switching target line to attack, the attacker can use (7-5) or (7-14) to construct a valid attack vector based on his knowledge on the system to decrease the real power flow on the line. The bigger real power flow on the switching target line, the more unstable the system is in a switching action as stated in Section 6. Therefore, the attack vector from (7-5) or (7-14) is highly likely to change the online stability check result and causes transient instability in the subsequent switching action.

7.3.2 Countermeasure

In previous literature [29], [72]-[73], the countermeasure for cyber-attack is to find key locations/measurements to protect. Once a set of basic measurements are secured, the existing false data will be detected easily. Based on that principle, a countermeasure for the FDIA in transmission switching actions is proposed to protect key substations. A transient stability index CSF is calculated in the power system day-ahead planning stage in Figure 7-1 as stated in Section 6. The CSF shows the maximum allowed real power flow for a stable switching action. And when the real power flow is greater than the CSF, a switching action becomes unstable. Therefore, if the real power flow of a switching target line in the planning stage is close to the CSF as shown in (7-21), this line will have potential transient instability issue since the uncertainty of load and generation may cause the actual line flow greater than the CSF in the real-time operation.

$$\left|CSF_{ij} - P_{ij}\right| \leq M \tag{7-21}$$

Once a risky line in transmission switching actions is found by (7-21), the two substations at both ends of the line must be secured in case of the FDIA to affect system physical stability in operation.

7.4 Numerical study

The IEEE 24 bus RTS [66] is used for demonstration in this part. Among the 38 branches, 10 lines satisfy condition (7-20) and 3 of them are actually beneficial to the system operating cost if switched off with the corresponding dispatch. And 1 out of these 3 lines has potential transient stability issue in the transmission switching action. Thus, using publicly available LMPs and flow measurements in (7-20), the attacker has about 10% possibility to find a switching target line for the FDIA without full knowledge of the system.

The case of line 10-11 is illustrated in detail to show how the attacker can implement the FDIA as mentioned in Section 7.3. Switching off line 10-11 with the corresponding dispatch will decrease operating cost by 0.72%. And the CSF of it is calculated as 215.3 MW in the day-ahead planning stage. In the online case, the actual flow is 234.4 MW, which means the switching action will cause instability in the physical system.

Now, the perfect and imperfect FDIAs are conducted trying to decrease line flow below the CSF and change the result of the online stability check. In order to do so, it is aimed to decrease the system state δ_{11} by 1 degree. The results of the FDIAs are shown in Table 7-1. Here the threshold for the largest normalized residual test is 1.4395, which is the 85% confidence interval. It can be seen that in the perfect FDIA from (7-6)-(7-9), all measurements near bus 11 must be changed. The bad data detection cannot identify any bad data since residues are the same as in the scenario without any attack. The system state δ_{11} changes by 1 degree. As for the imperfect FDIA from (7-14), only system information around bus 11 is required and fewer measurements are changed. In the bad data detection, two correct reactive power flow measurements are eliminated as bad data and then it passes. Instead, measurements under the actual FDIA are concealed. The system state δ_{11} changes by 1.1 degrees with a slight difference from the planned change.

Table 7-1: The perfect and imperfect FDIAs: Reprinted with permission from [© 2017, IEEE]

Type	Measurements changed	Bad data detection	State change
Perfect FDIA	P_9, P_{10}, P_{11}, P_{13}, P_{14}, Q_9, Q_{10}, Q_{11}, Q_{13}, Q_{14}, $P_{9\,11}$, $P_{10\,11}$, $P_{11\,13}$, $P_{11\,14}$, $Q_{9\,11}$, $Q_{10\,11}$, $Q_{11\,13}$, $Q_{11\,14}$	pass	$\Delta\delta_{11} = 1.0°$
Imperfect FDIA	P_9, P_{10}, P_{11}, P_{13}, P_{14}, $P_{9\,11}$, $P_{10\,11}$, $P_{11\,13}$, $P_{11\,14}$	$Q_{11\,13}$, $Q_{12\,13}$ eliminated and then pass	$\Delta\delta_{11} = 1.1°$

Then the change of the state variable will affect the real power flow on the switching target line as well as related nodal power injections. With the assumption that generation data is accurate, false load values are thus obtained from false nodal power injections in the FDIA in the nearby area of bus 11. Table 7-2 shows the load change and the flow change on the switching target line in the FDIA. $P_{10\,11}$ is decreased to 215.0 MW and 213.1 MW in the perfect FDIA and imperfect FDIA respectively. The false load redistribution and flow change will affect the result of the online stability check significantly.

Table 7-2: Load and line flow changes in the FDIAs: Reprinted with permission from [© 2017, IEEE]

Type	Load change	$\Delta P_{10\,11}$
Perfect FDIA	$\Delta P_9^L = -18.8\text{MW},\ \Delta P_{10}^L = -19.2\text{MW}$ $\Delta P_{11}^L = 110.8\text{MW},\ \Delta P_{13}^L = -35.7\text{MW}$ $\Delta P_{14}^L = -38.8\text{MW}$	234.4MW-215.0MW (19.4MW)
Imperfect FDIA	$\Delta P_9^L = -20.9\text{MW},\ \Delta P_{10}^L = -20.8\text{MW}$ $\Delta P_{11}^L = 119.7\text{MW},\ \Delta P_{13}^L = -37.2\text{MW}$ $\Delta P_{14}^L = -41.7\text{MW}$	234.4MW-213.1MW (21.3MW)

The physical impacts of the perfect and imperfect FDIAs on power system stability are shown in Figure 7-3. In the true system without any FDIA, the online stability check shows the system loses synchronism in the switching action, which should be forbidden. However, with either the perfect FDIA or the imperfect FDIA achieved in the state estimation, the online stability check will be altered showing that the switching action is stable. As a consequence, the allowed switching action will destabilize the power system due to the influence of the FDIAs.

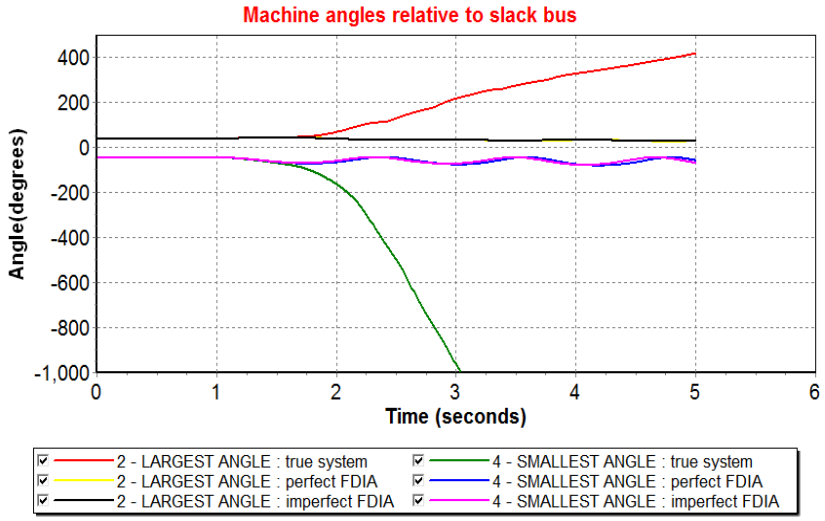

Figure 7-3: Online stability check results: Reprinted with permission from [© 2017, IEEE]

The proposed defending method is applied in this case. *M* in (7-21) is selected to be 30 so that line 10-11 will be found to have potential transient stability issue in the planning stage. Therefore, substations at bus 10 and 11 are specially protected and measurements at these substations cannot be compromised. The result of the AC state estimation and the bad data detection are shown in Table 7-3. With two key substations secured, all bad data can be identified and eliminated by using the largest normalized residual test. The calculated states of the online

case are authentic which will further yield accurate online stability check results. The unstable switching action is avoided in the online operation.

Table 7-3: State estimation with two substations secured: Reprinted with permission from [© 2017, IEEE]

Type	Measurements changed	Bad data detection	$\Delta P_{10\,11}$
Perfect FDIA	P_9, P_{13}, P_{14}, Q_9,Q_{13}, Q_{14}	P_9, P_{13}, P_{14}, Q_9, Q_{13}, Q_{14} eliminated and then pass	0
Imperfect FDIA	P_9, P_{13}, P_{14}	P_9, P_{13}, P_{14} eliminated and then pass	0

7.5 Summary

Modern power systems are cyber-physical systems. The integrity of data is crucial for power system control and operation since many applications rely on the result of the state estimation in the EMS. As an emerging technology, transmission switching is proposed to achieve better economy and solve contingencies. This new application also requires correct data for the necessary online stability check. Thus, an FDIA on the cyber layer may affect the physical system operation and eventually physical stability of the system through this kind of new technology.

In Section 7, the perfect FDIA and imperfect FDIA against the AC estimation are proposed for transmission switching applications. They are aimed to decrease the real power flow on the switching target line in order to alter the result of the online stability check. Also, a practical method to increase the possibility of finding a switching target line in an attacker's perspective is given based on LMPs and line flow measurements. Case studies on the IEEE RTS show that the perfect FDIA can change the real power flow without increasing any residues in the system. And

the imperfect FDIA can also achieve the same goal but some correct measurements are identified as bad data. Both FDIAs will cause serious instability in the physical system through transmission switching actions by altering the online stability check result. An effective countermeasure is provided to pinpoint key substations to protect based on the CSF in the planning stage.

8. SUMMARY

In Section 8, a brief summary of the dissertation is presented. And some potential research topics are discussed for future research.

8.1 Dissertation summary

With large-scale renewable resources integrated in the grid, there will be an unprecedented challenge for power system economical operations. The intermittent wind and solar generations together with the daily load fluctuation may cause transmission congestion in a system at different geographical locations during a day. Thus, the optimal topology of a modern power system is not fixed any more in the daily operations. To deal with this new challenge, OTS is proposed in recent years to track the optimal operating state of a power system. In OTS, transmission lines are actively switched on/off together with the corresponding generation dispatch to optimize the system operation. Although this emerging technology is promising in solving the problem raised by the integration of large-scale renewable generations, there are many key problems that need to be investigated before actual implementation.

In this dissertation, three major problems of OTS are studied thoroughly. The first major problem is how to formulate the OTS problems properly and solve the optimization problems accurately and efficiently. In Section 2, the deterministic formulation of OTS problems incorporated with energy storage devices is given based on the ACOPF. The co-optimization of OTS and batteries shows a superior performance in minimizing the operational cost of the system. Next, the uncertainties of the grid, especially the uncertainties of renewable sources, are taken into consideration in the OTS problems in Section 3. SP is used to represent the uncertainties in the optimization problems. Numerical results demonstrate that SP has a better performance than

deterministic optimization method when uncertainties are presented in the decision-making. In Section 4, we move forward to investigate on how to solve the SP formulation of the AC-OTS efficiently. A new mathematical formulation is proposed and a GBD based algorithm is built to achieve the goal. Numerical studies show that the proposed approach can handle large-scale SP problems efficiently without any sacrifice of accuracy.

The second major problem associated with OTS is the transient stability concern. A switching action may involve a large disturbance in the system and thus the system could lose the synchronism. Investigating under which condition the problem could happen and how to avoid the instability is crucial for this new technology. In Section 5, the basic methods to analyze the transient stability of switching actions are introduced. TCSC and batteries are proved to be effective in enhancing the system transient stability in switching actions. Then Section 6 presents a new transient stability index called CSF for switching actions. Based on the developed index, a preventive stabilizing redispatch scheme is built to avoid unstable switching actions in the online operation stage.

The third major problem is the cyber-security issue associated with OTS. The power system is a cyber-physical system and the control decisions are determined based on the acquired data. In Section 7, it is shown that the FDIA against the state estimator in the EMS could let the operator believe that it is safe to perform a switching action while the switching action is highly risky. The vulnerability is analyzed given that the attacker either has perfect information of the system or only has limited knowledge. To defend such kind of attack, a countermeasure is proposed to identify a subset of risky lines, whose measurements should be secured with extra efforts.

8.2 Future research

Although the three major problems of OTS are investigated in this dissertation, additional research is needed before it is possible to fully implement OTS. The following topics, as the extension of the completed research, are discussed for future research.

8.2.1 Stability issues of switching on actions

In this dissertation, we mainly discuss the transient stability issue of switching off actions since switching on a transmission line usually strengthens the system and will not cause any problem. However, a switching on action can also introduce disturbance in a system because of power imbalance at the switching moment. As we wish to use OTS as a routine method everyday, it is necessary to study whether there is a guarantee that switching on actions are always stable. If not, we need to be aware of which condition could lead to instability. This research may be related to transient stability, small signal stability, voltage stability and subsynchronous oscillation.

8.2.2 Transient stability issues of multiple switching actions

In Section 6, a transient stability index, CSF, is proposed for a switching action and the corresponding preventive stabilizing redispatch scheme is built. However, in OTS, sometimes multiple switching actions are needed. It is still a tough problem about how to determine the sequence of switching actions while keeping the he system stable. The developed scheme is not efficient enough for multiple switching actions right now. And further research should be conducted to revise the scheme or to develop a new scheme.

8.2.3 Power market design for OTS

Currently, a large area of USA is in the deregulated energy market. When implementing OTS in the deregulated area, corresponding market rules should also be designed. The implementation of OTS will have a significant impact on the market operations. For example, the

financial transmission rights and congestion revenue rights may be affected since we will switch lines on/off frequently during a day.

8.2.4 Machine learning for OTS problems

Although a lot of efforts has been taken to accelerate the computation of OTS problems, the computational speed is still relatively slow and not fast enough for online calculation. Using machine learning techniques seems to be a promising way to solve the problem. We can use machine learning to learn the relationship between the system operating state and the optimal line to switch. A massive historical data is available now and could be used for the offline study. Then, in the online operation stage, we can avoid the complicated calculation and implement the OTS action directly based on the real-time measurements and the learned relationship. However, the comprehensive scheme must be developed and make sure the machine learning results will not lead to any bad switching decisions in terms of system cost and system stability.

REFERENCES

[1] R. P. O'Neill, R. Baldick, U. Helman, M. H. Rothkopf and W. Stewart, "Dispatchable transmission in RTO markets," *IEEE Transactions on Power Systems*, vol. 20, no. 1, pp. 171-179, Feb. 2005.

[2] E. B. Fisher, R. P. O'Neill and M. C. Ferris, "Optimal Transmission Switching," *IEEE Transactions on Power Systems*, vol. 23, no. 3, pp. 1346-1355, Aug. 2008.

[3] K. W. Hedman, R. P. O'Neill, E. B. Fisher and S. S. Oren, "Optimal Transmission Switching—Sensitivity Analysis and Extensions," *IEEE Transactions on Power Systems*, vol. 23, no. 3, pp. 1469-1479, Aug. 2008.

[4] K. W. Hedman, R. P. O'Neill, E. B. Fisher and S. S. Oren, "Optimal Transmission Switching With Contingency Analysis," *IEEE Transactions on Power Systems*, vol. 24, no. 3, pp. 1577-1586, Aug. 2009.

[5] K. W. Hedman, M. C. Ferris, R. P. O'Neill, E. B. Fisher and S. S. Oren, "Co-Optimization of Generation Unit Commitment and Transmission Switching With N-1 Reliability," *IEEE Transactions on Power Systems,* vol. 25, no. 2, pp. 1052-1063, May 2010.

[6] K. W. Hedman, S. S. Oren and R. P. O'Neill, "A review of transmission switching and network topology optimization," in 2011 *IEEE Power and Energy Society General Meeting*, San Diego, CA, 2011, pp. 1-7.

[7] J. D. Fuller, R. Ramasra and A. Cha, "Fast Heuristics for Transmission-Line Switching," *IEEE Transactions on Power Systems*, vol. 27, no. 3, pp. 1377-1386, Aug. 2012.

[8] J. C. Villumsen, G. Brønmo and A. B. Philpott, "Line capacity expansion and transmission switching in power systems with large-scale wind power," *IEEE Transactions on Power Systems*, vol. 28, no. 2, pp. 731-739, May 2013.

[9] J. Wu and K. W. Cheung, "Incorporating Optimal Transmission Switching in Day-Ahead Unit Commitment and scheduling," in *2015 IEEE Power & Energy Society General Meeting*, Denver, CO, 2015, pp. 1-5.

[10] Z. Yang, H. Zhong, Q. Xia and C. Kang, "Optimal Transmission Switching With Short-Circuit Current Limitation Constraints," *IEEE Transactions on Power Systems*, vol. 31, no. 2, pp. 1278-1288, March 2016.

[11] M. Soroush and J. D. Fuller, "Accuracies of Optimal Transmission Switching Heuristics Based on DCOPF and ACOPF," *IEEE Transactions on Power Systems*, vol. 29, no. 2, pp. 924-932, March 2014.

[12] M. Khanabadi, H. Ghasemi and M. Doostizadeh, "Optimal Transmission Switching Considering Voltage Security and N-1 Contingency Analysis," *IEEE Transactions on Power Systems*, vol. 28, no. 1, pp. 542-550, Feb. 2013.

[13] F. Capitanescu and L. Wehenkel, "An AC OPF-based heuristic algorithm for optimal transmission switching," in *2014 Power Systems Computation Conference*, Wroclaw, 2014, pp. 1-6.

[14] Y. Bai, H. Zhong, Q. Xia and C. Kang, "A Two-Level Approach to AC Optimal Transmission Switching With an Accelerating Technique," *IEEE Transactions on Power Systems*, vol. 32, no. 2, pp. 1616-1625, Mar. 2017.

[15] B. Kocuk, S. S. Dey and X. A. Sun, "New Formulation and Strong MISOCP Relaxations for AC Optimal Transmission Switching Problem," *IEEE Transactions on Power Systems*, vol. 32, no. 6, pp. 4161-4170, Nov. 2017.

[16] C. Coffrin, H. L. Hijazi, K. Lehmann and P. Van Hentenryck, "Primal and dual bounds for Optimal Transmission Switching," In *2014 Power Systems Computation Conference*, Wroclaw, 2014, pp. 1-8.

[17] P. Dehghanian and M. Kezunovic, "Probabilistic Decision Making for the Bulk Power System Optimal Topology Control," *IEEE Transactions on Smart Grid*, vol. 7, no. 4, pp. 2071-2081, Jul. 2016.

[18] A. Nikoobakht, M. Mardaneh, J. Aghaei, V. Guerrero-Mestre and J. Contreras, "Flexible power system operation accommodating uncertain wind power generation using transmission topology control: an improved linearised AC SCUC model," *IET Generation, Transmission & Distribution*, vol. 11, no. 1, pp. 142-153, Jan. 2017.

[19] G. M. Huang, W. Wang, and J. An, "Stability issues of smart grid transmission line switching," *IFAC Proceedings Volumes*, vol. 47, pp. 7305-7310, 2014.

[20] H. H. Al Marhoon, I. Leevongwat and P. Rastgoufard, "A fast search algorithm for Critical Clearing Time for power systems transient stability analysis, " in *Power Systems Conference (PSC)*, 2014 Clemson University, 11-14 March 2014, pp.1-7.

[21] L. G. W. Roberts, A. R. Champneys, K. R. W. Bell and M. di Bernardo, "Analytical Approximations of Critical Clearing Time for Parametric Analysis of Power System Transient Stability," *IEEE Journal on Emerging and Selected Topics in Circuits and Systems*, vol. 5, no. 3, pp. 465-476, Sep. 2015.

[22] D. Gautam, V. Vittal and T. Harbour, "Impact of Increased Penetration of DFIG-Based Wind Turbine Generators on Transient and Small Signal Stability of Power Systems," *IEEE Transactions on Power Systems*, vol.24, no.3, pp.1426-1434, Aug. 2009.

[23] M. A. Chowdhury, W. Shen, N. Hosseinzadeh and H. R. Pota, "Quantitative assessment and comparison of fault responses for synchronous generator and wind turbine generators based on modified transient energy function," *IET Renewable Power Generation*, vol.8, no.5, pp.474-483, Jul. 2014.

[24] P. Kundur, Power system stability and control, 1th ed. New York: McGraw-Hill, 2012.

[25] P. M. Anderson and A. A. Fouad, Power system control and stability, 2th ed. New York: Institute of Electrical and Electronics Engineers, Inc., 1994.

[26] H.-D. Chiang, F. Wu and P. Varaiya, "Foundations of direct methods for power system transient stability analysis," IEEE Trans. Circuits Syst., vol. 34, no. 2, pp. 160-173, Feb 1987.

[27] T. L. Vu and K. Turitsyn, "Lyapunov Functions Family Approach to Transient Stability Assessment," IEEE Trans. Power Syst., vol. 31, no. 2, pp. 1269-1277, Mar. 2016.

[28] M. A. Rahman and H. Mohsenian-Rad, "False data injection attacks against nonlinear state estimation in smart power grids," in *2013 IEEE Power & Energy Society General Meeting*, Vancouver, BC, 2013, pp. 1-5.

[29] G. Liang, J. Zhao, F. Luo, S. R. Weller and Z. Y. Dong, "A Review of False Data Injection Attacks Against Modern Power Systems," in *IEEE Transactions on Smart Grid*, vol. 8, no. 4, pp. 1630-1638, Jul. 2017.

[30] N. Li, C. Uçkun, E. M. Constantinescu, J. R. Birge, K. W. Hedman and A. Botterud, "Flexible Operation of Batteries in Power System Scheduling With Renewable Energy," *IEEE Transactions on Sustainable Energy*, vol. 7, no. 2, pp. 685-696, Apr. 2016.

[31] J. Hazra, M. Padmanaban, F. Zaini and L. C. De Silva, "Congestion relief using grid scale batteries," in *2015 IEEE Power & Energy Society Innovative Smart Grid Technologies Conference (ISGT)*, Washington, DC, 2015, pp. 1-5.

[32] W. Bai and K. Y. Lee, "Modified optimal power flow on storage devices and wind power integrated system," in *2016 IEEE Power and Energy Society General Meeting (PESGM)*, Boston, MA, 2016, pp. 1-5.

[33] N. T. A. Nguyen, D. D. Le, G. G. Moshi, C. Bovo and A. Berizzi, "Sensitivity Analysis on Locations of Energy Storage in Power Systems With Wind Integration," *IEEE Transactions on Industry Applications*, vol. 52, no. 6, pp. 5185-5193, Nov.-Dec. 2016.

[34] A. H. Land and A. G. Doig, "An automatic method of solving discrete programming problems," *Econometrica*. vol. 28, no. 3, pp. 497–520, Jul. 1960.

[35] F. Capitanescu and L. Wehenkel, "An AC OPF-based heuristic algorithm for optimal transmission switching," in *2014 Power Systems Computation Conference*, Wroclaw, 2014, pp. 1-6.

[36] J. R. Birge and F. Louveaux, *Introduction to Stochastic Programming*. Belmont, CA: Duxbury Press, 2003.

[37] [Online] Available: https://www.ieee-pes.org/presentations/td2014/td2014p-000698.pdf

[38] D. P. Larson, L. Nonnenmacher, C. F.M. Coimbra, Day-ahead forecasting of solar power output from photovoltaic plants in the American Southwest, *Renewable Energy*, vol. 91, pp. 11-20, Jun. 2016,

[39] S. Talari, M. Yazdaninejad, M.-R. Haghifam, "Stochastic-based scheduling of the microgrid operation including wind turbines, photovoltaic cells, energy storages and responsive loads," *IET Generation, Transmission & Distribution*, vol.9, no.12, pp.1498-1509, Apr. 2015.

[40] Javad Modarresi, Eskandar Gholipour, Amin Khodabakhshian, "A comprehensive review of the voltage stability indices," *Renewable and Sustainable Energy Reviews*, vol. 63, pp. 1-12, Sep. 2016.

[41] J. F. Benders, “Partitioning procedures for solving mixed-variables programming problems,” *Numerische Mathematik*, vol. 4, no. 1, pp. 238-252, Feb. 1962.

[42] R. M. Van Slyke and Roger Wets Source, “L-Shaped Linear Programs with Applications to Optimal Control and Stochastic Programming,” *SIAM Journal on Applied Mathematics*, vol. 17, no. 4, pp. 638-663, Jul. 1969.

[43] A. Nasri, S. J. Kazempour, A. J. Conejo and M. Ghandhari, “Network-Constrained AC Unit Commitment Under Uncertainty: A Benders’ Decomposition Approach,” *IEEE Trans. Power Syst.*, vol. 31, no. 1, pp. 412-422, Jan. 2016.

[44] G. Laporte, F. V. Louveaux, “The integer L-shaped method for stochastic integer programs with complete recourse,” *Operations Research Letters*, vol. 13, no. 3, pp.133-142, Apr. 1993.

[45] [Online] available: http://people.tamu.edu/~lantian/modified IEEE-118_case3

[46] X. Li, A. Tomasgard and P. I. Barton, “Nonconvex Generalized Benders Decomposition for Stochastic Separable Mixed-Integer Nonlinear Programs,” *Journal of Optimization Theory and Applications*, vol. 151, pp. 425-454, Dec. 2011.

[47] A. M. Geoffrion, “Generalized Benders decomposition,” *Journal of Optimization Theory and Applications*, vol. 10, no. 1, pp. 237-260, Oct. 1972.

[48] N.V. Sahinidis, I.E. Grossmann, “Convergence properties of generalized benders decomposition,” *Computers & Chemical Engineering*, vol. 15, no. 7, pp. 481-491, Jul. 1991.

[49] A. Ruszczynski, *Nonlinear Optimization*. Princeton, NJ: Princeton University Press, 2006.

[50] P. Balasubramanian, M. Sahraei-Ardakani, X. Li and K. W. Hedman, "Towards smart corrective switching: analysis and advancement of PJM's switching solutions," *IET Generation, Transmission & Distribution*, vol. 10, no. 8, pp. 1984-1992, 5 19 2016.

[51] S. Zhao and C. Singh, "Studying the Reliability Implications of Line Switching Operations," *IEEE Transactions on Power Systems*, vol. 32, no. 6, pp. 4614-4625, Nov. 2017.

[52] M. Lu, H. Nagarajan, E. Yamangil, R. Bent, S. Backhaus and A. Barnes, "Optimal Transmission Line Switching Under Geomagnetic Disturbances," *IEEE Trans. Power Syst.*, vol. 33, no. 3, pp. 2539-2550, May 2018.

[53] P. Xiong and C. Singh, "Optimal Planning of Storage in Power Systems Integrated With Wind Power Generation," *IEEE Transactions on Sustainable Energy*, vol. 7, no. 1, pp. 232-240, Jan. 2016.

[54] C. Coffrin, H. L. Hijazi and P. Van Hentenryck, "The QC Relaxation: A Theoretical and Computational Study on Optimal Power Flow," *IEEE Transactions on Power Systems*, vol. 31, no. 4, pp. 3008-3018, July 2016.

[55] [Online] Available: http://icseg.iti.illinois.edu/southcarolina500/

[56] *PSS/E 33.4 Program Operation Manual*, Siemens Industry, Inc., Schenectady, NY, 2013.

[57] [Online] Available: https://www.powerworld.com/WebHelp/

[58] *TSAT User Manual*, Powertech Labs Inc., Surrey, British Columbia, Canada, 2017.

[59] [Online] Available: https://hvdc.ca/webhelp/ol-help.htm

[60] T. A. Nguyen, D. Van Hertem and J. Driesen, "Transient stability enhancement by TCSC controllers using remote input signals," In *9th IET International Conference on AC and DC Power Transmission (ACDC 2010)*, London, 2010, pp. 1-5.

[61] G. Huang and T. Zhu, "TCSC as a transient voltage stabilizing controller," in *2001 IEEE Power Engineering Society Winter Meeting. Conference Proceedings (Cat. No.01CH37194)*, Columbus, OH, USA, 2001, pp. 628-633 vol.2.

[62] K. Kawabe and A. Yokoyama, "Effective utilization of large-capacity battery systems for transient stability improvement in multi-machine power system," in *2011 IEEE Trondheim PowerTech*, Trondheim, 2011, pp. 1-6.

[63] E. M. Stewart, S. Kiliccote, D. Arnold, A. von Meier and R. Arghandeh, "Accuracy and validation of measured and modeled data for distributed PV interconnection and control," in *2015 IEEE Power & Energy Society General Meeting*, Denver, CO, 2015, pp. 1-5.

[64] WECC Renewable Energy Modeling Task Force (2014). *WECC Wind Plant Dynamic Modeling Guidelines* [Online]. Available: http://www.wecc.biz

[65] W. Wang, G. M. Huang, "Impacts of Smart Grid Topology Control on Power System Stability with Renewable Integration," in *2016 North American Power Symposium (NAPS)*, Denver, CO, Sep.18-20 2016, pp. 1-6.

[66] P. Wong, *et al.*, "The IEEE Reliability Test System-1996. A report prepared by the Reliability Test System Task Force of the Application of Probability Methods Subcommittee," *IEEE Transactions on Power Systems*, vol.14, no.3, pp.1010-1020, Aug 1999.

[67] [Online] Available: http://people.tamu.edu/~lantian/modified IEEE-118_case1

[68] [Online] Available: http://icseg.iti.illinois.edu/synthetic-power-cases/texas2000-june2016/

[69] G. Huang, J. Zaborszky and S. Y. Lin, "Reactive and Real Power Control for Computationally Effective Voltage and Thermal Management," *IEEE Trans. Power App. Syst.*, vol. PAS-104, no. 7, pp. 1728-1737, July 1985.

[70] W. Y. Ng, "Generalized Generation Distribution Factors for Power System Security Evaluations," *IEEE Trans. Power App. Syst.*, vol. PAS-100, no. 3, pp. 1001-1005, March 1981.

[71] A. Abur, A. G. Exposito, Power System State Estimation: Theory and Implementation, 1st ed. New York: Marcel Dekker, 2004.

[72] J. Kim and L. Tong, "On Topology Attack of a Smart Grid: Undetectable Attacks and Countermeasures," *IEEE Journal on Selected Areas in Communications*, vol. 31, no. 7, pp. 1294-1305, July 2013.

[73] A. Anwar, A. N. Mahmood, Z. Tari, “Identification of vulnerable node clusters against false data injection attack in an AMI based Smart Grid”, *Information Systems*, vol. 53, pp. 201-212, October 2015.